MEASUREMENT AND MAPPING OF PULSE COMBUSTION IMPINGEMENT HEAT TRANSFER RATES

A Thesis
Presented to
The Academic Facility

By

Charles C Hagadorn III

In Partial Fulfillment
Of the Requirements for the Degree
Master of Science in Mechanical Engineering

Georgia Institute of Technology

December 2005

MEASUREMENT AND MAPPING FOR PULSE COMBUSTION HEAT TRANSFER RATES

Approved by:

Dr. Frederick W. Ahrens
School of Mechanical Engineering
Georgia Institute of Technology

Dr. Timothy Patterson
School of Mechanical Engineering
Georgia Institute of Technology

Dr. David Orloff
School of Mechanical Engineering
Georgia Institute of Technology

Date Approved: August 19, 2005

ACKNOWLEDGEMENTS

First I would like to thank Dr. Fred Ahrens and Dr. Tim Patterson for their support and guidance thought this process. I have learned many important lessons from these two during the research and writing process that has improved my understanding of engineering and research.

I would also like to thank James Loughran for the many many hours he devoted in and out of the lab helping to construct and fix equipment and in gathering data. I would also like to thank Tex Sammons for the time and effort he spent working in the laboratory. Without James and Tex the research would not be where it is today.

Finally many thanks go to Mark Urbin, Perry Arrington and the people at GTRI Machine Services for their design and construction assistance.

TABLE OF CONTENTS

LIST OF TABLES

LIST OF FIGURES

LIST OF SYMBOLS

P	Pressure
P_{atm}	Atmospheric Pressure
Sh	Sherwood Number
Nu	Nusselt Number
Re	Reynolds Number
H	Impingement Gap Height
r	Radius or Radial Distance
D	Diameter of Tail Pipe
A	Amplitude of Velocity Oscillation
V_m	Mean Velocity
q	Heat Transfer Rate
A	Area
q''	Heat Flux
$\dot{E}$	Rate of Energy Transfer
T	Temperature
c_p	Specific Heat
$\dot{m}$	Mass Flow Rate
π	Pi
Pr	Prandlt Number
H	Coefficient of Heat Transfer
k	Thermal Conductivity

SUMMARY

After tissue and other types of paper leaves the press section of a paper machine it enters the drying section. Typically the drying section consists of either steam heated rolls over and around which the paper moves as it is dried or an impingement section where hot air is impinged on the paper to increase drying rates before continuing to the heated roll section.

Current research shows that pulse combustion impingement drying is an improvement over the steady impingement drying currently in commercial use. Pulse combustion impingement has higher heat transfer rates and a lower impact on the environment.

Commercialization of pulse impingement drying is the goal of the Pulsed Air Drying group at IPST. To that end the objective of this project is to develop a system that will allow researchers to measure heat transfer rates at the impingement surface from the impinging air.

A water cooled impingement plate with temperature and heat flux measuring capabilities was developed which accurately measures and records the desired information. The impingement plate was tested and its results were verified by comparison with previous literature.

Finally a preliminary comparison between steady and pulse combustion impingement was carried out. The study shows pulsed combustion impingement to be superior to steady impingement.

CHAPTER 1

INTRODUCTION

Project Purpose

In the paper drying process steady impingement drying is used to dry many types of products. Pulsed impingement drying is thought to be an improvement compared to steady impingement drying. The Pulsed Air Drying (PAD) group at IPST at Georgia Tech is researching the commercialization of the pulse combustion drying technique. The focus of this project was two fold. The first was to create a device that will allow measurement of impingement heat flux data relative to position. The second was to use the heat flux measurement device and paper drying tests to compare pulsed and steady impingement drying techniques in support of the PAD group's current and future efforts.

Project Background

When manufacturing tissue and other light weight papers the pulp slurry flows from the head box and onto the forming screen. At this point the paper is typically less than 1% solids. A vacuum is pulled from beneath the forming screen and increases the solids content. From here the fiber web enters the press section of the paper machine. In the press section the paper web is mechanically compressed and the solids content rises to approximately 40%.

From here the tissue paper will enter the drying section of the paper machine. The Yankee dryer has been in use for several decades in the paper drying industry. It typically consists of a large cylinder, around which the paper travels, with a dryer hood

over it. The large cylinder is heated internally with steam. In the hood hot air used for drying is expelled though nozzles onto the paper; the hood works to contain the impinging air and to remove the hot moist air from the process after impinging on the paper. Io this was the sheet is heated from both sides, increasing the rate of water removal.

More recently, a new process for drying tissue type paper has been in development. Pulse combustion impingement drying shares many of the physical systems and parts of the Yankee dryer but instead of steady air impingement on the paper sheet the pulsed air dryer produces reversing pulsed impingement air flow onto the paper. Pulse combustion drying has been shown to have many benefits over steady impingement. As outlined by Kudra (2003), the main advantages are as follows:

- Increased heat transfer and drying rates
- Increased production
- Decrease in pollutants, namely NO_x
- Decrease in production costs
- Easily retrofit into current Yankee dryers

In this study the increase in heat transfer and drying rates were investigated.

Project Methodology

Production scale tissue drying equipment uses an array of nozzles through which the impingement air flows to dry the paper. For complexity reasons, in most lab scale studies a single nozzle is used, this study also used a single nozzle for heat flux and drying tests.

In order to measure heat flux and surface temperature as a function of position relative to the combustion nozzle outlet, an impingement surface with a heat flux transducer and thermocouple was developed. A water cooled plate provided the impingement surface. The heat flux transducer was mounted flush with the surface in the middle of the water cooled plate to allow measurement of heat flux and surface temperature. The combined assembly was then mounted on a programmable 2-axis positioning system which allowed the experimenter to record data with respect to position.

In this project temperature and heat flux data were recorded with the heat flux transducer and the pulse combustor tail pipe exit jet temperature was recorded using a thermocouple. With this data, Newton's Law of cooling was to determine the local coefficient of heat transfer. The heat flux and position data were used to determine local Nusselt numbers. The Nusselt number is a dimensionless number that provides a measure of the convection heat transfer rate. Moreover, the local results were averaged over the entire surface to give average heat transfer rates.

Also, drying tests were conducted using blotter paper samples to study drying rates for pulse combustion impingement. The data from these tests can also be used to back calculate the heat transfer rate from the impingement jet on a real sample of paper.

By comparing the results from each type of test, the effectiveness of the heat flux measurement device in predicting drying rates was made. If the two tests show a high degree of correlation then testing can be done using the heat flux measuring device with many different geometries without having to do the tests with paper samples, thus reducing man hours spent in experimentation.

CHAPTER 2

LITERATURE REVIEW

Paper machine description

In the first stage of a paper machine a pulp slurry consisting of 99% water mass or higher is evenly laid onto the forming screen by way of the head box, from this point on the main propose of the paper machine it to remove the water and leave the pulp fiber. In the first stage of dewatering water drains through the forming screen, or wire, without assistance. As the water and pulp mixture travels over the forming screen it eventually enters a section where water removal is done via a vacuum from beneath the forming screen. By the time the pulp slurry reaches the end of the forming screen it has formed a thin mat of fibers and is now a sheet of wet paper.

From the forming screen the paper enters the press section of the paper machine. In the press section of the machine the paper is transported on a layer of "felt". The felt and paper are pressed between heavy steel rollers and water is removed from the paper into the felt. At this point the paper has typically reached 60% water by mass and further water removal via mechanical pressing is not possible due to sheet quality constraints, reduced felt lifetime and/or insufficient dwell time in each press.

At this point water is removed via thermal processes. Two main types of thermal dewatering are used. In the first type the paper travels over many steam filled drying cylinders. These drying cylinders heat the water in the paper, turning it to steam which travels though the felt and into the ambient air. Another option is to have hot air blown onto the sheet evaporating the water. It is this type of drying method that pulsed

combustion drying improves upon. After the paper has completed the drying section the paper making process is finished. From here the paper is packaged as ordered by the customer.

Pulsed Combustor Technology

At the heart of pulse combustor technology is the combustion chamber and its exhaust tail pipe. The combustion chamber and tail pipe together act as a Helmholtz resonator. For purposes of this study a Helmholtz resonator is generically defined as a gas chamber which contains a body of air and a pipe attached to a hole at one end of the chamber which contains a slug of air that can oscillate back and forth. The air in the chamber acts as a spring connected to the air in the tail pipe which acts as the mass in this spring-mass system. The frequency of the system is dependant on the density of the air, the length and volume of the tail pipe and the volume of the chamber.

The cyclical process of pulsed combustion is shown in simplified form in Figure 2.1 from Zbicinski.

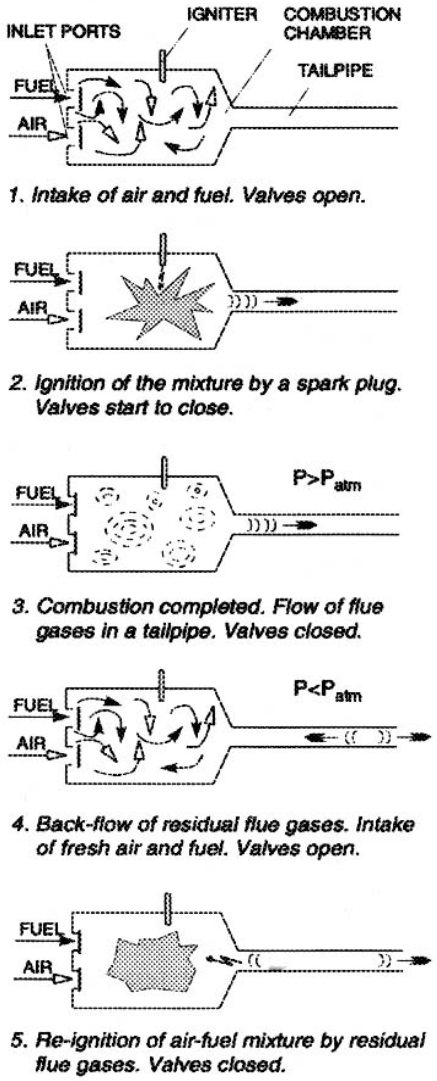

Figure 2.1: Pulsed Combustion Process from Zbinski (2002)

Although this figure uses flapper valves on the air and gas inlets to the combustion chamber, an aerodynamic valve would serve the same purpose. A description of the pulse combustion process follows:

1. In the first step fuel and air are forced into the combustion chamber though the intake valves and the gases mix together.

2. The first combustion cycle requires an ignition source. When the gas is ignited the pressure inside the chamber rises forcing hot gasses to leave the combustion chamber though the tail pipe and also causes the inlet valves to close.
3. At the completion of the combustion process the gas continues to flow out the tail pipe and the inlet valves remain closed.
4. The momentum of the gases in the tail pipe cause the pressure in the combustion chamber to eventually drop below atmospheric pressure causing the intake valves to be pulled open bringing in fresh air and fuel. The lower pressure in the combustion chamber also causes some of the flue gases in the tail pipe to be drawn back into the combustion chamber.
5. Re-ignition of the gases in the combustion chamber is now caused by the heat from the flue gasses and the heat contained in the walls of the combustion chamber.

After the initial warm up period the combustion process will continue indefinitely, as long as fresh air and fuel are sent into the chamber during each cycle.

Steady Impingement

In 1977 Holger Martin published a paper titled "Heat and Mass Transfer between Impinging Gas Jets and Solid Surfaces". In this, first of its kind, paper Martin reviewed more than 60 separately written papers published between 1952 and 1974. The author then presented complete theoretical models for impingement heat transfer under an

assortment of operating conditions, including single round nozzles, slotted nozzles, nozzle arrays and etc.

For round nozzles two qualitative conclusions were reached in regards to plots of the Nusselt and Sherwood numbers: monotonically decreasing bell shaped curves for large nozzle-to-plate distances and curves with a distinct bump or second maximum for small nozzle-to-plate distances. The secondary maximums were shown to be less distinct with decreasing Reynolds numbers. Figure 2.2 shows the plots from Martin (1977).

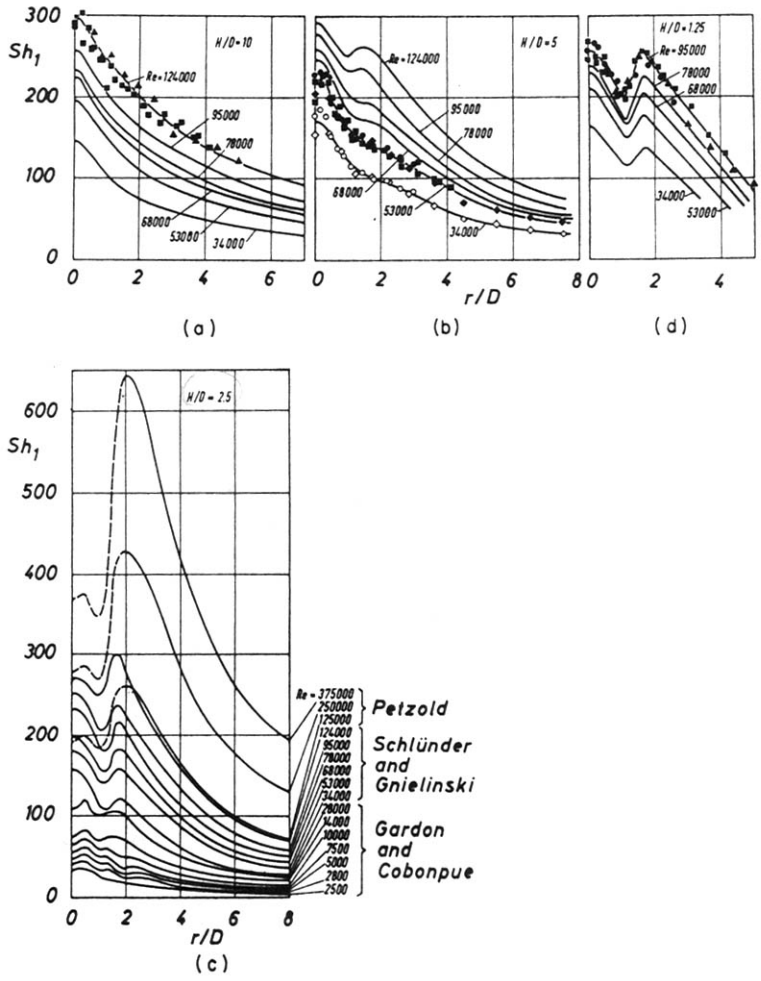

Figure 2.2: Plots of Sherwood Number Contours

In Figure 2.2 H/D is the ratio of impingement gap to nozzle diameter, r/D is the radial position as a function of nozzle diameter, for example, an r/D of 2 means that the measurement is 2 nozzle diameters from the nozzle centerline. The symbol Re is the Reynolds number of the air flow through the tail pipe for each specific plot. Sh is the Sherwood number which is the mass transfer analogy for Nusselt number. Also in Figure 2.2 (c); the names on the right side of the graph refer to the researchers who performed the work.

Although Martin's (1977) paper discussed steady impingement in great detail there are no similarly detailed discussions for pulsed impingement drying. There is no study equivalent to the Martin (1977) paper dealing with pulsed impingement heat transfer.

Pulsed Impingement Vortices

One of the main proposed mechanisms for the improvement in heat transfer seen with pulsed impingement is the effect of the toroidal vortices that are created by the pulsating and reversing jet. Two companion papers written by Keller (1991) and Eibeck (1991) studied, both numerically and experimentally, the strong toroidal vortices formed by the pulsing flow and the increase in heat transfer resulting from the pulsating flow.

Figures 2.3 and 2.4 show how the vortices form and travel as a function of cycle time. At t = 0 the positive flow begins and gas exits the tail pipe at a low velocity and a vortex ring is released. As time continues the velocity of the exit gas increases and with it the strength of the vortex. By the time the positive flow period is completed the vortex is at least 2 tail pipe diameters from the tail pipe exit. When the cycle enters the negative

flow period air is pulled back into the tail pipe. The reverse flow only pulls in air from the perimeter region around the tail pipe exit. The toroidal vortex continues to travel away from the tail pipe. Their calculations also showed that fluid beyond 2 diameters from the tail pipe exit was not affected by the reverse flow. Because of this the region affected by the reverse flow was much less than the region affected by the positive flow jet.

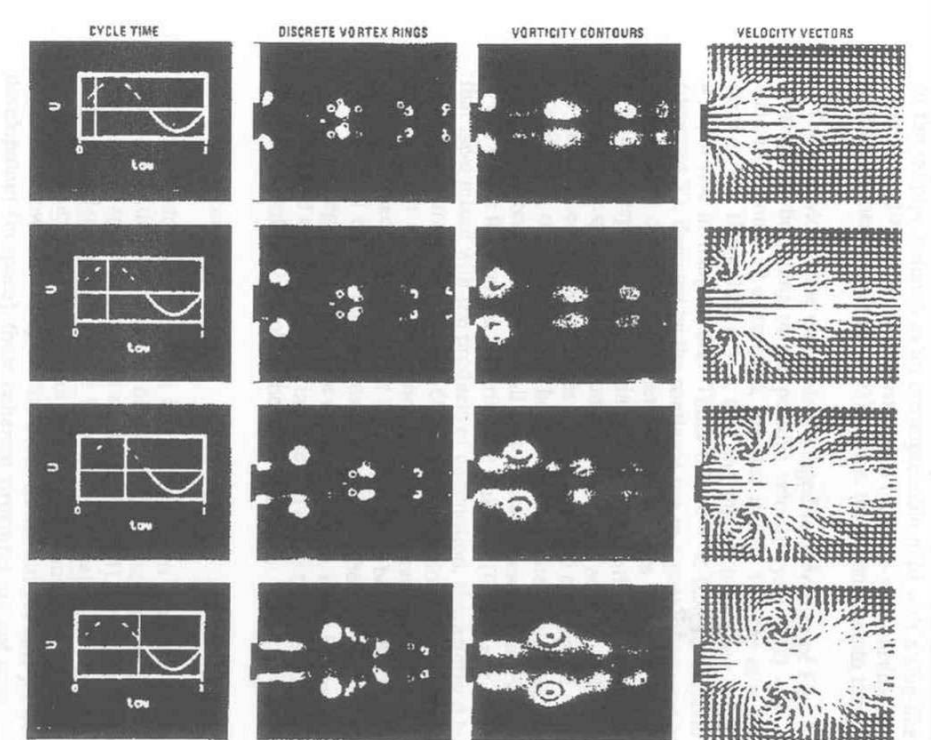

Figure 2.3: Pulse Combustion Vortices from Eibeck (1991)

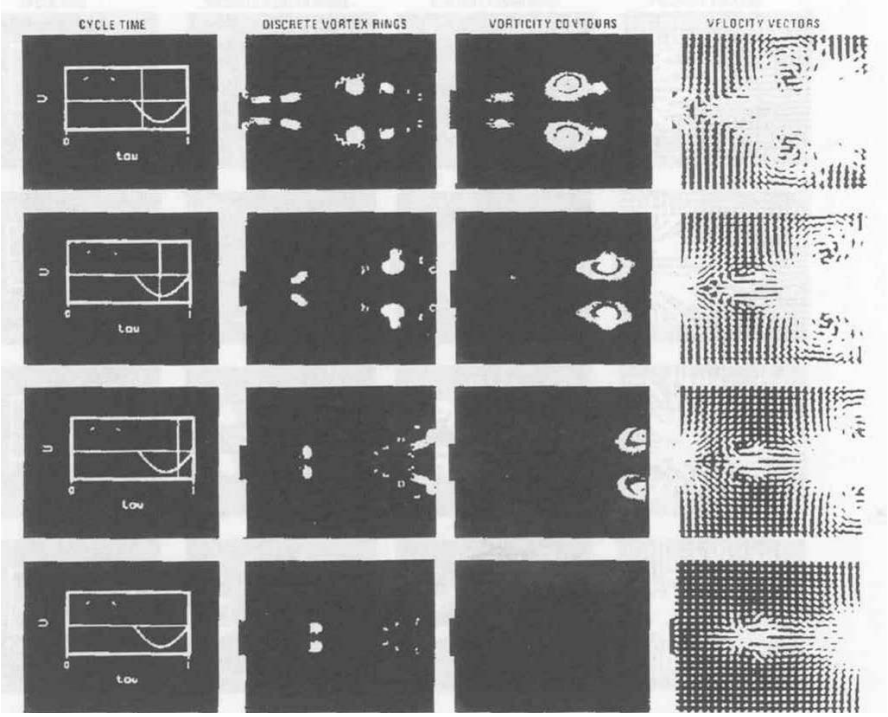

Figure 2.4: Pulse Combustion Vortices from Eibeck (1991)

In their study Eibeck and Keller concluded that for a separation distance of less than 4 pipe diameters improvements in heat transfer as high as 2.5 times could be obtained. Beyond 4 pipe diameters the effects of pulsed impingement with reverse flow were worse than that of standard steady impingement. The reduction in heat transfer beyond 4 diameters was thought to be due to entrainment of ambient air in the toroidal vortex, which at greater distances disrupted the flow in the exit jet.

The Amplitude Ratio

The amplitude ratio is a measure of the mean tail pipe exit velocity to the amplitude of the pulsing velocity and is of significant importance to the study of pulse impingement heat transfer. Equation 2.1 shows the relationship.

$$Amplitude \quad Ratio = \frac{A}{V_m} \qquad \text{Eq (2.1)}$$

Hanby (1969) investigated the relationship between amplitude ratio and heat transfer to the wall of the pulse combustor tail pipe and showed a significant and direct relationship between the two. The relationships showed that, above an amplitude ratio of one, heat transfer with the tail pipe wall increased linearly as the amplitude ratio increases. It is expected that a similar relationship, where the heat transfer increases with amplitude, exists for pulse combustion impingement heat transfer.

Retrofit

A driving force behind pulsed combustion technology in the paper industry is the relative ease with which existing dryers can be retrofitted with pulsed combustion technology. A diagram of a typical Yankee dryer and its hot air supply is shown in Figure 2.5.

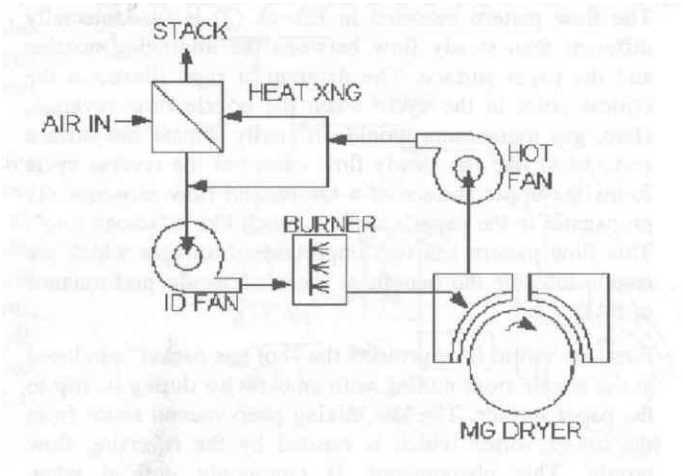

Figure 2.5: Typical Yankee Dryer Process Diagram from States (2003)

The Yankee dryer system consists of an induced draft fan to force air into the burner which heats the air and then blows it into the dryer hood where the air impinges onto the paper. Another fan pulls the hot air and steam from the dryer hood where it is

sent to a heat exchanger to preheat the incoming air and then the exhaust air is sent out the stack.

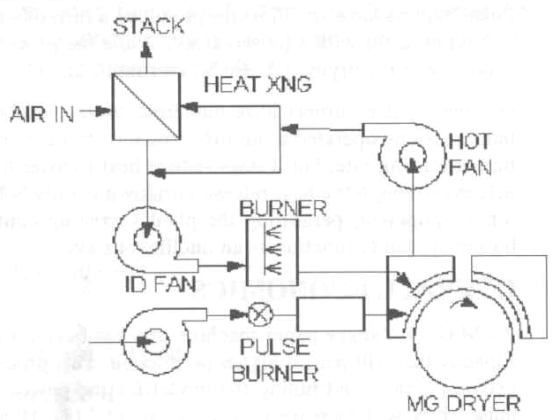

Figure 2.6: Possible Pulse Combustion Retrofit from States (2003)

In one pulse combustion retrofit concept most of the existing equipment was used, but a third fan and the pulse combustion chamber was added to the system, the same dryer hood was used. This system is shown in figure 2.6.

By utilizing a majority of the previously installed equipment the pulse combustion impingement drying process can be added to existing paper machines with relatively little capital cost and risk.

CHAPTER 3

METHODOLOGY

Cooling Plate Design

This investigation of pulsed impingement drying used an experimental apparatus to measure the heat flux as a function of distance from the tail pipe centerline. There are several functional requirements that were developed in specifying the function of the heat flux measurement apparatus in this study:

1. It should have a flat impingement surface.
2. It should have a response time on the order of several seconds or less to allow for quick measurements.
3. The plate must work with the existing pulse combustion apparatus without modifications.
4. The heat flux data from the plate needs to be verifiable.

In attempting to meet these requirements two different plates were designed. The first heat flux measuring apparatus relied solely on free convection and radiation for cooling. After experimentation with the first apparatus, a second improved plate was designed and built. The second plate used built in water channels to cool the impingement surface. A complete discussion of both experimental apparatuses follows.

Free Convection Cooled Plate

The first apparatus consisted of a heat flux meter, an ITI model HT-50, embedded in an 460 mm square by 13 mm thick steel plate. The heat flux meter was 19 mm in diameter and 3 mm deep. This specific heat flux meter was chosen for its relatively small size, its ability to measure surface temperature and heat flux at the same time, and its ability to function in a wide range of temperatures. The output of the heat flux transducer is a voltage that was proportional to the temperature difference between the top and bottom of the transducer. Because the thermal conductivity and the geometry of the material between the top and bottom of the transducer were known by the manufacturer, the output voltage was used to calculate the heat flux through the transducer using manufacturer supplied data. The design of the plate met requirements 1 and 3, having a flat impingement surface and working with the existing apparatus, respectively.

The procedure for testing the plate involved starting up the pulse combustor and allowing it to reach steady state. Once steady state was reached the data acquisition system was started and the heat flux plate was quickly moved into position, lining up the heat flux meter with the centerline of the tail pipe. Figure 3.1 is a graph of heat flux and plate temperature versus time and is representative of the data recorded using the heat flux meter embedded in the plate.

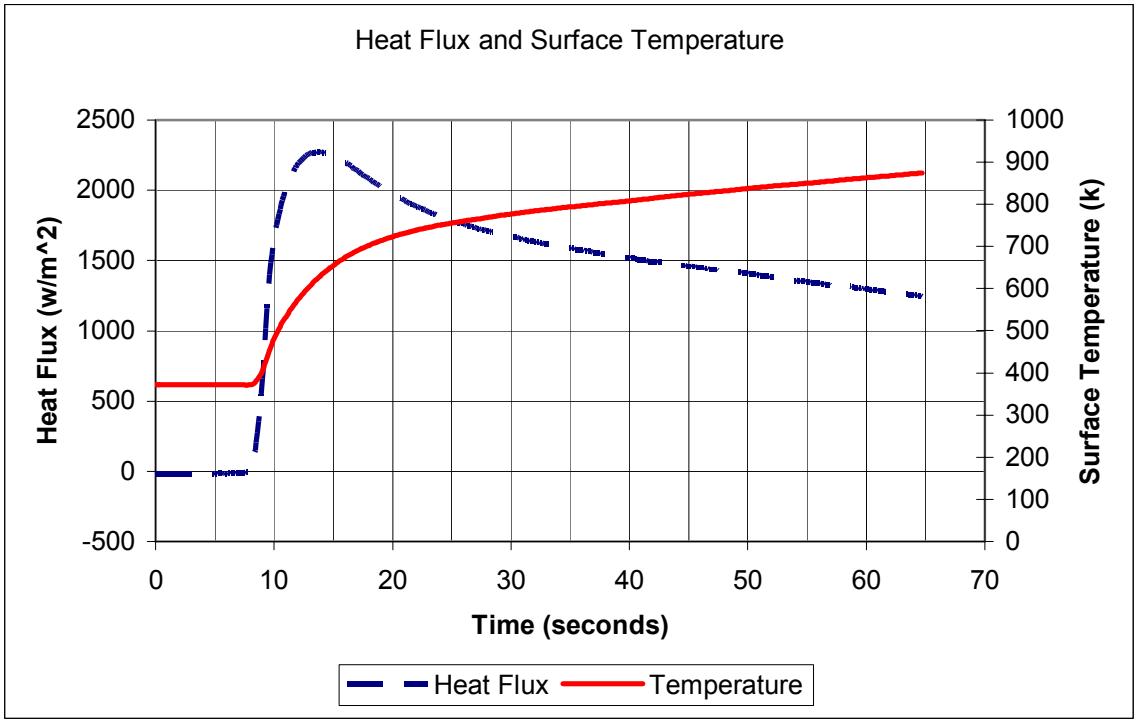

Figure 3.1 Heat Flux and Surface Temperature Versus Time

As can be seen from Figure 3.1 the plate never reached steady state. The temperature continued to rise throughout the experiment. Also interesting is that the heat flux peaked after 5 seconds of exposure to the jet and then declined for the duration of the experiment. It was thought that the initial sharp raise in heat flux followed by a steady decrease was due to heat conduction through the plate. When the plate was initially cool and placed under the exit jet, the exposed surface increased in temperature rapidly and the temperature difference between the top surface and the bottom surface of the heat flux meter as high. As the plate warmed up heat was conducted though the heat flux meter and the temperature difference between the top and the bottom of the heat flux meter declined thereby reducing the heat flux measured by the meter.

A simple finite difference model was used to test this theory. The one-dimensional conduction model consisted of an initially cool rod insulated at one end, exposed to a heat source at the other and divided into twenty elements. Using generic material data the chart in Figure 3.2 was derived.

Figure 3.2 is a graph of temperature difference verses time between a pairs of points along the rod. Although not a quantitative analysis, the finite difference graph of Figure 3.2 has many of the qualities of the heat flux graph from Figure 3.1. It was inferred from this analysis that the heat flux meter would not produce usable data in this configuration. It did not meet requirement 2. Furthermore, the impingement surface temperature reached an extremely high level. For these reasons a water cooled heat flux plate was developed.

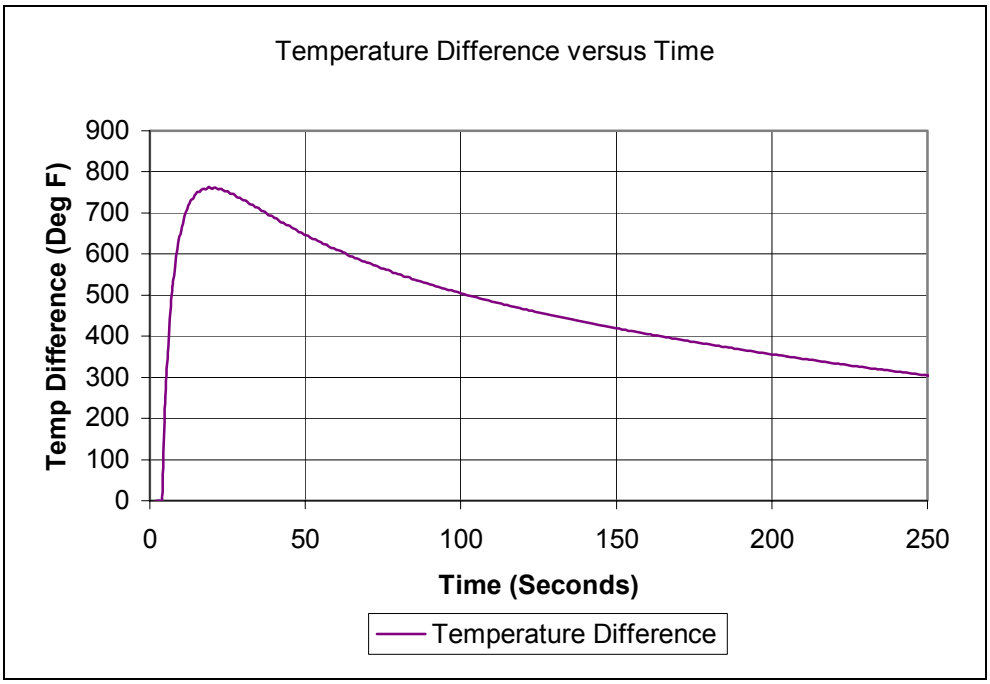

Figure 3.2: Temperature Difference versus Time for Finite Difference Approximation

Water Cooled Heat Flux Plate

For the heat flux plate to reach steady state the energy entering the plate from the pulse combustor must equal the amount of energy leaving the plate. The first plate failed to reach steady state in a reasonable about of time because it relied on free convection and radiation in air to remove heat from the plate which proved to be insufficient. Using forced convection to cool the plate will allow energy to be removed at a faster rate.

A constant supply of water at 16 ^{o}C was available in the laboratory and was chosen as the preferred method to remove energy from the heat flux plate. To do this a plate was designed with two separate flows. The two flows cool different parts of the plate, one for the heat flux meter and the other for the main surface of the plate. Using two separate flows allowed the operator to adjust the flow rate in the two areas independently of each other and ensured adequate cooling was provided to both the main surface of the plate and to the heat flux meter.

The first flow consisted of a spiral channel machined into the back of the plate. It started 50 mm from the center of the plate and spiraled outward, increasing in radius at a rate of 20.3 mm per revolution creating 5.5 total revolutions. The total path length of the flow was 3.59 m. The channel was 15.2 mm wide and 15.9 mm deep with 7.6 mm radius corners at the bottom of the channel. Figure 3.3 is a three dimensional model of the plate viewed from the bottom and shows the path of the channel. Figure 3.4 is a cross-section of the plate and shows the profile of the channel. This flow path cooled 60% of the plate surface, but did not cool the heat flux meter.

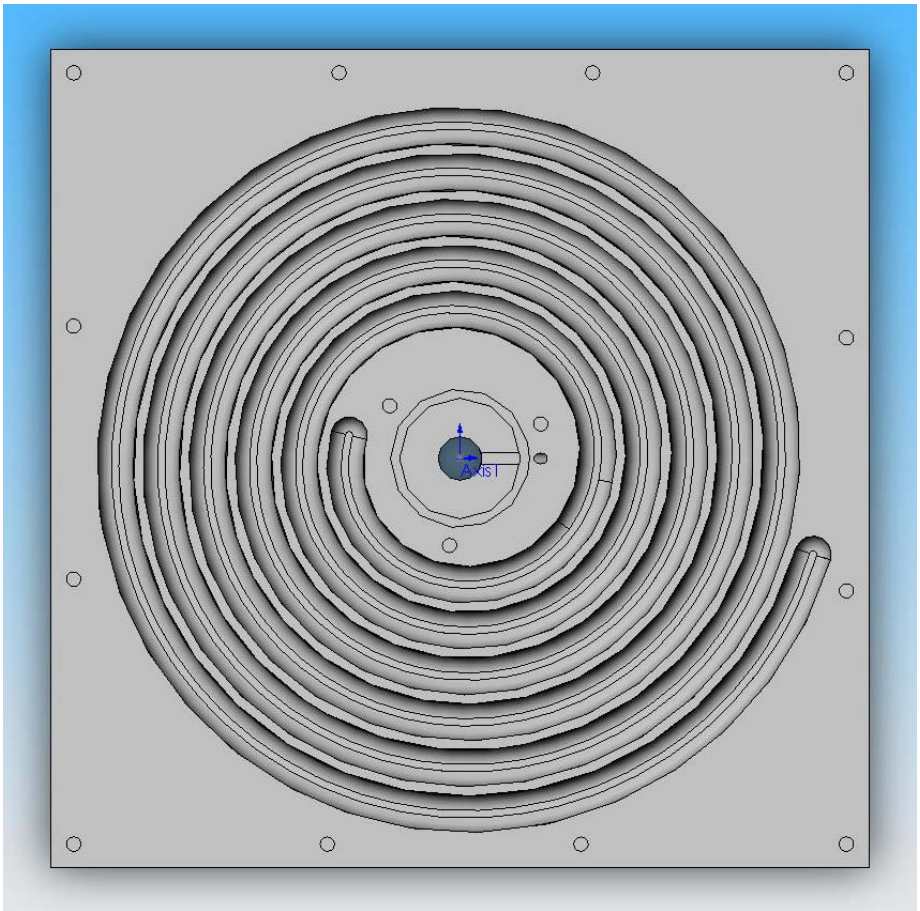

Figure 3.3: Diagram of Heat Flux Plate, Bottom View

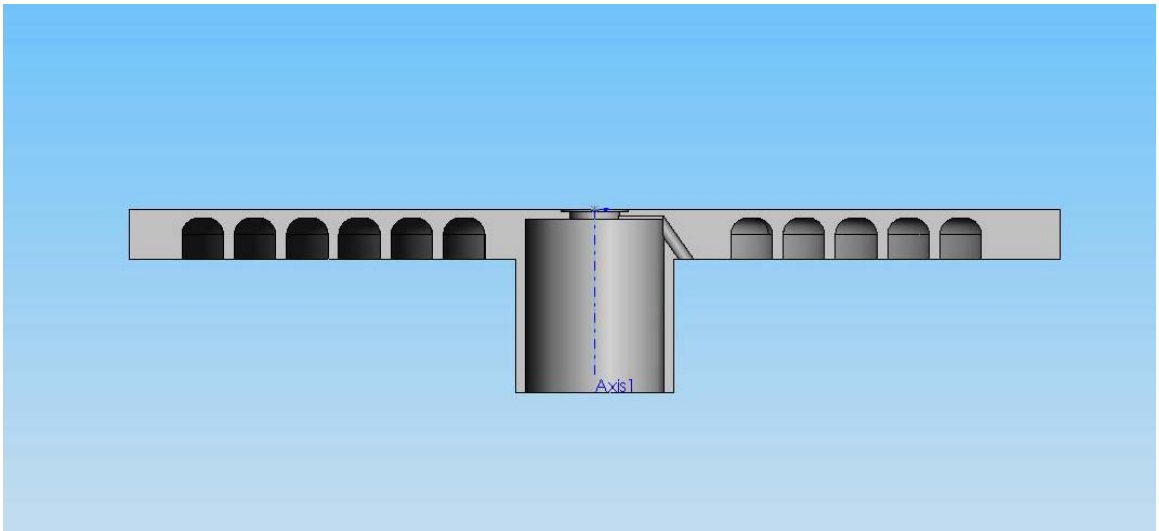

Figure 3.4: Diagram of Heat Flux Plate, Cross Section Side View

A 6.4 mm plate provided the bottom cover of the cooling channel. The plate had inlet and outlet nipples to provide connections for the cooling water. The cover was secured with 12 1/4x20 bolts and was sealed with high temperature silicone. Figure 3.5 shows the completed plate with the cover installed.

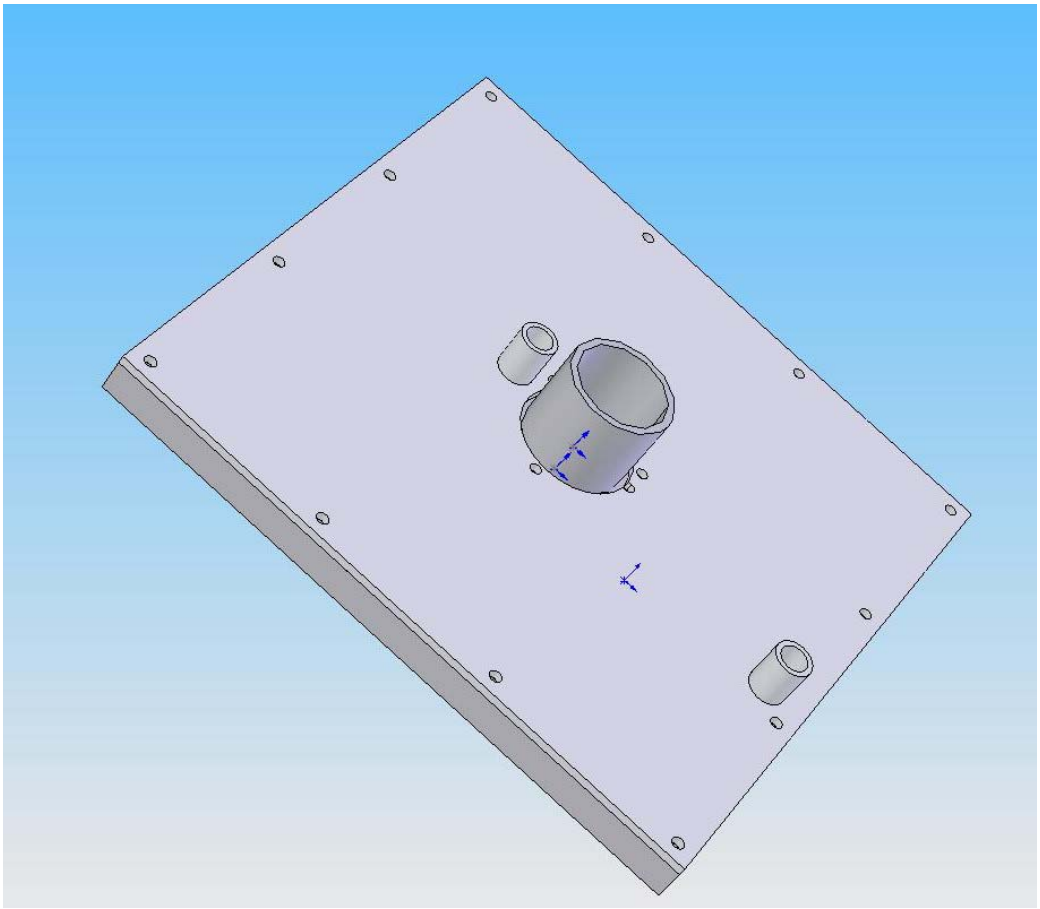

Figure 3.5 Diagram of Heat Flux Plate with Cover

The second water flow path was designed specifically to cool the heat flux meter and the plate surface immediately surrounding the meter. Figure 3.6 shows a cross section of the final design for the heat flux meter cooling path.

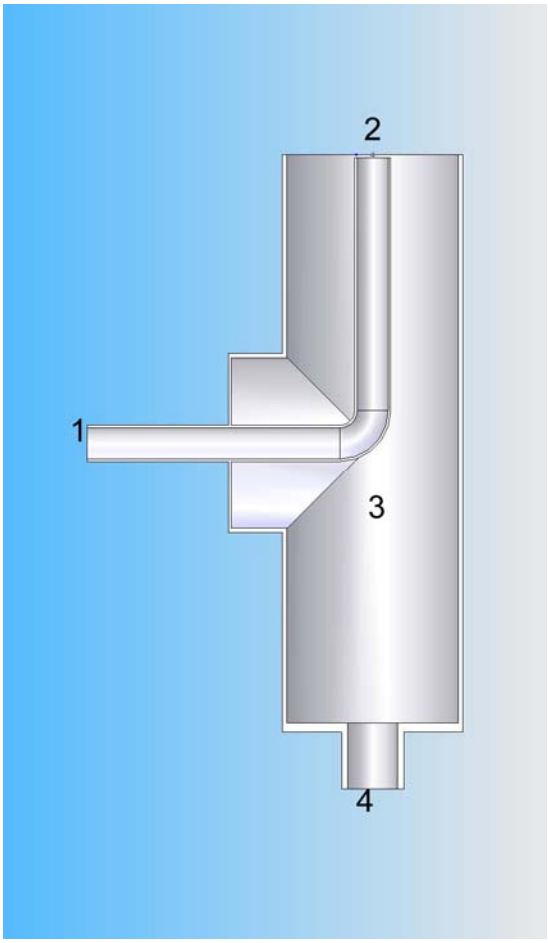

Figure 3.6 Diagram of Heat Flux Cooling Water System

The heat flux meter cooling water entered the flow path through point 1 as marked on the figure and flowed through the 9.5 mm diameter tube. There was a 3.2 mm gap between the end of the tube and the heat flux meter, marked point 2. When the water exited the tube it immediately impinged on the back surface of the heat flux meter and then entered the main chamber marked 3 on the diagram. Finally the cooling water exited the chamber though the exit marked 4 on the diagram. Figures 3.7 and 3.8 show the model and a photo of the final assembly of the water cooled heat flux plate respectively.

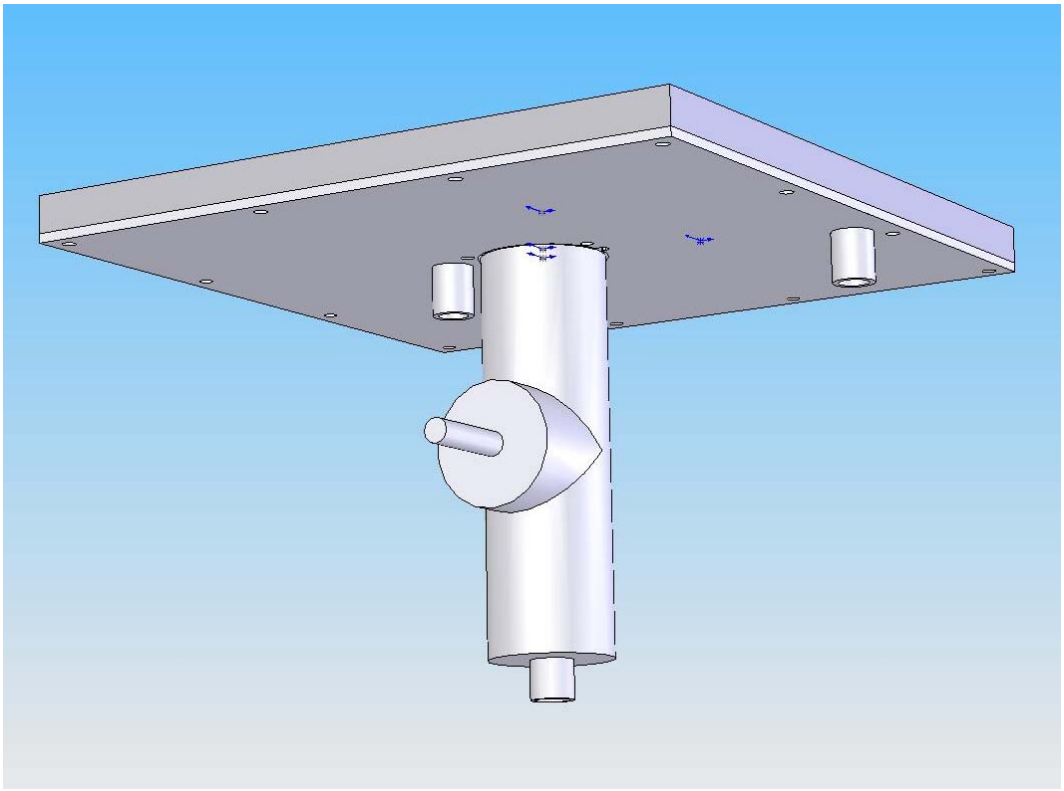

Figure 3.7 Diagram of assembled water cooled heat flux plate

Figure 3.8: Photo of heat assembled water cooled heat flux plate

Because the cooling water for the heat flux meter exited though the bottom of the chamber it was necessary to verify that the chamber would remain full during operation and that cooling water was always in contact with the plate and heat flux meter surface. A simple experiment determined the minimum necessary flow rate to keep the cooling chamber full at all times. For purposes of this simple experiment the heat flux meter cooling chamber was considered a control volume with inlet 1, chamber 3 and exit 4 as marked in Figure 3.9.

In order for the chamber to fill with water before each test the inlet water flow rate must be higher than the outlet flow rate. When filling the chamber only the static pressure of the column of water in the chamber forces the water out the exit. After the chamber is filled the pressure of the main water line will force the water out of the chamber. The following simple experiment was used to determine the outlet flow of the chamber while it is filling and was conducted before attaching the chamber to the plate.

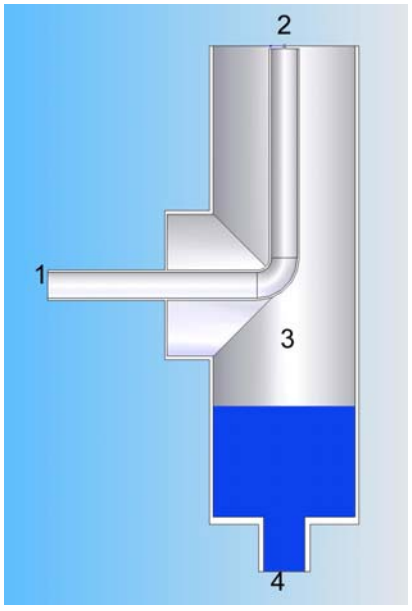

Figure 3.9 Cooling Water Flow Diagram

The procedure to determine the cooling water flow rate was as follows:

1. The exit was open to the atmosphere and the chamber was filled through the inlet.
2. When the chamber was full the inlet flow rate was adjusted until inlet and exit flow rates were equal and the water level was at the top of the chamber.
3. At this point the flow rate into the chamber that causes it to remain full had been determined and was recorded.

For this specific cooling chamber the flow necessary to keep it filled with water was 8 liters per minute When the heat flux plate was in use a flow rate of more than 8 LPM was kept to insure that the chamber was full at all times. In all experiments with this chamber the flow rate was set to at least 8.8 LPM giving a 10% margin for error.

Because the water that flowed through the plate removed most of the heat that the pulse combustor transferred to the plate the water cooled plate reached steady state more quickly, and at a lower surface temperature, than the non water cooled plate. Also, because the inlet and outlet flow rate and temperature of the cooling water could be measured a secondary heat balance for the plate was made to verify the data from the heat flux meter. This will be discussed in greater detail in the calibration section.

Positioning System

In order to position the plate under the pulse combustor accurately and to move the plate while the pulse combustor is in operation an automated positioning system was required. The design requirements for the positioning system are listed below:

1. Repeatable position accuracy of 2 mm or less
2. Must fit within the existing pulse combustor structure
3. Must be able to program specific paths for the plate to travel while recording data
4. Must work in the hot environment of the pulse combustor

With these requirements the positioning system was designed. The basic components of the system were as follows:

1. Industrial Devices R2A Series linear actuators
2. Industrial Devices Model S6962 controller
3. UniMeasure LX Series draw wire transducers

The linear actuator's positioning plate as moved by a stepper motor and was configured for 20,000 steps per revolution and 21.34 mm per revolution. The actuator had a published repeatable positioning accuracy of 0.25 mm. This provided more than enough positioning accuracy to satisfy the requirements.

The controller had several different operating modes, including a manual positioning mode and a preprogrammed mode. It was also capable of controlling two

different axes at the same time. More specific information about using and programming the controller is located in Appendix A.

Draw wire transducers vary their voltage output based on position. These particular transducers had a variable resistance linear potentiometer that forms a voltage divider. As the wire was pulled out of the transducer the adjustment knob on the potentiometer was turned, the resistance changed and therefore the output voltage changed. The UniMeasure LX series draw wire transducers were accurate to 0.5% full scale, approximately 3 mm.

Each axis of the positioning system consisted of a linear actuator with motor and an attached draw wire transducer. To allow the plate to be positioned anywhere in two dimensions under the pulse combustor one linear actuator was mounted on the moveable platform of the other and their axes were orientated 90 degrees to each other. Figure 3.10 shows a side view of one axis of the positioning system and Figure 3.11 shows the completed positioning system before mounting of the heat flux plate.

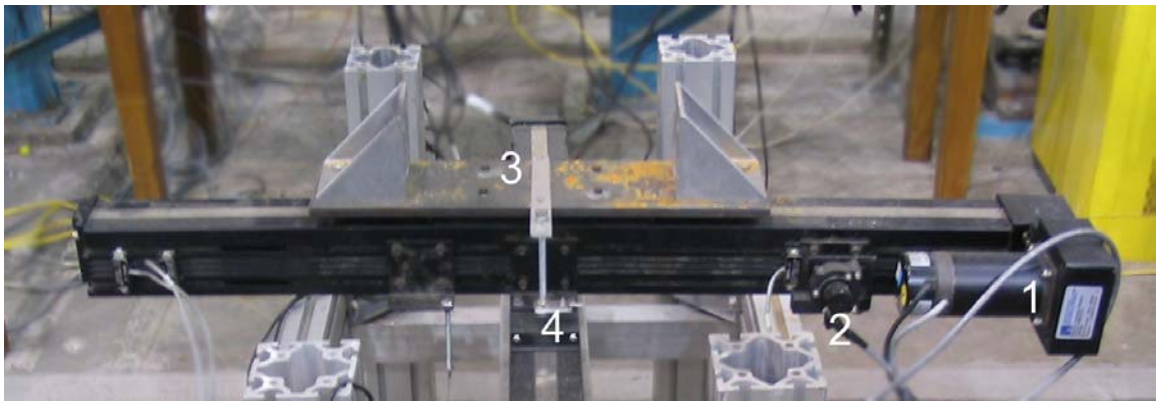

Figure 3.10: Positioning System Side View

In Figure 3.10 1 is the stepper motor, 2 is the draw wire transducer, 3 is the positioning platform and 4 is the connection between the positioning platform and the draw wire transducer.

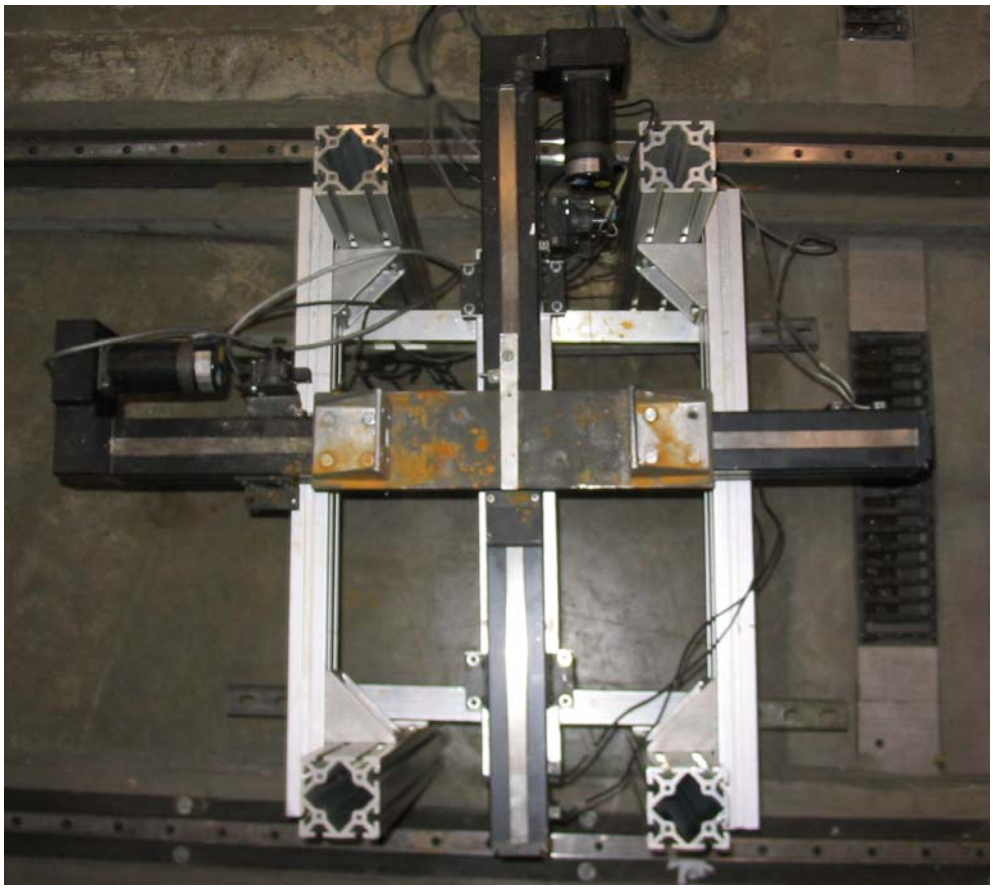

Figure 3.11 Positioning System Top View

Heat Flux Meter Calibration

As discussed earlier this study involved measuring heat flux at different radial positions starting from the pulse combustor centerline and moving outward. The heat flux measurements were then used to calculate the heat transfer rate into the plate.

Although the manufacturer claimed a specific accuracy of the heat flux meter it must be determined whether the output from the heat flux meter in this specific setup could be used to calculate the quantities desired. The heat flux meter's accuracy was verified using a secondary, and more fundamental, method of measuring overall heat transfer into the plate.

The two methods used to measure heat flux into the plate were called the heat flux meter method and the second, more fundamental method, was called the cooling water energy balance method. Both methods are described in detail below.

Heat flux method

In the heat flux method the plate was positioned under the tailpipe of the pulse combustor and during operation heat flux measurements were made at specific radial positions. Each radial position was then assigned a specific plate area which depended on its distance from the center of the plate and corresponded to the annular shaped area that the heat flux measurement represented.

Table 3.1 shows the positions at which heat flux measurements were recorded, the area corresponding to the annular region assigned to each radial position along with the inner and outer radii of the annular region and sample data from each position to be used in an example to follow. The heat flux measurements were multiplied by their corresponding area and the results from all the areas were then added together to calculate the total rate of energy transfer into the plate. The final result was the total heat transfer rate into the plate's surface. Equations 3.1 and 3.2 show the equations used to determine the total heat flux into the plate.

Table 3.1: Heat Flux Radial Position Data

Radial Position	Area	Heat Flux
(m)	(m^2)x10^3	(W/m^2)
0.000	0.29	604
0.006	0.00	603
0.013	0.00	586
0.019	2.28	574
0.025	0.00	558
0.038	3.64	542
0.051	4.05	508
0.064	5.07	469
0.076	6.08	426
0.089	7.09	404
0.102	8.11	350
0.114	9.12	303
0.127	10.13	281

Calculating heat transfer for area A1 corresponding to position 0.00:

$$q_{A1} = A_1 * q''_{A1} \qquad \text{Eq (3.1)}$$

This calculation was carried out for each position and the results put into equation 3.2 to calculate the total heat transfer:

$$q_{Total} = q_{A1} + q_{A2} + \ldots + q_{a13} \qquad \text{Eq (3.2)}$$

The area at positions 6.4, 13 and 25 mm were ignored here because the diameter of the heat flux transducer, 19 mm, is greater than the increase in radial position and would have caused a great deal of overlap in measurement areas. This is why their areas were set to 0.

Water Balance Method

The water balance method of determining the heat transfer into the plate was simpler than the heat flux method. In this method the whole heat flux plate was

considered a control volume at steady state. In this case the total energy that entered the control volume was equal to the total energy leaving the control volume and there was no change in energy stored in the control volume. Energy entered the system from the pulse combustor and the cooling water inlet and left the system through the cooling water exit, all other sources of energy transfer were ignored. Equation 3.3 is the conservation of energy equation which states the energy stored in a system is equal to the energy entering the system plus the energy generated in the system minus the energy leaving the system.

$$\dot{E}_{in} + \dot{E}_{g} - \dot{E}_{out} = \dot{E}_{st} \qquad \text{Equ (3.3)}$$

In this experiment there was no energy generated in the system and at steady state there was no change in the amount of energy stored in the system. For these reasons equation 3.3 simplifies to equation 3.4.

$$\dot{E}_{in} - \dot{E}_{out} = 0 \qquad \text{Equ (3.4)}$$

Inputting the known and unknown variables for our specific experiment equation 3.4 becomes equation 3.5.

$$\dot{E}_{WaterOut} - \dot{E}_{WaterIn} = \dot{E}_{impingement} \qquad \text{Equ (3.5)}$$

Finally, the energy entering and leaving the control volume via the cooling water were known through measurement of the cooling water flow rate and inlet and outlet water temperatures. Equation 3.6 shows how the rate of energy entering and leaving the system though the cooing water was determined based on its specific heat capacity, temperature and mass flow rate.

$$\dot{E}_{WaterOut} - \dot{E}_{WaterIn} = \dot{m} * c_{p} * \left(T_{out} - T_{in}\right) \qquad \text{Equ (3.6)}$$

Equation 3.6 can now be solved for the only unknown, the heat transfer to the plate from the pulse combustor.

Calibration Data Analysis

With the procedures for determining the heat flux via the water balance and the heat flux meter methods established, a comparison and analysis of the results was made.

Cooling water data were taken over two days of trials resulting in 10 cooling water energy balance data points to compare to the heat flux meter measurements. The data came from several different operating conditions, steady state and pulsating air flows, 25 mm and 71 mm diameter tail pipes and high and low mass flow though the combustor. By using several different operating conditions the analysis should not be biased for or against any particular operating condition.

Table 3.2 shows the cooling water data recorded from the 10 trials. This includes the run number, inlet water temperature, which was the same for both water flows, the outlet water temperature, flow rate and energy gain for both flows.

Table 3.2: Cooling Water Data

Heat Flux Transducer Cooling Water				
Run	**Temp In**	**Temp Out**	**Flow Rate**	**Heat Transfer**
(#)	(deg C)	(deg C)	(L/min)	(J/hour)
1	17.00	17.61	8.41	1290000
9	18.00	19.22	8.45	2600000
13	18.50	20.22	8.45	3660000
16	18.72	21.50	8.45	5900000
17	17.33	18.61	8.63	2770000
20	17.44	20.11	8.63	5780000
24	17.78	20.33	8.63	5540000
25	18.72	20.44	8.13	3520000
28	18.89	21.61	8.13	5560000
33	18.22	19.83	8.82	3570000
Spiral Channel Cooling Water				
Run	**Temp In**	**Temp Out**	**Flow Rate**	**Heat Transfer**
(#)	(deg C)	(deg C)	(L/min)	(J/hour)
1	17.00	22.72	13.5	19300000
9	18.00	27.39	13.7	32400000
13	18.50	22.22	13.2	12300000
16	18.72	26.83	12.5	25500000
17	17.33	21.56	12.5	13300000
20	17.44	27.06	13.6	32900000
24	17.78	26.94	15.8	36400000
25	18.72	22.06	15.8	13200000
28	18.89	26.78	15.8	31300000
33	18.22	36.17	11.1	50200000

Figure 3.12 shows the total energy gained by the cooling water versus energy transferred using the heat flux meter data.

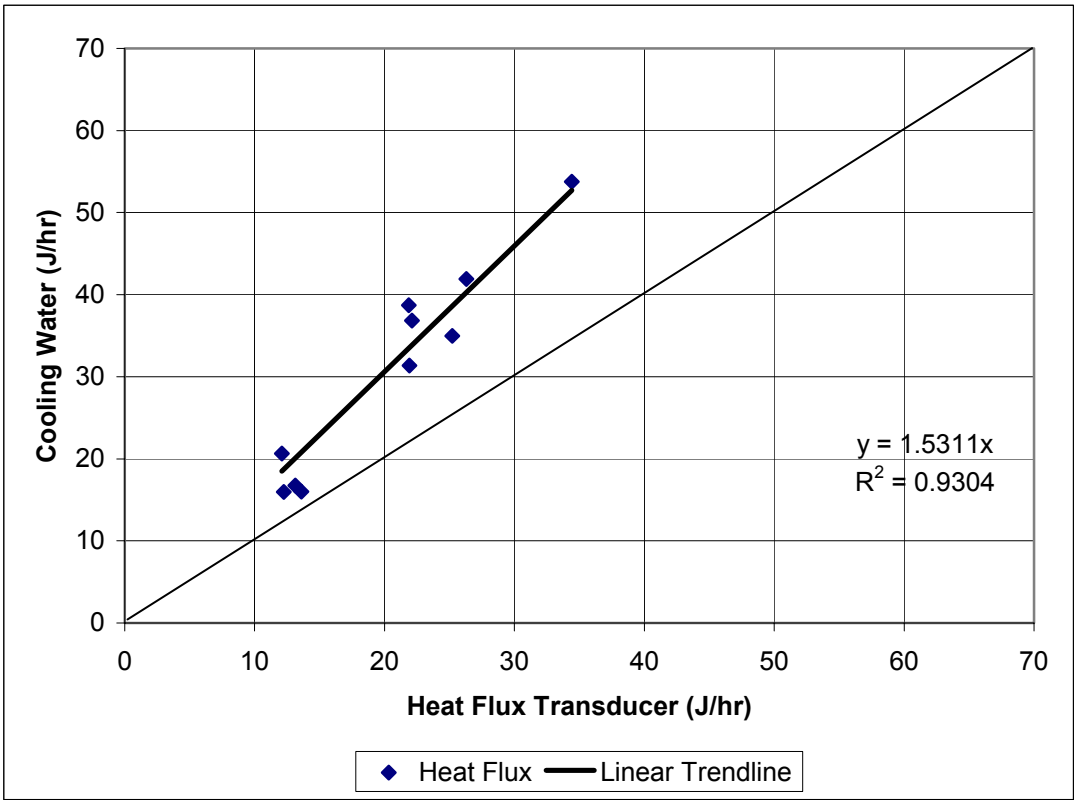

Figure 3.12: Cooling Water vs Heat Flux Transducer Energy Transfer Rate

As can be seen from Figure 3.12 the two energy calculations did not match. This was most likely due to the fact that measurements were only made out to 127 mm from the center of the plate and the plate was 356 mm square. The current method did not account for the heat flux beyond 127 mm from the center of the plate.

Two adjustments were made to the heat flux method in order to account for the heat transfer beyond 127mm. The square plate was treated as if it were a circle of similar surface area with radius r. This transformation is shown in equation 3.7.

$$r_{circ} = \sqrt{\frac{A_{sq}}{\pi}} \qquad \text{Equ (3.7)}$$

Second an estimation of the heat flux beyond 127 mm was made. For purposes of this analysis two different assumptions about the heat flux beyond 5 inches were made, the first was that the heat flux was constant beyond 127 mm and the second was that the heat flux decreased at a constant rate beyond 127 mm and was equal to the rate the heat flux decreased between the last two measurements, at 114 and 127 mm. Figure 3.13 is a graph of heat flux verses radial position and shows the difference between these two methods.

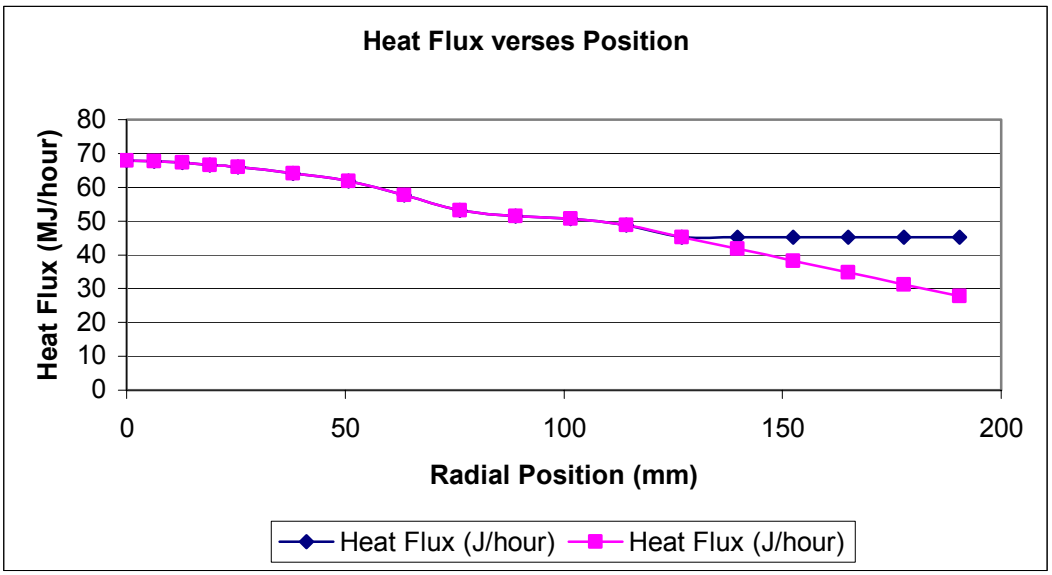

Figure 3.13: Plot of Heat Flux Methods

Finally, figures 3.14 and 3.15 are graphs of cooling water energy measured verses heat flux meter energy measured using the constant heat flux and linear decreasing heat flux methods, a linear regression best fit line is shown for both cases.

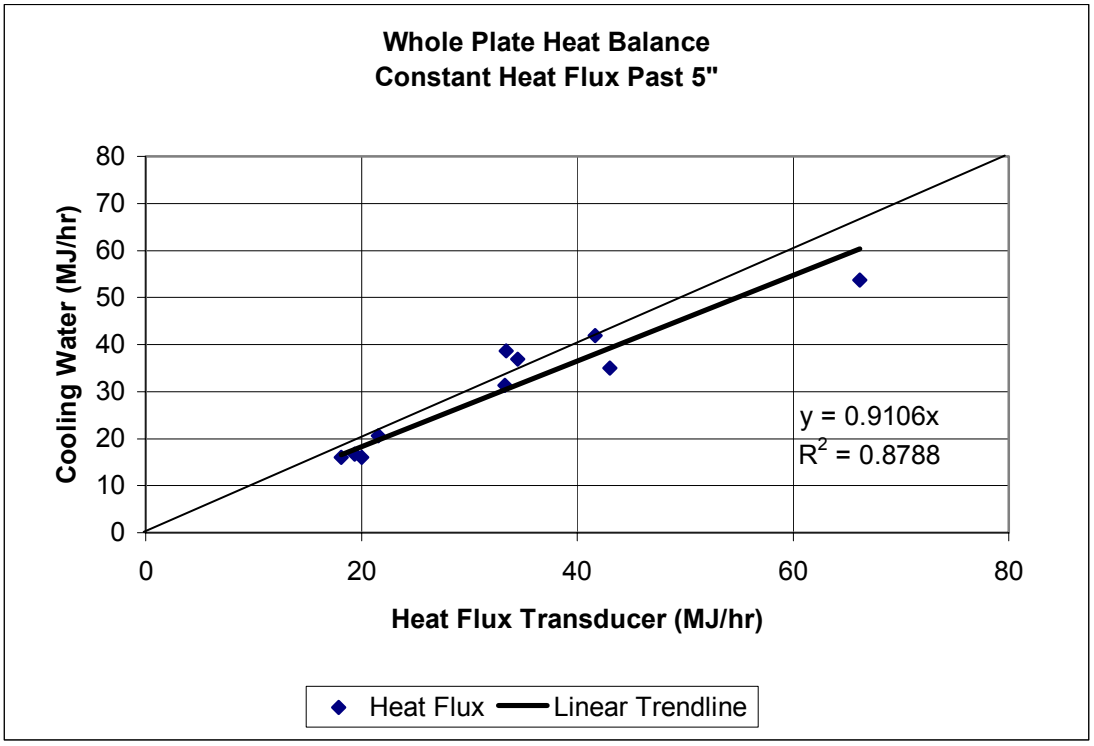

Figure 3.14: Plot of Heat Flux Plate Energy Balance, Constant Heat Flux

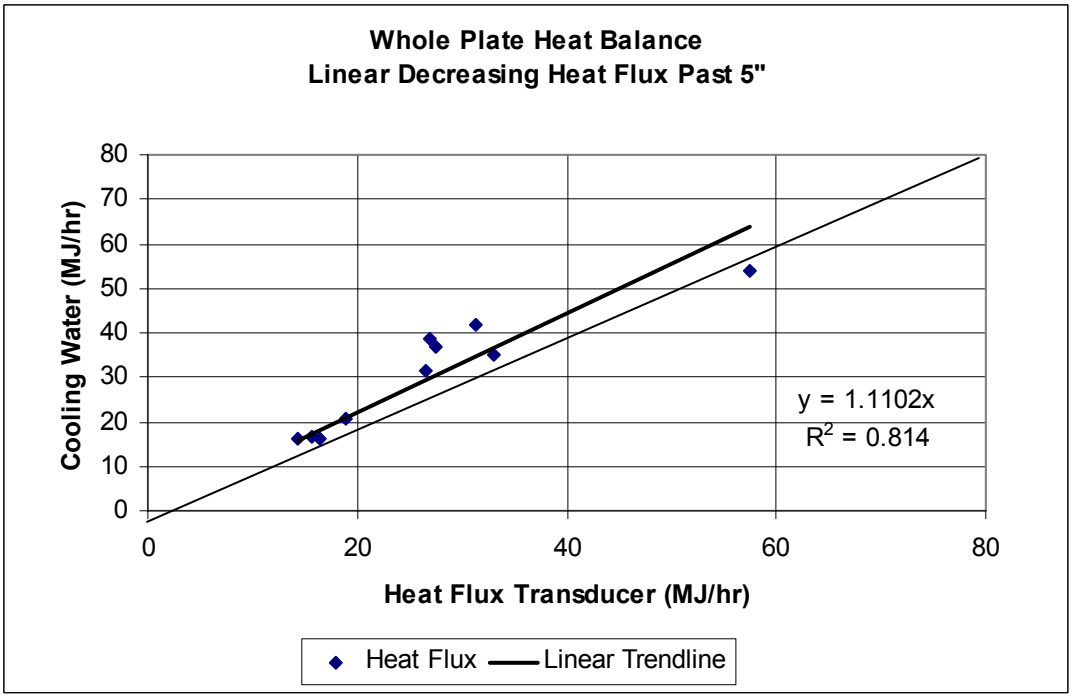

Figure 3.15: Plot of Heat Flux Plate Energy Balance, Linear Decreasing Heat Flux

Linear regression analysis showed that the linearly decreasing and the constant heat flux assumption had a better than 12% agreement between the cooling water and heat flux meter methods of calculating the energy transferred to the heat flux plate and had R^2 values above 0.80 showing an acceptable relationship. The two methods also bracket the expected one-to-one relationship between the heat flux meter and cooling water balance methods, meaning that the best relationship lies somewhere in between the two methods evaluated here.

From the analysis of the heat flux meter it has been shown that the meter and positioning system could accurately measure the heat flux as a function of position and the results could be used to calculate an area average of thermal energy transferred to the plate's surface.

Pulse Combustor and Support Equipment

In the background section of the paper, the general operation of a pulse combustor was described. This section will describe the specific equipment used in the trials conducted for this report, their function and their purpose.

The air used in the combustion process was supplied from the ambient air in the laboratory. An Ametek model DR S13 pump, driven by a Delta model VFD-B variable frequency drive, pumped the air through a 101 mm diameter pipe and into the combustion system. There was a pressure tap located just beyond the pump outlet that was connected to a manometer used to measure the static pressure of the pump. Pump curves used to correlate the static pressure of the pump and the frequency of the drive to the pump's air flow rate are shown in Appendix B. It has been found through previous

testing that an average of 25% of the volumetric flow from the pump leaked out of the system prior to entering the combustion chamber though imperfect seals in the piping. This loss was accounted for in all data reported.

From the pump the air flowed into the headbox located above the combustion and mixing chambers. The headbox had a volume significantly larger than the combustion chamber and was used to dampen any pressure pulses that move upstream from the combustion chamber. The headbox also acted as a buffer in the opposite direction by helping to insulate the combustion chamber from any intermittent changes in air pressure supplied by the pump.

From the headbox the air then flowed into the mixing chamber where propane, supplied from a tank, was also feed into the chamber. From the mixing chamber the air and gas mixture then passed through the aerodynamic valve and into the water jacketed combustion chamber. The combustion chamber used in these experiments was 152 mm in diameter and 241 mm long. The combustion chamber was immersed in a water bath that cools the chamber walls.

From the combustion chamber the flue gases exited the combustion camber though a hole in the bottom of the chamber. If steady impingement tests were conducted there was no tailpipe connected to the chamber. If pulsed impingement tests were run then the flue gas flowed though a 406 mm long tailpipe before impinging on the drying surface.

Figure 3.16 is a photograph showing the pulse combustor setup in the laboratory using a 25 mm tail pipe, three other tailpipes were used to divert excess flow away from the impingement surface.

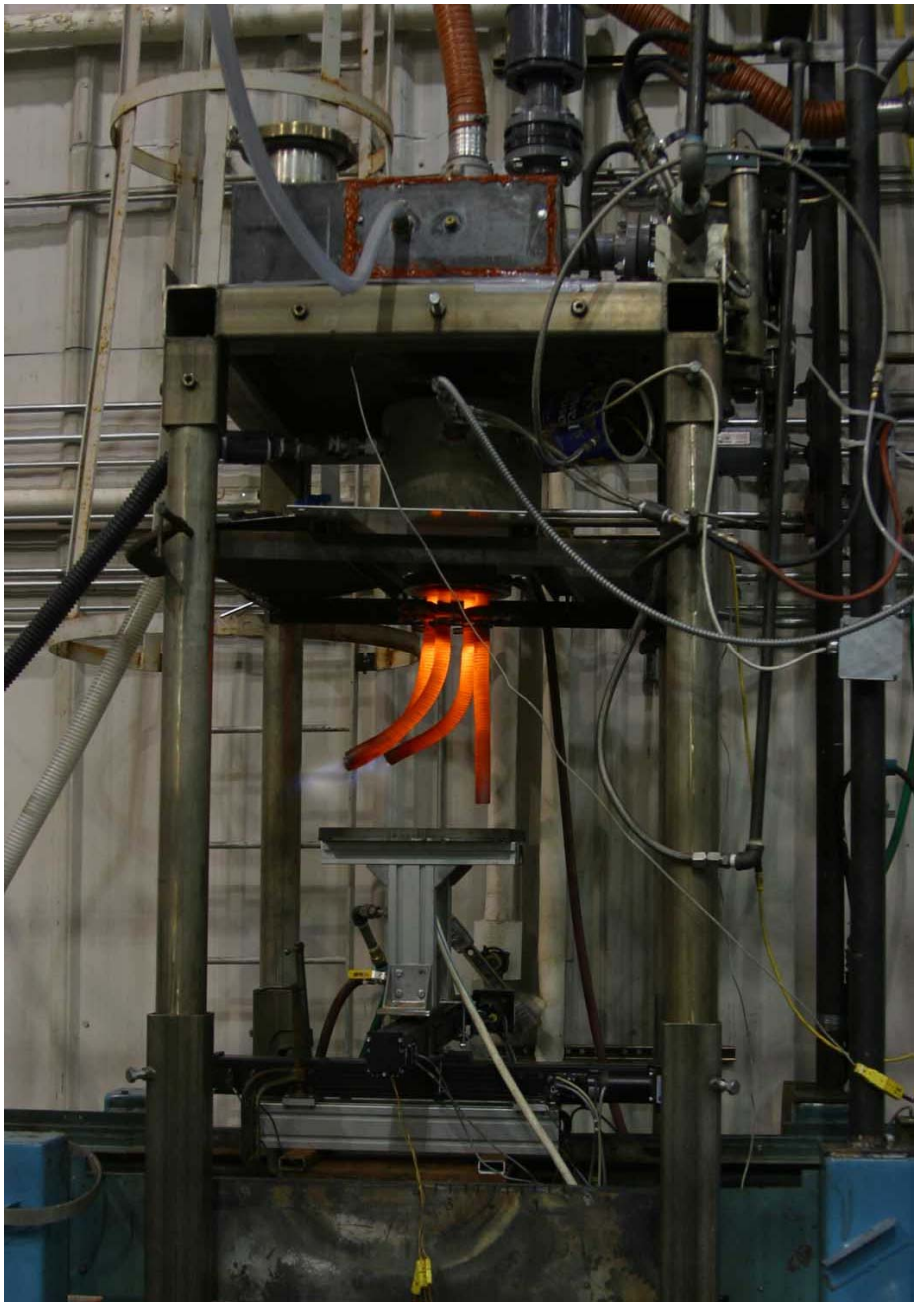

Figure 3.16: Pulse Combustor Lab Setup

The data acquisition system used in the testing was a DaqBook 216 system connected to a laptop computer for recording data. Data sheets on the data acquisition system are located in Appendix D.

Figure 3.17 is a drawing of the pulse combustor without a confinement roof and cooling plate with the important geometric properties and measurement locations labeled. Figure 3.18 is a drawing of the pulse combustor with confinement roof. Finally figure 3.19 is a top down view showing approximate location of heat flux measurements relative to the heat flux plate and tail pipe centerline.

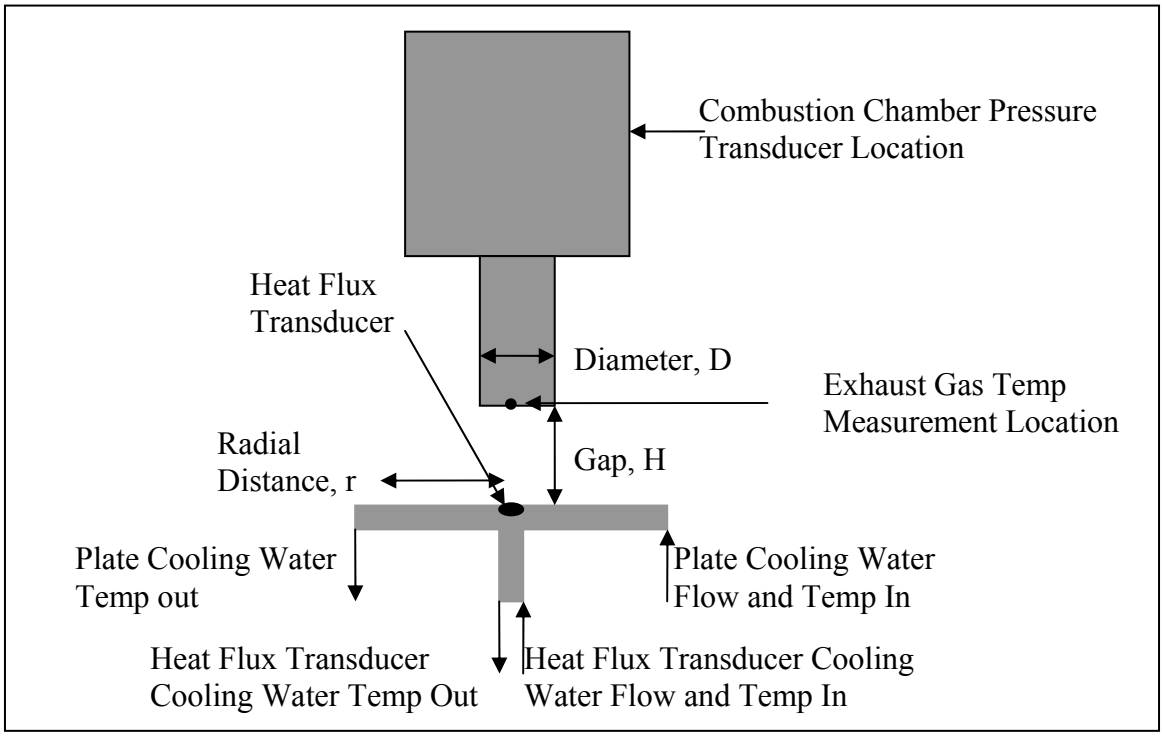

Figure 3.17: Labeled, Unconfined Pulse Combustor Setup

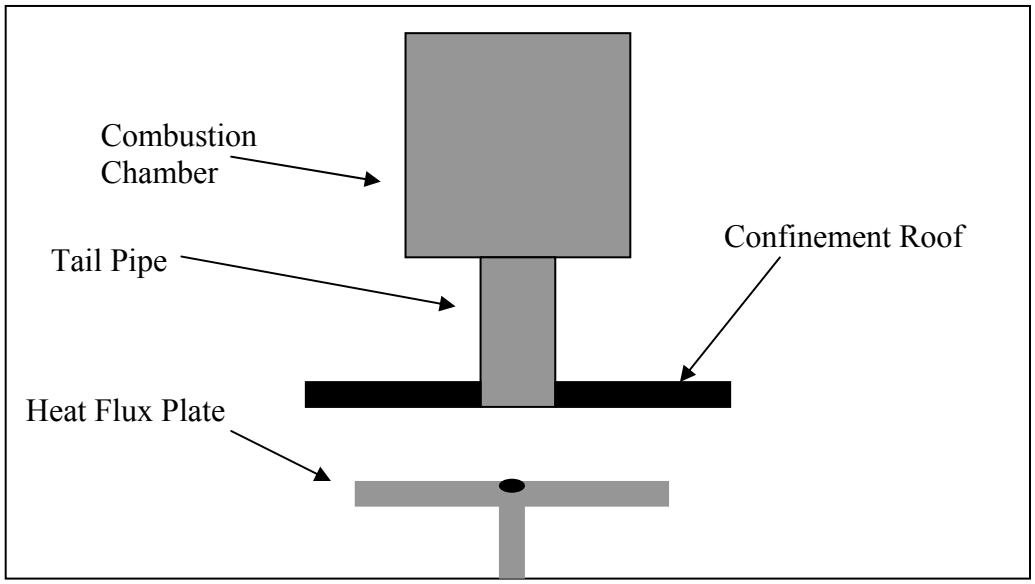

Figure 3.18: Confined Pulse Combustor Setup

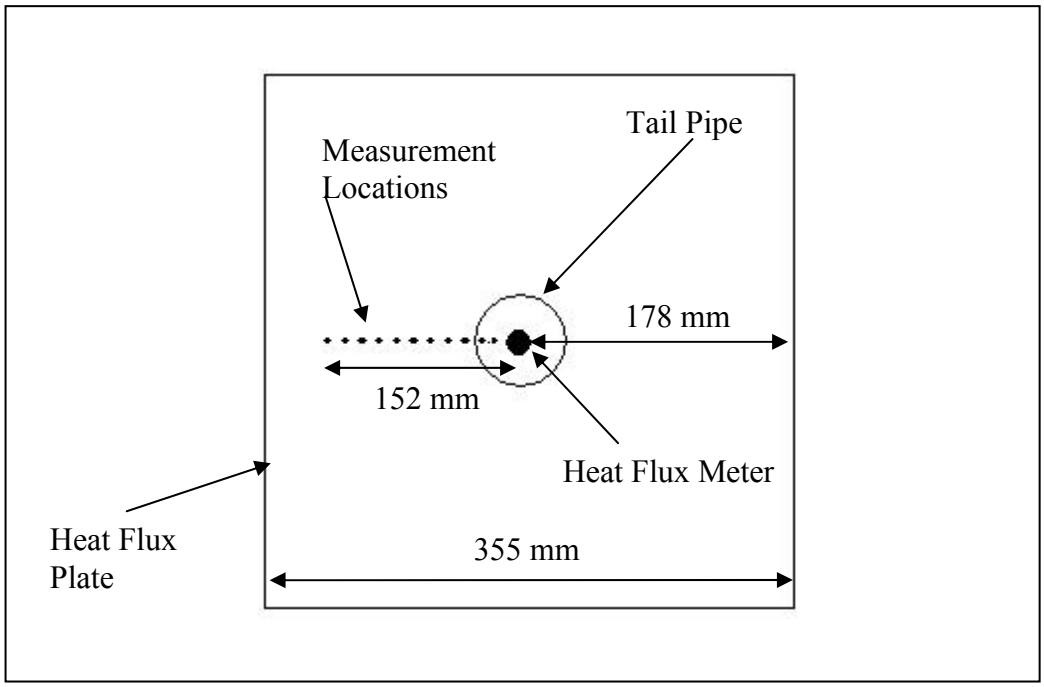

Figure 3.19: Heat Flux Measurement Locations

Pulse Combustor Startup Procedure

Depending on the type of test conducted different procedures were followed. For this reason the procedure is split into three parts, the procedure for general startup of the pulse combustor, a heat flux plate measurement procedure and a drying procedure.

1. If the test called for using a confinement roof the roof was installed between 6 and 13 mm above the end of the tail pipe.
2. Setup of either the heat flux plate or the drying experiment was done, as explained below.
3. The pulse combustor gas and air flow were set to the low setting and ignition was started.
4. After 10 seconds of forced ignition the combustor would ignite on its own and forced ignition was halted.
5. Gas and air flow rates were slowly increased until the desired flow rates were met. Care was taken to increase both air and gas flow rates at a similar rate. If one flow rate was raised much higher than the other combustion would cease and the ignition process would be restarted from the beginning.
6. When the desired flow rates were met the combustor was run for approximately 5 minutes in order for it to reach steady state. The system was determined to be at steady state when the exit gas temperature was steady.
7. The tailpipe exit temperature, fuel flow rate, air pump drive frequency and air pressure were all recorded.

8. If pulsed impingement tests were being conducted the data acquisition system recorded 1 second of combustion chamber pressure pulse data at a rate of 4,000 samples per second.
9. The system was now at steady state and the pulse combustor operating conditions have been recorded and heat flux or drying procedure would begin.

Heat Flux Plate Procedure

1. The positioning system and heat flux plate were assembled under the pulse combustor tail pipe exit. The proper impingement gap was set, taking into account a 6 mm tail pipe length growth due to thermal expansion if a 406 mm pipe was used
2. The plate was aligned with the heat flux meter centered under the tail pipe.
3. Cooling water to the heat flux plate was turned on and the flow rate was set to 8.8 liters per minute. The Spiral channel could handle much more flow than the heat flux cooling channel. For this reason the spiral channel took the balance of the flow from the water line, this was usually 12-14 liters per minute.
4. At this point the pulse combustor startup procedure was followed as described above.
5. Once steady state was reached the heat flux plate to tail pipe alignment was double checked and adjustments were made as necessary to center the heat flux meter under the tail pipe. This was done due to occasional uneven thermal expansion of the tail pipe.

6. Data acquisition was begun, recording plate temperature, heat flux and plate position at a rate of 10 samples per second.
7. The heat flux position program was run. The plate was positioned at radial distances of 0.00, 0.006, 0.013, 0.019, 0.025, 0.028, 0.051, 0.064, 0.076, 0.089, 0.102, 0.114 and 0.127 m. At each radial distance the plate stopped for 12 seconds to allow the heat flux meter to reach a steady value.

After the raw data had been recorded some manipulation was done before it was ready for analysis. There tended to be a lot of noise in the position and heat flux data. In order to reduce the effect of noise on the data a moving average of 10 data points, or one second of data, was used. Figure 3.20 shows an example of the raw data recorded during a heat flux measurement experiment data after the moving average was applied.

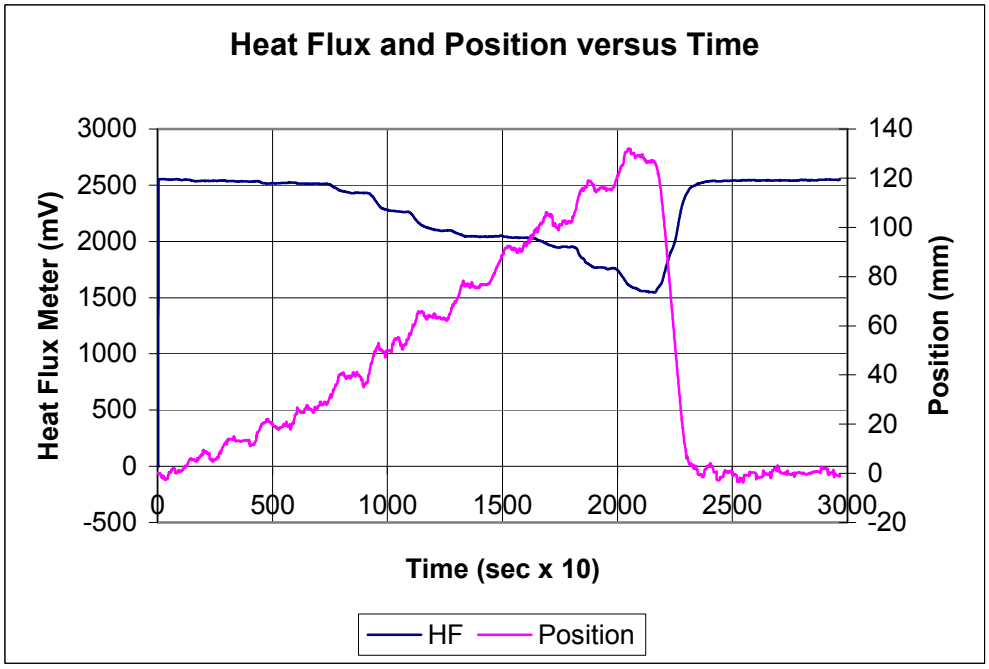

Figure 3.20: Plot of Moving Average Heat Flux Data

Using the moving average data the heat flux and temperature data were picked out for each position. These were the heat flux data used for analysis. The coefficient of heat transfer from each point was found from the temperature difference between the plate surface and the jet exit and from the heat flux measured at the point. Figure 3.21 shows an example of the discrete heat flux, plate surface temperature and coefficient of heat transfer data for each position after it had been retrieved from the moving average data.

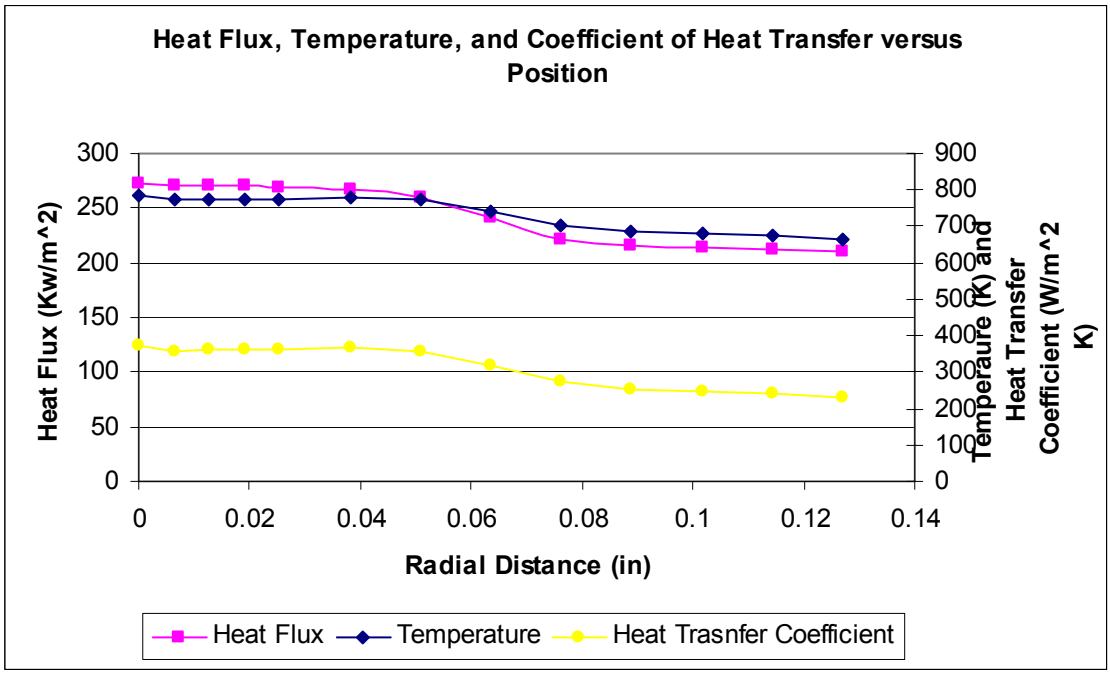

Figure 3.21: Plot of Discrete Heat Flux Data

Heat flux data were taken for the conditions show below in Table 3.3 and 3.4. Figure 3.3 contains the tests conditions for confined experiments where a roof was placed near the tail pipe exit in order to reduce ambient air entrainment. Figure 3.4 contains the test conditions for unconfined experiments without a confinement roof.

Table 3.3: Heat Flux Test Conditions, Confined

Confined				
Diameter	Tail Pipe Length	Impingement Gap	Pulsed or Steady	Number of Flows
71	406	25	Pulsed	2
71	406	71	Pulsed	2
71	406	142	Pulsed	2
25	406	25	Pulsed	4
25	406	71	Pulsed	4
71	76	25	Steady	2
71	76	71	Steady	2
71	76	142	Steady	2
25	0	25	Steady	2
25	0	71	Steady	2

Table 3.4: Heat Flux Test Conditions, Unconfined

Unconfined				
Diameter	Tail Pipe Length	Impingement Gap	Pulsed or Steady	Number of Flows
71	406	25	Pulsed	4
71	406	71	Pulsed	4
71	406	142	Pulsed	4
25	406	25	Pulsed	4
25	406	51	Pulsed	4
25	406	71	Pulsed	4
71	76	71	Steady	4
71	76	25	Steady	4

Drying Procedure

1. The samples to be dried were prepared. They were 127 mm diameter blotter paper wet to a solids content of nominally 30% by mass.
2. The sample tray height was set for the desired impingement gap.
3. The pulse combustor was started as detailed above and reached steady state.
4. The plastic bags were weighed
5. The plastic bag with a wet sample inside was weighed

6. The sample was removed from the plastic bag and quickly paced on the sample tray. The sample tray was placed under the tail pipe exit jet and held there for a time between 1 and 8 seconds and then removed from under the jet. The time under the jet was recorded.
7. The dried sample was quickly placed back into the pre-weighed bag and reweighed.

A plot of mass loss verses time was made and the drying rate was the slope of the line formed from the data in the graph. Figure 3.22 is an example plot from a drying experiment.

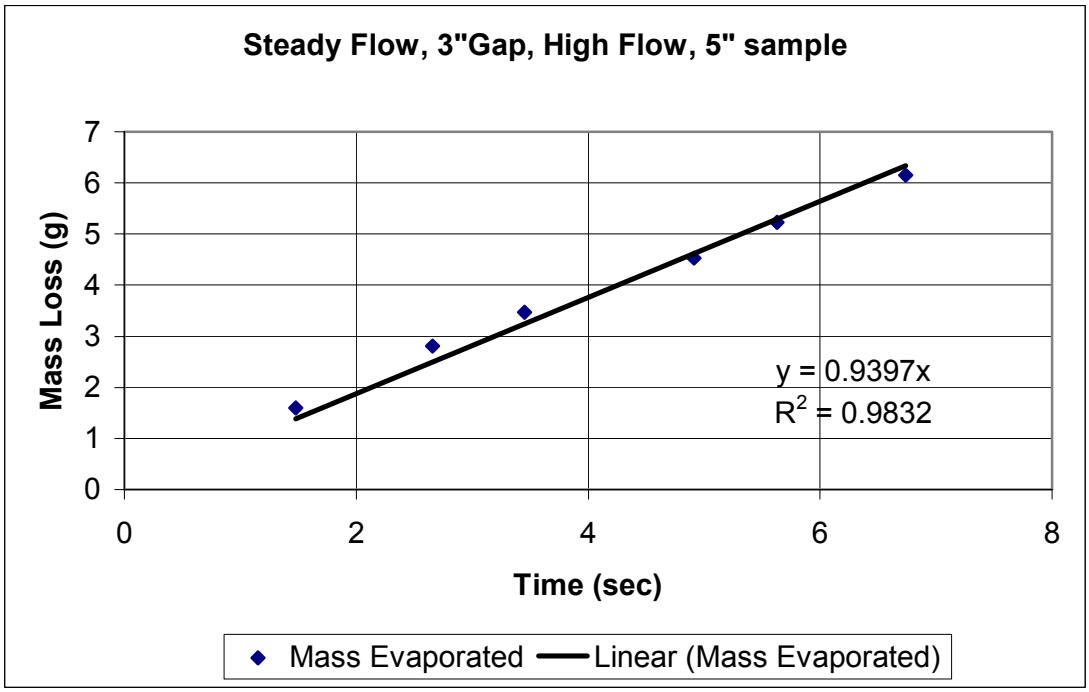

Figure 3.22: Example of Impingement Drying Data

CHAPTER 4

RESULTS AND DISCUSSION

In these experiments the control variables studied included the impingement gap height, tail pipe diameter, flow rate and tail pipe temperature for pulse combustion and steady impingement. It was commonly accepted in the impingement literature that the relationship between tail pipe diameter and impingement gap had a significant impact on the heat transfer rate, with increasing gap to diameter ratios came decreasing heat flux. Also, with increasing flow rates an increase in heat transfer rates was observed.

For comparisons made in this study all control variables were kept as equal was possible when comparing pulse and steady impingement. This was to make comparisons of heat flux as easy and straight forward as possible. If changes in many variables were made a straight heat flux comparison would not be valid. Also due to the project's overall aim of commercialization, a study of the actual energy transferred to the heat transfer plate was valuable. A complete fundamental analysis of pulse and steady impingement was unnecessary in this project and beyond the scope of the present investigation.

Unconfined Pulsed vs Steady

Figures 4.1 and 4.2 shows the heat flux as a function of position using a 71 mm diameter exit at 25 mm and 71 mm impingement gaps respectively. The test conditions for each trial along with the total heat transferred into the impingement surface are displayed in Table 4.1.

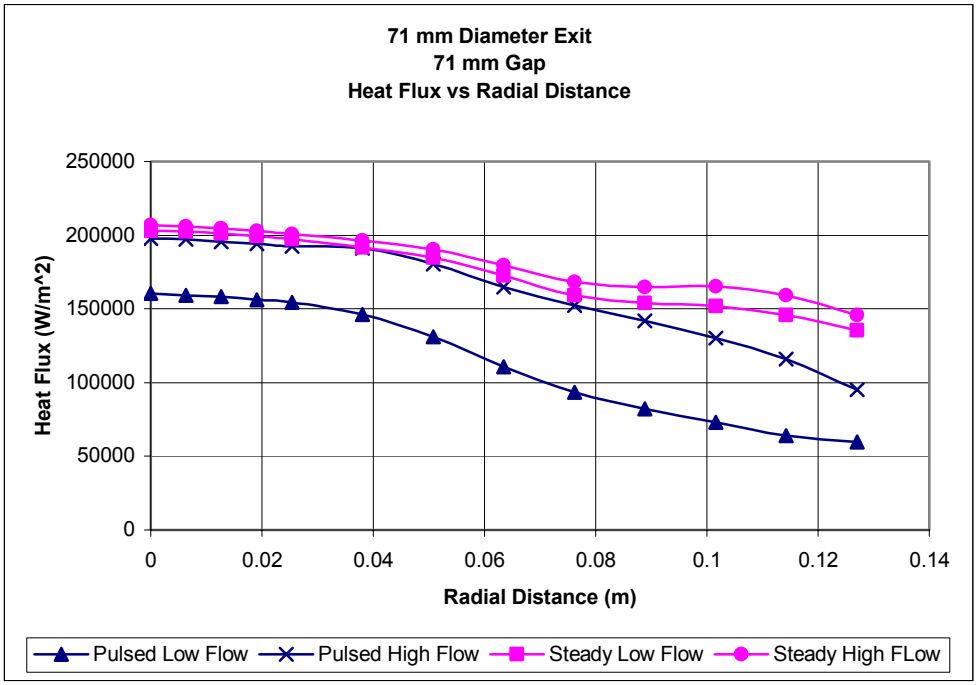

Figure 4.1: Heat Flux for Pulsed and Steady Impingement 71 mm Exit and Gap

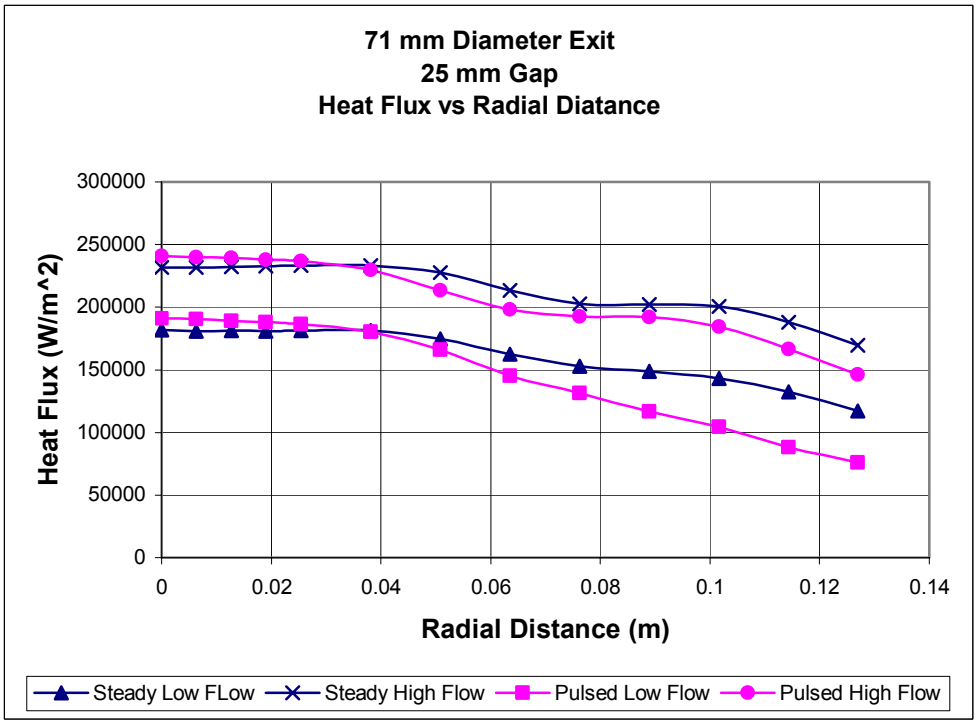

Figure 4.2: Heat Flux for Pulsed and Steady Impingement 71 mm Exit and 25 mm Gap

Table 4.1 Unconfined Impingement Test Conditions and Total Heat Transfer Rate

Run #	Pulsed or Steady	Exit Dia (mm)	Gap (mm)	Total Gas and Air Flow Rate (L/min)	Gas Exit Temp K	Total Heat Transfer Rate Watts
5	Pulsed	71	71	2124	1361	4667
33	Steady	71	71	2124	1373	8134
8	Pulsed	71	71	3908	1446	7288
36	Steady	71	71	4021	1433	8627
9	Pulsed	71	25	2124	1394	6217
29	Steady	71	25	2067	1356	7601
12	Pulsed	71	25	3908	1521	9598
32	Steady	71	25	4021	1430	10305

In the 25mm gap trials of Figure 4.2 the pulsed combustion heat flux tests showed a 12% to 16% increase in maximum heat flux over steady impingement. This was in contrast to the 71mm gap trials depicted in Figure 4.1 where the pulse combustion heat transfer was 12% to 15% less effective than similar conditions run using steady impingement. Under all conditions the total energy transferred into the impingement surface was lower for pulsed impingement than for steady impingement by 6% to 20%.

The inconsistency in these results and the reason the steady impingement was higher than the pulsed may have been caused by three sources. The first was uneven jet temperature during the steady impingement trials. The temperature of the exit gas varied by as much as 140 K across the exit diameter. Blue flame could be seen from one half the tail pipe while no flame could be seen from the other half. Figure 4.3 is an illustrated example of the problem. The dark area is representative of where flame was observed exiting the tail pipe. Because of the uneven exit gas temperature heat flux measurements could have been effected by small variations in alignment between the heat flux transducer and exit tail pipe and also from movement of the flame between trials. No

immediate cause or solution could be found for this problem. It would appear that the problem was due to an unknown issue in the gas flow inside the combustion chamber which resulted in uneven combustion and/or mixing.

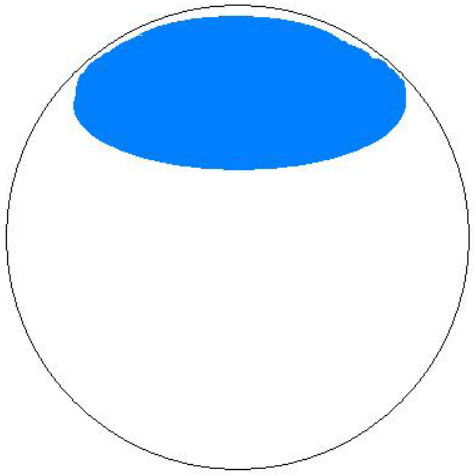

Figure 4.3: Tail Pipe Flame Characteristics

Uneven combustion of the steady impingement gas was not the only shortfall in the testing conducted without a confinement roof. Figure 4.4 depicts 4 trials, which used similar gas and air flow. There were three pulsed trials with 25 mm, 71 mm and 140 mm gaps and two steady trials using a 25 mm and 70 mm gap.

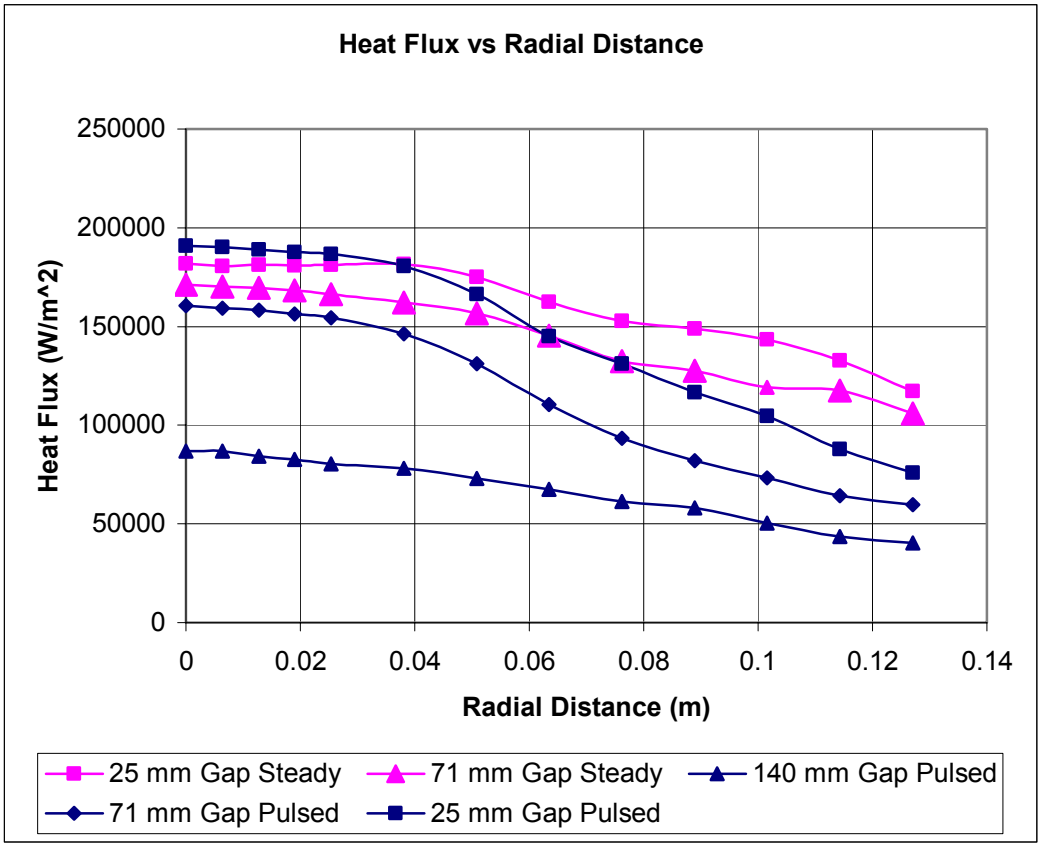

Figure 4.4: Rapid Falloff of Heat Flux

From inspection of the graph in Figure 4.4 it can be seen that the pulsed impingement heat flux dropped off at a rate significantly higher than the steady impingement configuration. Due to pulsed combustion's tendency to entrain ambient air around the jet it would be logical that the falloff was due to poor confinement around the tail pipe exit. Because this project was focused on industrial applications where there would be many other tailpipes in an array and entrainment of significantly cooler gas would be unlikely further tests were done with a more confined area around the tail pipe. For this reason testing was repeated using a confinement roof nearly flush with the tail pipe exit and an extension added to the heat flux impingement plate to further confine the

gas flow impinging on the plate. It was important to note that in previous studies a falloff in heat transfer using pulse combustion was observed (Eibeck, 1991), but the falloff was generally with an impingement gap greater than 4 nozzle diameters, whereas in this trial the falloff was observed at 2 nozzle diameters.

Finally, the Amplitude Ratio for all pulse impingement trials using the 71 mm had the relatively low amplitude ratio of 2.5. Increasing this ratio, which is a function of the physical characteristics of the pulse combustor, should increase the heat transfer rates.

Confined Pulsed Vs Steady

The results of the confined test were mixed just as were the results from the unconfined tests. Whether pulsed combustion or steady impingement showed higher heat transfer rates seemed to depend more on the diameter of the tail pipe than any other factor.

Figures 4.5, 4.6 and 4.7 depict the heat flux as a function of radial distance for a 71mm tail pipe at 25mm, 51mm and 71mm respectively. Table 4.2 contains the basic operating conditions for the 71mm trials along with the total heat transferred into the impingement surface.

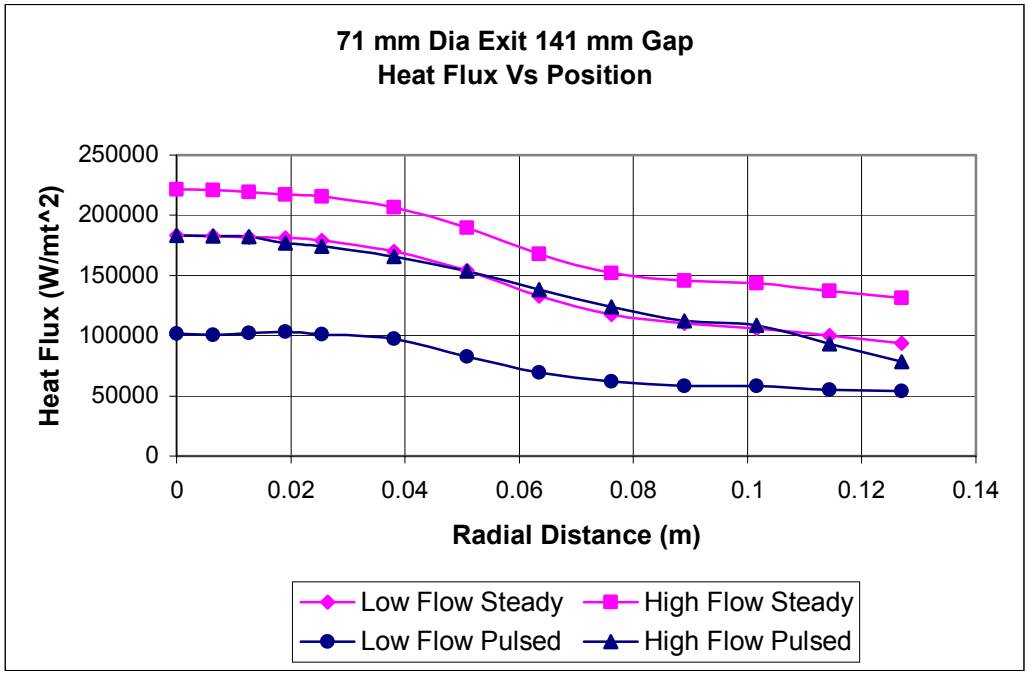

Figure 4.5: Heat Flux for Confined Impingement, 71 mm Exit and 141 mm Gap

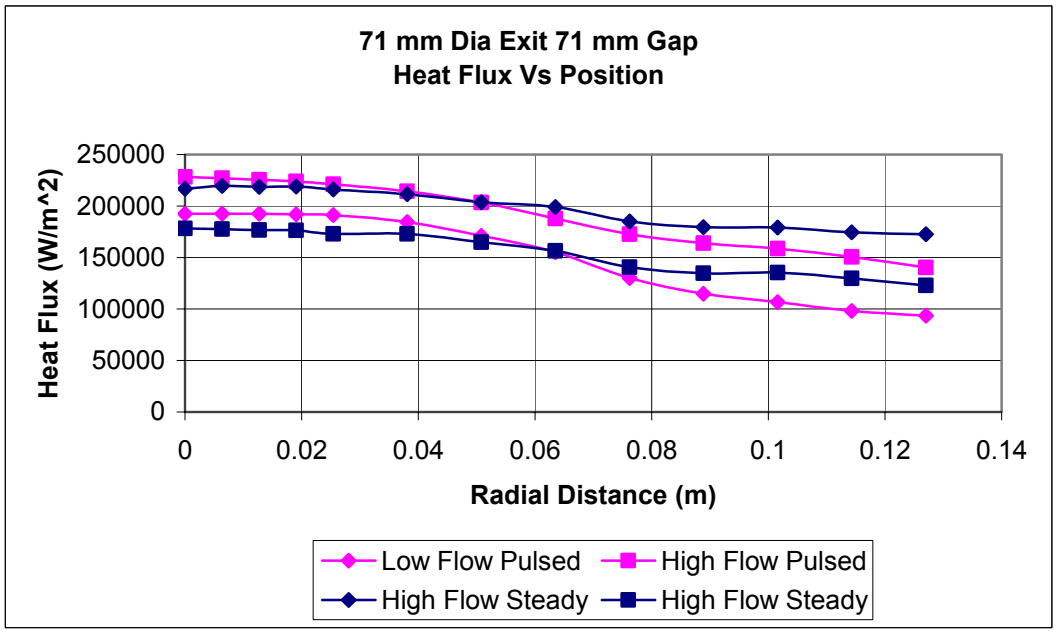

Figure 4.6: Heat Flux for Confined Impingement, 71 mm Exit and 71 mm Gap

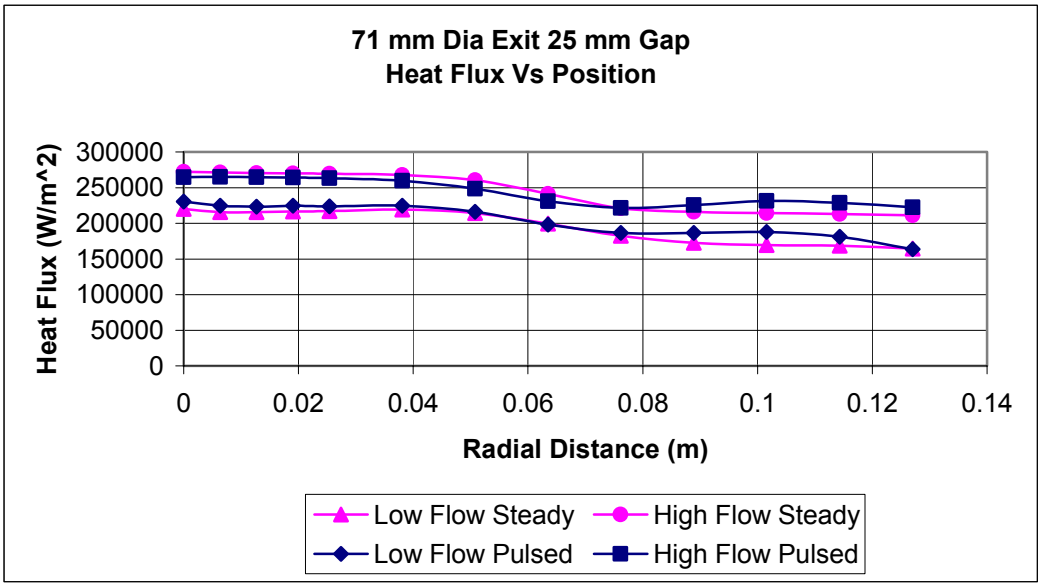

Figure 4.7: Heat Flux for Confined Impingement, 71 mm Exit and 71 mm Gap

Table 4.2: Test Conditions for Confined Impingement 71 mm Exit

Exit Dia (mm)	Gap (mm)	Pulsed or Steady	Gas Flow Rate (L/min)	Gas Exit Temp K
71	141	Pulsed	2124	1378
71	141	Steady	2124	1366
71	141	Pulsed	3823	1436
71	141	Steady	3823	1436
71	71	Pulsed	2124	1350
71	71	Steady	2124	1386
71	71	Pulsed	3717	1431
71	71	Steady	3504	1411
71	25	Pulsed	2124	1376
71	25	Steady	2124	1373
71	25	Pulsed	3823	1433
71	25	Steady	3717	1431

Beginning our analysis with the 71 mm tail pipe with 25 mm gap of Figure 4.7 it was observed that pulse combustion impingement shows a higher maximum heat flux at the lower flow rate and a lower heat flux at the higher flow rate. The differences between the two are small enough, in all cases less than 5%, that there was no meaningful

difference between the pulsed and the steady impingement cases with the 25 mm gap. The overall heat transferred into the plate was between 2% and 5% higher for pulse combustion impingement. This was an improvement over the unconfined tests where the steady impingement energy transfer was higher than the pulsed impingement.

The data from the 71 mm gap of Figure 4.6 shows that the maximum pulse combustion impingement heat flux was higher, although not significantly, than the steady impingement in all cases. In the lower flow trial, pulse combustion increased the maximum heat flux by 3% while at the higher flow pulse combustion improves heat flux by 5%. As with the 25 mm gap the differences between the pulse combustion and steady impingement were relatively small; for all practical purposes they were identical. In contrast to the 25 mm gap test where heat transfer was improved using pulse combustion, in the 71 mm gap test pulse combustion produced lower overall heat transfer by 8-11%.

The 140 mm gap test results in Figure 4.5 show that the steady impingement heat flux was significantly higher than the pulsed impingement flux. At the lower flow rate the steady impingement heat flux was nearly double the pulsed combustion value.

The results were more promising for the 25 mm tail pipe. The improvements in heat transfer for pulsed impingement are 50% to 80% higher than steady impingement under similar conditions. Table 4.3 shows the conditions run and the percent increase in heat transfer for pulsed combustion over steady impingement. The trials used for comparison in table 4.3 were chosen because the energy, based on enthalpy, in the steady jet was higher than the energy in the pulsed jet while the heat transfer in the pulsed jet was higher than in the steady jet.

Table 4.3: Test Conditions for Confined Impingement 25 mm Exit

Diameter	Gap	Steady or Pulsed	Flow Rate	Jet Temp	Enthalpy of Jet	Energy of Jet	Energy Transfer to Plate	% Increase in Energy Transfer to Plate
mm	mm		l/min	K	KJ/kg	KJ/s	J/s	
25	71	Steady	195	1322	1420	34795	3570	
25	71	Pulsed	180	1244	1327	31901	5227	46.40
25	71	Steady	105	1239	1325	18659	2303	
25	71	Pulsed	74	1329	1430	13136	4095	77.80
25	25	Steady	195	1272	1360	34639	4051	
25	25	Pulsed	176	1239	1325	31316	7242	78.70
25	25	Steady	105	1239	1325	18659	3508	
25	25	Pulsed	71	1344	1445	12721	5521	57.30

Figures 4.8 and 4.9 are plots of heat flux versus positions for the same trials as shown in Table 4.3.

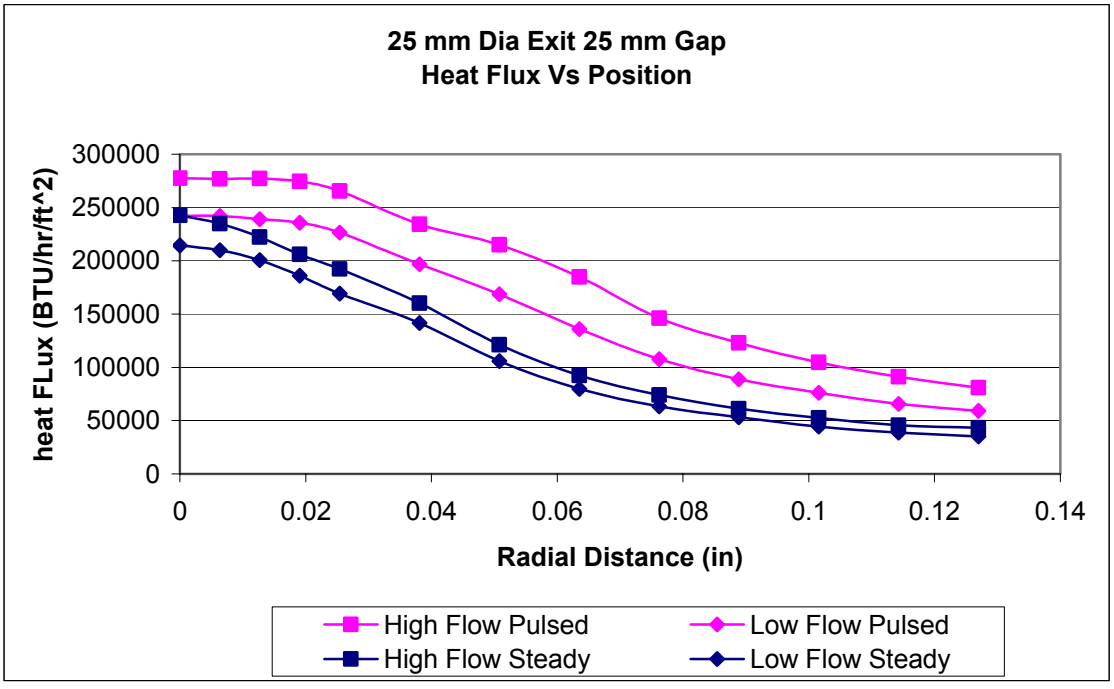

Figure 4.8: Heat Flux for Confined Impingement, 25 mm Exit 25 mm Gap

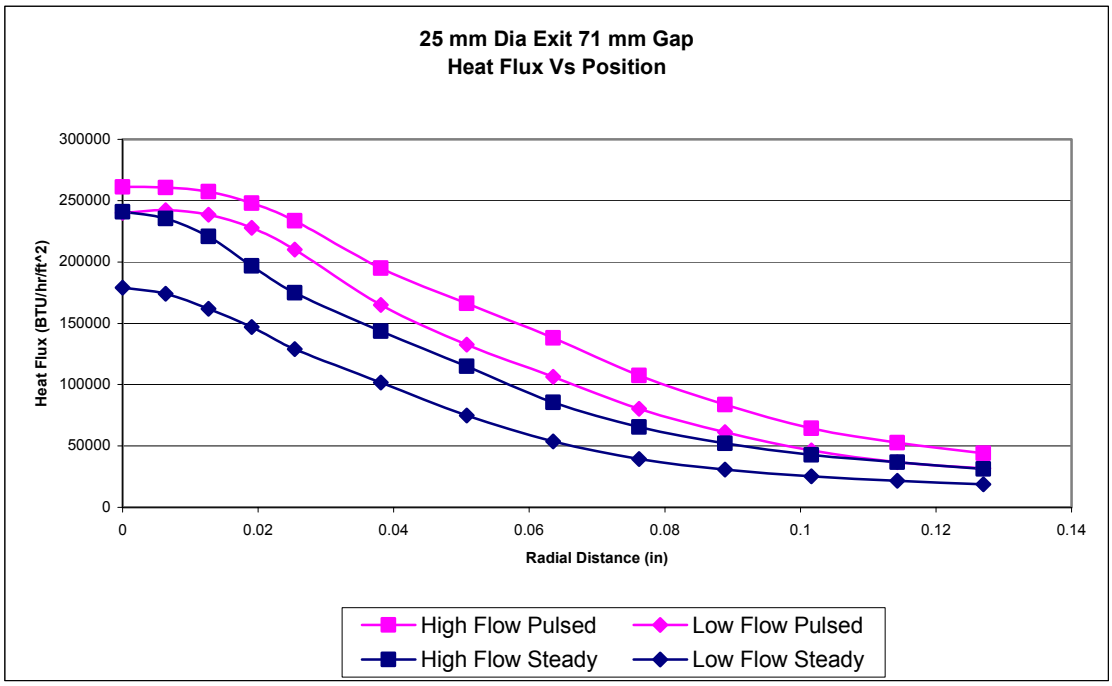

Figure 4.9: Heat Flux for Confined Impingement, 25 mm Exit 71 mm Gap

Amplitude ratios for the 25 mm tail pipe were between 0.45 and 0.56 for all cases. This means that there was little chance for reverse flow with the 25 mm tail pipe and also that much greater heat transfer rates are possible if the pulse combustor produced higher amplitude ratios.

Confined vs Unconfined

The confinement roof was added to answer the question, 'How much improvement, if any, is made when a confinement roof is installed?' The answer is that there was improvement and in many cases the improvement was significant. Table 4.4 shows the operating conditions that were compared. Although more data were recorded this table represents the cases were the confined experiment most closely matches the

unconfined experiment. Cases where the flow or temperature of the confined experiment differs significantly from the unconfined experiment were not evaluated.

The average rate of heat transfer into the plate and the percent increase when using the confinement roof are also included in Table 4.4 shown below.

Table 4.4: Impact of Confinement Roof on Heat Flux

Pulsed or Steady	Diameter	Gap	Flow	Temp	Confined Heat Transfer	Unconfined Heat Transfer	Percent Increase
	(mm)	(mm)	(L/min)	(K)	(W)	(W)	
Steady	71	25	2067	1355		94	
Steady	71	25	2124	1373	115		22
Steady	71	25	4021	1430		128	
Steady	71	25	3710	1431	143		12
Steady	71	71	2124	1344		83	
Steady	71	71	2124	1350	90		9
Steady	71	71	3483	1405		100	
Steady	71	71	3540	1411	117		17
Pulsed	71	25	2124	1394		77	
Pulsed	71	25	2124	1376	121		58
Pulsed	71	25	3908	1521		119	
Pulsed	71	25	3823	1433	147		23
Pulsed	71	71	3908	1444		90	
Pulsed	71	71	3823	1428	108		20
Pulsed	71	142	2152	1383		36	
Pulsed	71	142	2152	1378	41		14
Pulsed	71	142	3993	1437		61	
Pulsed	71	142	3823	1436	75		22
Pulsed	25	25	3908	1379		68	
Pulsed	25	25	3908	1383	113		67

Depending on the experimental setup increases in heat transfer as high as 67% could be made when using the confinement roof.

Drying Analysis

The improvements seen using the confinement roof were discovered prior to any drying experiments. For these reasons all drying experiments were conducted with the confinement roof. A majority of the drying experiments were conducted by Dr. Isaak Rudman, Dr. Timothy Patterson and Mr. James Loughran, with initial data processing done by Mr. Loughran. The following drying analysis is a combination of work done by Mr. Loughran and original analysis by the author. All drying analysis was conducted with a 127 mm diameter paper sample.

The 71 mm and 25 mm tail pipe trial conditions and results are shown in Table 4.5. The results from the trials show that pulse combustion impingement drying resulted in a 20% to 35% increase in drying rates over steady impingement at similar conditions.

Table 4.5: Impingement Drying Tests for 71 mm Exit

Diameter	Gap	pulsed/steady		Exit temp	Evap rate	% Increase In Evaportaion Rate
mm	mm		L/min	k	Kg/m^2	
71	25	steady	2888	1377	2.0	
71	25	pulsed	2917	1383	2.6	29
71	25	steady	4332	1405	2.4	
71	25	pulsed	4219	1413	3.3	35
71	71	steady	2888	1378	1.7	
71	71	pulsed	2917	1374	2.1	25
71	71	steady	5777	1417	2.4	
71	71	pulsed	5493	1439	3.0	22
25	25	steady	991	1316	1.6	
25	25	pulsed	991	1321	2.0	24
25	25	steady	1303	1303	2.1	
25	25	pulsed	1218	1289	2.7	30
25	71	steady	991	1316	1.2	
25	71	pulsed	963	1322	1.6	26
25	71	steady	1303	1283	1.7	
25	71	pulsed	1218	1322	2.0	21

Heat Flux as a Predictor of Drying Improvement

With the limited data gathered thus far no relationship between the heat flux plate measurements and the drying measurements could be found that would work for both the 25mm and 71mm diameter tail pipes. In fact the 71mm heat flux measurements showed a decrease in heat transfer using pulsed combustion when compared to steady combustion while the drying tests showed a 20% to 30% increase. The reasons behind this conflicting data were not entirely understood. It may have been due to differences in the impingement surfaces and the non-uniform exit temperature in the steady impingement configuration.

With the 25mm tail pipe the results were different. The heat flux measurements and the drying measurements both showed improvement for pulse combustion impingement over steady impingement. The heat flux test showed a 50-80% increase in heat flux while the drying test showed a 21-30% increase in drying rates. When similar conditions were compared between the drying tests and the heat flux tests we see that the heat flux plate over predicted the increase in drying rates by about 150%.

It is important to note that when discussing comparisons between the drying tests and heat flux tests that the impingement surface was not the same in both tests. In the heat flux measurements the jet impinged onto a 355mm square plate, while with the drying tests the jet impinged onto a 127mm diameter paper surface. The difference in the size of the impingement surface may have had a significant impact on the ability to compare the two types of tests.

Comparison with Literature

In Martin's (1977) study of steady impingement he recommended using Equation 4.1 to compute average Nusslet numbers for an unconfined single round nozzle.

$$\frac{\overline{Nu}}{\mathrm{Pr}^{0.42}} = G\left(\frac{r}{D}, \frac{H}{D}\right) F_1(\mathrm{Re}) \qquad \text{Eq (4.1)}$$

$$F_1 = 2\,\mathrm{Re}^{0.5}\left(1 + 0.005\,\mathrm{Re}^{0.55}\right)^{0.5} \qquad \text{Eq (4.2)}$$

$$G = \frac{D}{r}\frac{1 - 1.1D/r}{1 + 0.1(H/D - 6)D/r} \qquad \text{Eq (4.3)}$$

The results from the Martin (1977) prediction were compared with the experimental data in the current study. To compute the average Nusselt number from experimental data Incropera and Dewitt suggested equation 4.4

$$\overline{Nu} = \frac{\bar{h}D}{k} \qquad \text{Eq (4.4)}$$

Use of equation 4.1 requires an r/D of 2.5 or greater. In the present study measurements were only conducted out to an r/D of 1.8. Fortunately several sources including Martin (1977), Eibeck (1991) and Hwang (2001) show that the Nusselt number, which is a function of heat transfer coefficient, is approximately linear for the rage of r/D from 1.75 to 3. For this reason the slope of the heat transfer coefficient calculated for the last two data points in the experimental data was extrapolated out to an r/D of 2.8. The overall average heat transfer coefficient, calculated after extrapolation, is used in equation 4.4.

Due to the high temperature of the exit gas the temperature data from the thermocouple was corrected for radiation according to Equation 4.5 from Shaddix (1998).

$$T_{gas} = T_{TC} + \sigma \varepsilon d\left(T_{TC}^4 - T_{Env}^4\right)/\left(k \cdot Nu\right) \qquad \text{Eq (4.5)}$$

Tavener (2002) recommends that ideally the thermocouple would be inserted 15 diameters into the medium to be measured for a conduction related error less than 0.001%. In this study the thermocouple was inserted approximately 10 diameters directly into the jet and was also exposed to the exit gases out to approximately 30 diameters. For these reasons conduction through the thermocouple was considered negligible.

The results of this comparison are shown in Figure 4.10. The experimental average Nusselt number was within 15 to 25% of Martin's predicted average Nusselt number. The agreement between the experimental results and Martin's equation showed that the heat flux plate is reasonably accurate measurement of the heat flux from the impinging jet. Results may be improved if the heat flux was measured past 5 inches, rather than extrapolating the data.

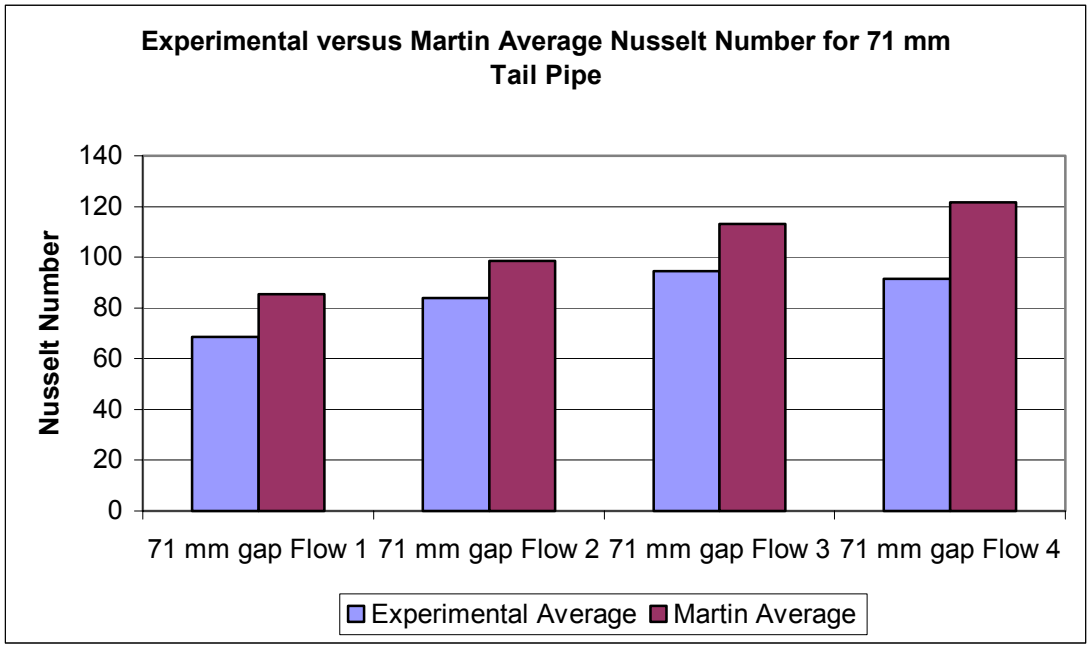

Figure 4.10: Experimental versus Martin (1977) Average Nusselt Number

In the Eibeck (1991) study the coefficient of convective heat transfer was plotted against non dimensional radial distance from the tail pipe centerline. In computing the coefficient of heat transfer Eibeck (1991) used equation 4.6, where T_{aw} is the adiabatic wall temperature. In the present study all calculations used equation 4.7 and rather than T_{aw} as a reference temperature, this study has used T_{jet} .

$$q'' = h(T_s - T_{aw}) \qquad \text{Eq (4.6)}$$

$$q'' = h(T_s - T_{Jet}) \qquad \text{Eq (4.7)}$$

The adiabatic wall temperature is the temperature at which no conduction or radiation heat transfer occurs. This value was not measured in the present study. But Eibeck (1991) did publish complete data for the heat transfer coefficient at the tail pipe centerline. Using only tail pipe centerline data and correcting for differing Reynolds numbers using Equation 4.7, a comparison was made between Eibeck's (1991) experimental data and data collected in the present study. Table 4.6 shows the results of this analysis. The column representing the present study shows calculated Nusselt numbers while the column representing the Eibeck (1991) data shows Nusselt numbers that were corrected for Reynolds number effects.

Table 4.6: Nusselt Numbers at Tail Pipe Centerline

	Current Study	Eibeck (1991)
Reynolds Number	Nusselt Number	Nusselt Number
12400	86	267
13800	104	286
16700	140	324
21400	156	380

The results show that Eibeck's (1991) data had Nusselt numbers 2 to 3 times higher than the results from the current study. After correcting for Reynolds number the only significant difference in operating conditions between the two studies was the amplitude ratio. The pulse combustor with 71 mm tail pipe in the current study produced an amplitude ratio of 2.4-2.5 while the Eibeck (1991) pulse combustor's amplitude ratio was 6. As noted in the paper by Hanby (1969), the amplitude ratio has a significant effect on the heat transfer coefficient when studying heat transfer to the wall of the tail pipe. Preliminary numerical modeling by Mr. Liewkongsataporn suggested that this is also the case for pulsed impingement heat transfer. The increases in heat transfer due to increases in the amplitude ratio predicted by both Hanby (1969) and Liewkongsataporn are comparable to the increases seen between the current study and Eibeck (1991).

CHAPTER 5

CONCLUSIONS AND RECOMMENDED FUTURE WORK

A heat flux measuring impingement plate was designed and built that:

- Can be accurately positioned manually or in preprogrammed mode to measure heat flux as a function of position
- Correctly measured total heat transfer to within 10% of the energy gained by the cooling water
- Measured heat flux data accurate to within 5% of the literature's predicted value

The results from this study show that the heat flux measuring impingement plate is a validated tool that can be used in future experiments with proven accuracy.

An analysis of confined versus unconfined impingement shows that confined impingement heat transfer rates were higher than unconfined heat transfer rates. This discovery will help guide future PAD research at IPST towards concentrating on confined impingement.

Pulse combustion impingement versus steady impingement analysis shows that pulse combustion impingement produced greater heat transfer rates than steady impingement in many cases. The greatest improvement in heat transfer rates was observed when using the small tail pipe.

In comparing pulse combustion data with the literature significant room for improvement exists.

Recommended improvements to the pulse combustion equipment are as follows:

- The amplitude ratio of the pulse combustion system needs to be increased. The current setup does not fully realize the benefits of pulsed combustion due to its low amplitude ratio
- If research continues at the 71 mm diameter tail pipe then a more uniform exit gas temperature should be achieved. This may involve using a separate apparatus to heat the air evenly.
- A steady state apparatus that allows for the addition of longer tail pipes should be used to allow for fully developed flow at the tail pipe exit.

These improvements would allow for a better understanding of the improvements gained though the use pulse combustion. It also allows for a similar geometry between pulse and steady experiments.

The full potential of the heat flux plate has not yet been fully tested. When studies are preformed using an array of tail pipes the heat flux plate will be able to accurately measure the heat flux as a function of position in two dimensions. Although arrays of steady impinging nozzles have been studied, a search of the literature seems to imply that this type of investigation into pulse combustion heat transfer has yet to be carried out. The heat flux plate would provide valuable information in regards to arrays of tail pipes. One possible array type is shown in figure 5.1.

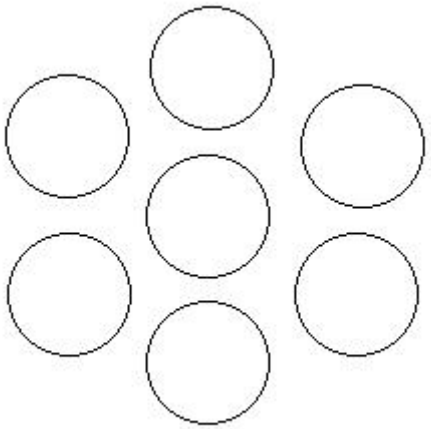

Figure 5.1: Hexagonal Nozzle Array

This hexagonal array was recommended due to the tight packing allowed by hexagonal arrays and because this array type is currently used in some steady impingement hoods. The array also allows for uniform distance between the centerline of each tail pipe and all those around it.

In studying drying rates and comparing them to the measured heat flux a loose correlation was found with the 25 mm tail pipe. The results were not entirely conclusive and further study is needed. Improvements to the drying tests are recommended. In tests for this study the blotter paper was placed on a wire screen. The screen may not provide the impingement surface necessary for the effects of pulsed combustion to be realized. It is further recommended that a solid impingement surface of similar size to that used in the heat flux measurements be used in the drying experiments.

APPENDIX A

Positioning System Operating Guide

Connecting the System

There are four subsystems that need to be properly connected for the positioning system and heat flux transducer to function.

1. Draw Wire Transducers: The draw wire transducers send position data to the data acquisition system. The connector for the transducers is the 9-pin serial type connector. One side of the connector attaches to the transducers while the other end connects to the power supply and the data acquisition system.
2. The Heat Flux Meter: The heat flux meter has three connectors, one for the k-type thermocouple and two for the heat flux transducer. All three connect to the data acquisition system. It is important that the heat flux transducer be connected with the correct polarity. Match the unmarked connectors to each other and the marked connectors to each other to insure proper polarity. The Data acquisition system has its internal gain set to 500 due to the small voltage created by the heat flux transducer. The current heat flux transducer has a calibration of 14.97 BTU/hr,ft^2,uV
3. Linear Actuator Limits: This is the large 25-pin serial type connector. This connects the actuator position limits to the motor controller. These must be connected for the position system to function.

4. Motor Power: These are two yellow connectors marked ‘1’ and ‘2’. These are connected differently depending on how the position system in orientated under the pulse combustor. When connected and before turning on the pulse combustor jog the position system to make sure the positioning system’s axis are connected correctly, if they are not the switch the motor power connectors with each other. The two possible connection schemes are 1->1, 2->2 and 1->2, 2->1.

Control Box

The control box controls the movement of the two actuators. A complete user’s manual with program guide is located at:
http://www2.idcmotion.com/Support/Manuals/S69R20.pdf

Power the controller up by plugging it in to 120v from any wall socket. After initializing there are two things you can do. Actually there are more than two but we only need to concern ourselves with two. The two functions are Jog and Run Program.

- Jogging the Motors: Jogging is used to properly set the initial position of the plate, usually with the heat flux meter directly under the tail pipe centerline. To jog the motors push the RUN button followed by the F2 (JOG) button. You are now able to move the motors along each axis by pressing the arrow keys. You can change between LO and HIGH settings by pressing the F1 and F2 keys. Be aware that the motors do not stop moving when you stop pressing the arrow keys,

the motors begin to decelerate when you stop pressing the arrow keys. It takes more than an inch to stop the motors in HIGH speed and about 0.2 inches in LO speed.

- Run a Program: To run a program press the RUN key followed by the F1 (PROG) Key. At this point you can use the arrow keys to scroll though all the programs or use the number pad to key in the desired program. Currently the only program used in the PAD project is program 10. After the desired program has been scrolled to or its number entered press the ENTER key. The program will now start immediately.

The current program and the one used in the project moves axis 1 and shown below:

```
AC4 VE4 DI.25 GO
TD12 DI.25 GO
TD12 DI.25 GO
TD12 DI.25 GO
TD12 DI.5 GO
TD12 DI.5 GO
TD12 DI.5 GO
TD12 DI.5 GO
TD12 DI.5 GO
```

TD12 DI.5 GO

TD12 DI.5 GO

TD12 DI.5 GO

TD12 DI.5 GO

The commands used in this program are as follows:

AC: Sets acceleration rate to 4 in/s^2

VE: Sets velocity to 4 in/s

TD: Time delay for 12 seconds

DI: Move 0.25, 0.5, or -5.0 inches

GO: Execute the command

APPENDIX B

Pump Curves

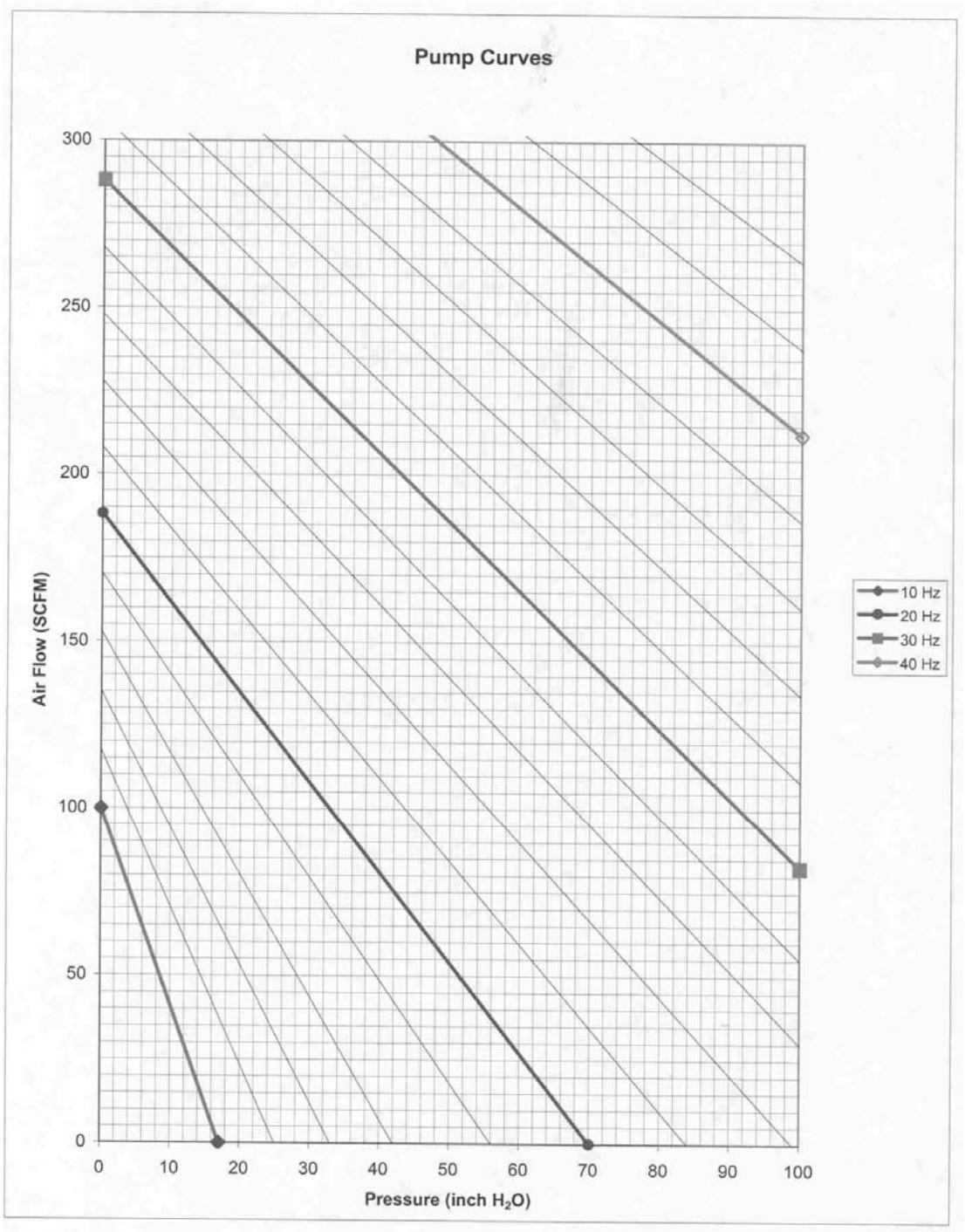

Figure B.1: Ametek Pump Curves

APPENDIX C

RAW DATA

Table C.1: Unconfined Test Conditions

				Gas Flow		Air Settings		Air Flow
Run	Pulsed or Steady	Tail Pipe Dia	Gap					
#		(mm)	(mm)	(L/m)	(scfm)	(Hz)	(in H2O)	(scfm)
1	Pulsed	71	142	80	2.9	14.4	10.4	76
2	Pulsed	71	142	100	3.8	17.9	15.3	93
3	Pulsed	71	142	120	4.4	21.2	21.1	111
4	Pulsed	71	142	140		26.5	30.7	141
5	Pulsed	71	71	80	2.85	14.4	9.6	75
6	Pulsed	71	71	100	3.7	17.7	14.9	93
7	Pulsed	71	71	120	4.4	21.3	21.3	112
8	Pulsed	71	71	140		26.5	30.6	138
9	Pulsed	71	25	80	2.85	14.4	9.3	75
10	Pulsed	71	25	100	3.8	17.7	14.6	93
11	Pulsed	71	25	120	4.4	21.3	20.3	112
12	Pulsed	71	25	140		26.6	29.3	138
13	Pulsed	25	25	80	2.9	14.2	10.5	70
14	Pulsed	25	25	100	3.75	17.8	16.6	90
15	Pulsed	25	25	120	4.4	21.2	22.6	112
16	Pulsed	25	25	140		26.5	31.6	138
17	Pulsed	25	51	80	2.95	14.4	10.9	71
18	Pulsed	25	51	100		17.9	16.7	90
19	Pulsed	25	51	120	4.35	21.2	22.4	112
20	Pulsed	25	51	140		26.6	31.8	138
21	Pulsed	25	76	80	2.9	14.5	10.7	71
22	Pulsed	25	76	100		17.8	16.5	90
23	Pulsed	25	76	120	4.4	21.2	22.3	112
24	Pulsed	25	76	140		26.7	31.9	138
25	Pulsed	25	25	80	2.8	14.3	10.4	71
26	Pulsed	25	25	100	3.75	17.8	16.4	90
27	Pulsed	25	25	120	4.4	21.3	22.6	112
28	Pulsed	25	25	140		26.7	32.1	138
29	Steady	71	25	72	2.42	12.6	5.6	73
30	Steady	71	25	95	3.5	17.8	11	97
31	Steady	71	25	103	3.75	21.4	15.5	116
32	Steady	71	25	115		24.4	20	142
33	Steady	71	71	88	2.9	12.7	5.4	75
33 b	Steady	71	71	72	2.6	12.7	5.4	75
34	Steady	71	71	93	3.4	17.8	10.3	100
35	Steady	71	71	103	3.9	21.4	14.5	123
36	Steady	71	71	114		24.5	18.8	142

Table C.1: Unconfined Test Condtions (Continued)

	Cooling Water					Exit Jet Temp	Pulse Pressure Data		
Run	Temp in	Temp Out Flux	Temp Out Coil	Flow Rate Flux	Flow Rate Coil		Mean	Peak to Peak	Freq
#	(deg F)	(deg F)	(deg F)	(lbs/min)	(lbs/min)	(deg F)	(psi)	(psi)	(Hz)
1	62.6	63.7	72.9	18.5	29.6	2029	0.83	61	159
2		64.2	75.9			2164	0.47	79	159
3		65	79.1			2140	1.87	98	158
4		65.6	81.3			2127	5.07	125	162
5		65.7	77			1990	0.19	59	154
6		66.7	81.1			2132	1.12	77	160
7		66.9	85.4			2125	12.45	97	159
8		67	87.4			2143	5.21	122	158
9	64.4	66.6	81.3	18.6	30.2	2050	0.85	43	149
10		67.5	87.1			2163	2.27	51	144
11		68.1	92.7			2231	4.98	61	140
12		69.4	99.8			2278	7.95	77	135
13	65.3	68.4	72	18.6	30.2	1807	4.28	36	108
14		69	74.3			1922	6.61	46	107
15		69.5	76.8			1938	9.04	58	104
16	65.7	70.7	80.3			2022	6.61	46	106
17	63.2	65.5	70.8	19	27.5	1833	5.03	35	104
18		66.7	73.5			2010	6.86	49	119
19		67.3	77.8			2040	9.74	52	103
20	63.4	68.2	80.7			2070	13.58	63	100
21	63.6	66.2	70.8	19	27.5	1782	3.61	36	110
22		67.5	74.2			1989	6.33	44	109
23		67.9	76.6			2007	9.31	56	110
24	64	68.6	80.5			2065	14.42	66	107
25	65.7	68.8	71.7	17.9	34.75	1851	3.79	34	105
26		69.4	74.2			1857	6.61	50	112
27		69.5	76.6			2010	10.23	53	108
28	66	70.9	80.2			2004	14.26	64	105
29	64.8	68	92.4	19.4	24.5	1982			
30		68.8	102.2			2085			
31		68.7	103			2066			
32		69.4	109.1			2115			
33	64.8	67.7	97	19.4	24.5	2012			
33 b		67.2	89.8			1960			
34		68	96.4			2060			
35		68.1	100.4			2070			
36		68.6	102.8			2120			

Table C.2: Unconfined Test Data

Radial Position	Data Point	Time	Time	CDPosition	MDPosition	Plate Temp	Heat Flux
(in)	#	(HR:MIN:SEC)	(ms)	(V)	(V)	(F)	(mV)
Unconfined Trial # 1							
0.00	190	+000:00:18	900	1.28	1.57	433	921
0.25	340	+000:00:33	900	1.32	1.61	433	918
0.50	490	+000:00:48	900	1.67	1.66	425	892
0.75	640	+000:01:03	900	1.29	1.69	421	877
1.00	790	+000:01:18	900	1.30	1.73	408	848
1.50	970	+000:01:36	900	1.27	1.82	396	829
2.00	1150	+000:01:54	900	1.31	1.90	372	773
2.50	1330	+000:02:12	900	1.29	1.98	352	716
3.00	1510	+000:02:30	900	1.27	2.08	327	648
3.50	1690	+000:02:43	900	1.29	2.28	314	618
4.00	1870	+000:03:06	900	1.29	2.24	279	533
4.50	2050	+000:03:24	900	1.27	2.32	254	462
5.00	2230	+000:03:42	900	1.30	2.31	237	423
Unconfined Trial # 2							
0.00	120	+000:00:11	700	1.22	1.54	556	1206
0.25	270	+000:00:26	700	1.27	1.58	559	1218
0.50	420	+000:00:41	700	1.23	1.61	547	1187
0.75	570	+000:00:56	700	1.30	1.67	530	1147
1.00	720	+000:01:11	700	1.28	1.70	521	1118
1.50	900	+000:01:29	700	1.28	1.79	511	1097
2.00	1080	+000:01:47	700	0.90	1.87	488	1043
2.50	1260	+000:02:05	700	1.29	1.95	460	981
3.00	1440	+000:02:23	700	1.27	2.03	417	879
3.50	1620	+000:02:41	700	1.29	2.17	379	792
4.00	1800	+000:02:59	700	1.29	2.20	335	675
4.50	1980	+000:03:17	700	1.32	2.28	299	584
5.00	2160	+000:03:35	700	1.23	2.36	273	514
Unconfined Trial # 3							
0.00	130	+000:00:12	700	1.30	1.56	666	1475
0.25	280	+000:00:27	700	1.29	1.57	661	1448
0.50	430	+000:00:42	700	1.29	1.64	656	1446
0.75	580	+000:00:57	700	1.29	1.68	655	1452
1.00	730	+000:01:12	700	1.47	1.71	632	1375
1.50	910	+000:01:30	700	1.29	1.80	612	1342
2.00	1090	+000:01:48	700	1.29	1.87	566	1216
2.50	1270	+000:02:06	700	1.29	1.96	527	1130
3.00	1450	+000:02:24	700	1.32	2.04	467	993
3.50	1630	+000:02:42	700	1.41	2.14	434	929
4.00	1810	+000:03:00	700	1.28	2.22	409	870
4.50	1990	+000:03:18	700	1.23	2.29	360	734
5.00	2170	+000:03:36	700	1.30	2.34	322	650
Unconfined Trial # 4							
0.00	140	+000:00:13	700	1.29	1.48	703	1572
0.25	290	+000:00:28	700	1.29	1.57	701	1567
0.50	440	+000:00:43	700	1.29	1.62	691	1544
0.75	590	+000:00:58	700	1.42	1.65	687	1534
1.00	740	+000:01:13	700	1.21	1.70	667	1483
1.50	920	+000:01:31	700	1.29	1.79	640	1409
2.00	1100	+000:01:49	700	1.29	1.86	596	1299
2.50	1280	+000:02:07	700	1.29	1.95	538	1166
3.00	1460	+000:02:25	700	1.29	2.03	500	1071
3.50	1640	+000:02:43	700	1.29	2.12	468	1005
4.00	1820	+000:03:01	700	1.29	2.20	434	924
4.50	2000	+000:03:19	700	1.19	2.28	396	834
5.00	2180	+000:03:37	700	1.30	2.37	340	680

Table C.2: Unconfined Test Data (Continued)

Radial Position	Data Point #	Time	Time	CDPosition	MDPosition	Plate Temp	Heat Flux
(in)		(HR:MIN:SEC)	(ms)	(V)	(V)	(F)	(mV)
Unconfined Trial # 5							
0.00	80	+000:00:07	700	1.32	1.30	748	1699
0.25	230	+000:00:22	700	1.32	1.34	744	1690
0.50	380	+000:00:37	700	1.33	1.39	738	1673
0.75	530	+000:00:52	700	1.32	1.42	733	1656
1.00	680	+000:01:07	700	1.32	1.46	722	1635
1.50	860	+000:01:25	700	1.31	1.51	689	1549
2.00	1040	+000:01:43	700	1.31	1.62	627	1386
2.50	1220	+000:02:01	700	1.32	1.71	540	1167
3.00	1400	+000:02:19	700	1.31	1.79	458	986
3.50	1580	+000:02:37	700	1.32	1.87	411	869
4.00	1760	+000:02:55	700	1.32	1.96	369	774
4.50	1940	+000:03:13	700	1.31	2.08	331	681
5.00	2120	+000:03:31	700	1.32	2.12	313	631
Unconfined Trial # 6							
0.00	110	+000:00:10	700	1.34	1.27	876	2023
0.25	260	+000:00:25	700	1.32	1.34	875	2026
0.50	410	+000:00:40	700	1.32	1.38	868	2004
0.75	560	+000:00:55	700	1.31	1.34	863	1988
1.00	710	+000:01:10	700	1.32	1.46	854	1972
1.50	890	+000:01:28	700	1.32	1.54	825	1893
2.00	1070	+000:01:46	700	1.31	1.62	766	1739
2.50	1250	+000:02:04	700	1.20	1.71	678	1512
3.00	1430	+000:02:22	700	1.42	1.79	589	1294
3.50	1610	+000:02:40	700	1.31	1.87	538	1178
4.00	1790	+000:02:58	700	1.32	1.96	486	1063
4.50	1970	+000:03:16	700	1.33	2.04	413	888
5.00	2150	+000:03:34	700	1.32	2.12	357	704
Unconfined Trial # 7							
0.00	200	+000:00:19	700	1.31	1.33	894	2054
0.25	350	+000:00:34	700	1.32	1.36	891	2051
0.50	500	+000:00:49	700	1.31	1.40	888	2048
0.75	650	+000:01:04	700	1.33	1.43	885	2046
1.00	800	+000:01:19	700	1.32	1.47	881	2032
1.50	980	+000:01:37	700	1.32	1.56	862	1959
2.00	1160	+000:01:55	700	1.33	1.65	815	1860
2.50	1340	+000:02:13	700	1.32	1.72	751	1703
3.00	1520	+000:02:31	700	1.33	1.81	682	1532
3.50	1700	+000:02:49	700	1.28	1.88	636	1411
4.00	1880	+000:03:07	700	1.29	1.97	582	1279
4.50	2060	+000:03:25	700	1.33	2.06	512	1100
5.00	2240	+000:03:43	700	1.32	2.16	454	986
Unconfined Trial # 8							
0.00	100	+000:00:09	700	1.31	1.29	911	2099
0.25	250	+000:00:24	700	1.32	1.33	911	2079
0.50	400	+000:00:39	700	1.32	1.38	906	2076
0.75	550	+000:00:54	700	1.32	1.41	901	2056
1.00	700	+000:01:09	700	1.32	1.45	893	2041
1.50	880	+000:01:27	700	1.33	1.53	876	2020
2.00	1060	+000:01:45	700	1.40	1.63	834	1913
2.50	1240	+000:02:03	700	1.32	1.70	769	1740
3.00	1420	+000:02:21	700	1.41	1.78	713	1611
3.50	1600	+000:02:39	700	1.32	1.87	671	1502
4.00	1780	+000:02:57	700	1.31	1.95	621	1382
4.50	1960	+000:03:15	700	1.32	2.04	562	1234
5.00	2140	+000:03:33	700	1.32	2.13	470	1008

Table C.2: Unconfined Test Data (Continued)

Radial Position	Data Point #	Time	Time	CDPosition	MDPosition	Plate Temp	Heat Flux
(in)		(HR:MIN:SEC)	(ms)	(V)	(V)	(F)	(mV)
Unconfined Trial # 9							
0.00	90	+000:00:08	700	1.41	1.13	875	2022
0.25	240	+000:00:23	700	1.42	1.16	872	2018
0.50	390	+000:00:38	700	1.41	1.20	866	2001
0.75	540	+000:00:53	700	1.43	1.25	862	1988
1.00	690	+000:01:08	700	1.42	1.28	856	1976
1.50	870	+000:01:26	700	1.41	1.37	833	1911
2.00	1050	+000:01:44	700	1.38	1.45	773	1759
2.50	1230	+000:02:02	700	1.41	1.49	693	1536
3.00	1410	+000:02:20	700	1.41	1.75	639	1393
3.50	1590	+000:02:38	700	1.41	1.70	577	1235
4.00	1770	+000:02:56	700	1.50	1.79	513	1106
4.50	1950	+000:03:14	700	1.41	1.86	434	934
5.00	2130	+000:03:32	700	1.41	1.93	381	806
Unconfined Trial # 10							
0.00	110	+000:00:10	700	1.51	1.14	973	2263
0.25	260	+000:00:25	700	1.41	1.17	969	2252
0.50	410	+000:00:40	700	1.41	1.21	967	2251
0.75	560	+000:00:55	700	1.41	1.25	965	2239
1.00	710	+000:01:10	700	1.41	1.29	962	2231
1.50	890	+000:01:28	700	1.41	1.30	940	2169
2.00	1070	+000:01:46	700	1.42	1.38	874	2008
2.50	1250	+000:02:04	700	1.41	1.54	794	1812
3.00	1430	+000:02:22	700	1.41	1.62	751	1708
3.50	1610	+000:02:40	700	1.38	1.70	713	1606
4.00	1790	+000:02:58	700	1.41	1.79	652	1462
4.50	1970	+000:03:16	700	1.41	1.88	568	1242
5.00	2150	+000:03:34	700	1.58	1.95	496	1077
Unconfined Trial # 11							
0.00	120	+000:00:11	700	1.42	1.14	1029	2399
0.25	270	+000:00:26	700	1.41	1.09	1026	2392
0.50	420	+000:00:41	700	1.43	1.22	1021	2380
0.75	570	+000:00:56	700	1.41	1.29	1018	2378
1.00	720	+000:01:11	700	1.41	1.30	1012	2370
1.50	900	+000:01:29	700	1.41	1.37	983	2285
2.00	1080	+000:01:47	700	1.56	1.46	917	2118
2.50	1260	+000:02:05	700	1.40	1.53	846	1954
3.00	1440	+000:02:23	700	1.41	1.63	817	1882
3.50	1620	+000:02:41	700	1.41	1.73	807	1858
4.00	1800	+000:02:59	700	1.25	1.82	765	1747
4.50	1980	+000:03:17	700	1.41	1.91	693	1564
5.00	2160	+000:03:35	700	1.41	2.45	615	1375
Unconfined Trial # 12							
0.00	120	+000:00:11	700	1.41	1.13	1089	2550
0.25	270	+000:00:26	700	1.42	1.16	1085	2544
0.50	420	+000:00:41	700	1.41	1.17	1080	2533
0.75	570	+000:00:56	700	1.44	1.25	1077	2519
1.00	720	+000:01:11	700	1.41	1.28	1071	2510
1.50	900	+000:01:29	700	1.41	1.37	1042	2431
2.00	1080	+000:01:47	700	1.41	1.20	976	2259
2.50	1260	+000:02:05	700	1.41	1.53	905	2094
3.00	1440	+000:02:23	700	1.41	1.59	880	2039
3.50	1620	+000:02:41	700	1.41	1.74	878	2032
4.00	1800	+000:02:59	700	1.41	1.79	845	1953
4.50	1980	+000:03:17	700	1.41	1.86	781	1762
5.00	2160	+000:03:35	700	1.41	1.95	702	1547

Table C.2: Unconfined Test Data (Continued)

Radial Position	Data Point #	Time	Time	CDPositi	MDPositi	Plate Temp	Heat Flux
(in)		(HR:MIN:SEC)	(ms)	(V)	(V)	(F)	(mV)
Unconfined Trial # 13							
0.00	210	+000:00:20	700	1.48	0.79	983	2382
0.25	360	+000:00:35	700	1.48	0.79	969	2335
0.50	510	+000:00:50	700	1.44	0.87	915	2183
0.75	660	+000:01:05	700	1.47	0.90	824	1946
1.00	810	+000:01:20	700	1.47	0.94	727	1696
1.50	990	+000:01:38	700	1.47	1.02	594	1360
2.00	1170	+000:01:56	700	1.67	1.09	499	1115
2.50	1350	+000:02:14	700	1.48	1.19	393	841
3.00	1530	+000:02:32	700	1.48	1.28	311	618
3.50	1710	+000:02:50	700	1.49	1.35	256	479
4.00	1890	+000:03:08	700	1.49	1.45	218	383
4.50	2070	+000:03:26	700	1.48	1.52	192	316
5.00	2250	+000:03:44	700	1.47	1.60	173	264
Unconfined Trial # 14							
0.00	150	+000:00:14	700	1.48	0.79	1107	2687
0.25	300	+000:00:29	700	1.48	0.82	1084	2610
0.50	450	+000:00:44	700	1.48	0.85	1018	2445
0.75	600	+000:00:59	700	1.32	0.87	928	2225
1.00	750	+000:01:14	700	1.84	0.94	836	1990
1.50	930	+000:01:32	700	1.49	1.01	719	1682
2.00	1110	+000:01:50	700	1.49	1.09	615	1403
2.50	1290	+000:02:08	700	1.47	1.43	486	1067
3.00	1470	+000:02:26	700	1.49	1.28	382	808
3.50	1650	+000:02:44	700	1.48	1.37	309	613
4.00	1830	+000:03:02	700	1.48	1.44	256	480
4.50	2010	+000:03:20	700	1.48	1.47	222	390
5.00	2190	+000:03:38	700	1.47	1.57	199	330
Unconfined Trial # 15							
0.00	120	+000:00:11	700	1.47	0.76	1168	2857
0.25	270	+000:00:26	700	1.48	0.80	1141	2774
0.50	420	+000:00:41	700	1.48	0.83	1074	2609
0.75	570	+000:00:56	700	1.48	0.87	990	2409
1.00	720	+000:01:11	700	1.46	0.93	910	2210
1.50	900	+000:01:29	700	1.48	0.80	814	1932
2.00	1080	+000:01:47	700	1.48	1.09	701	1624
2.50	1260	+000:02:05	700	1.48	1.18	564	1267
3.00	1440	+000:02:23	700	1.48	1.26	448	979
3.50	1620	+000:02:41	700	1.48	1.38	360	750
4.00	1800	+000:02:59	700	1.47	1.68	299	593
4.50	1980	+000:03:17	700	1.41	1.52	255	478
5.00	2160	+000:03:35	700	1.48	1.59	224	392
Unconfined Trial # 16							
0.00	178	+000:00:17	500	1.48	0.76	1235	3045
0.25	328	+000:00:32	500	1.47	0.81	1225	2982
0.50	478	+000:00:47	500	1.46	0.85	1174	2829
0.75	628	+000:01:02	500	1.53	0.90	1106	2675
1.00	778	+000:01:17	500	1.38	0.93	1038	2522
1.50	958	+000:01:35	500	1.48	0.83	938	2258
2.00	1138	+000:01:53	500	1.52	1.09	830	1958
2.50	1318	+000:02:11	500	1.48	1.20	682	1567
3.00	1498	+000:02:29	500	1.48	1.25	537	1191
3.50	1678	+000:02:47	500	1.61	1.34	434	936
4.00	1858	+000:03:05	500	1.48	1.34	360	747
4.50	2038	+000:03:23	500	1.59	1.50	304	595
5.00	2218	+000:03:41	500	1.48	1.50	267	513

Table C.2: Unconfined Test Data (Continued)

Radial Position	Data Point #	Time	Time	CDPositi	MDPositi	Plate Temp	Heat Flux
(in)		(HR:MIN:SEC)	(ms)	(V)	(V)	(F)	(mV)
Unconfined Trial # 17							
0.00	118	+000:00:11	500	1.38	0.83	1049	2596
0.25	268	+000:00:26	500	1.37	0.74	1044	2548
0.50	418	+000:00:41	500	1.38	0.89	1006	2428
0.75	568	+000:00:56	500	1.38	0.94	921	2183
1.00	718	+000:01:11	500	1.41	0.98	822	1929
1.50	898	+000:01:29	500	1.38	1.02	687	1593
2.00	1078	+000:01:47	500	1.38	1.14	550	1239
2.50	1258	+000:02:05	500	1.38	1.24	412	900
3.00	1438	+000:02:23	500	1.38	1.33	319	706
3.50	1618	+000:02:41	500	1.39	1.41	256	521
4.00	1798	+000:02:59	500	1.38	1.49	215	423
4.50	1978	+000:03:17	500	1.38	2.02	188	350
5.00	2158	+000:03:35	500	1.38	1.65	171	295
Unconfined Trial # 18							
0.00	140	+000:00:13	700	1.38	0.85	1141	2775
0.25	290	+000:00:28	700	1.38	0.89	1139	2725
0.50	440	+000:00:43	700	1.38	0.93	1090	2576
0.75	590	+000:00:58	700	1.38	0.96	1007	2368
1.00	740	+000:01:13	700	1.31	0.99	912	2155
1.50	920	+000:01:31	700	1.38	1.08	789	1832
2.00	1100	+000:01:49	700	1.33	1.03	652	1472
2.50	1280	+000:02:07	700	1.38	1.13	491	1070
3.00	1460	+000:02:25	700	1.48	1.34	376	790
3.50	1640	+000:02:43	700	1.39	1.43	302	594
4.00	1820	+000:03:01	700	1.39	1.50	250	460
4.50	2000	+000:03:19	700	1.38	1.58	217	378
5.00	2180	+000:03:37	700	1.38	1.62	195	319
Unconfined Trial # 19							
0.00	140	+000:00:13	700	1.39	0.86	1173	2857
0.25	290	+000:00:28	700	1.38	0.90	1156	2779
0.50	440	+000:00:43	700	1.31	0.94	1103	2636
0.75	590	+000:00:58	700	1.38	1.06	1030	2474
1.00	740	+000:01:13	700	1.52	1.05	969	2338
1.50	920	+000:01:31	700	1.38	1.09	892	2119
2.00	1100	+000:01:49	700	1.40	1.19	762	1754
2.50	1280	+000:02:07	700	1.38	1.27	601	1349
3.00	1460	+000:02:25	700	1.36	1.35	473	1030
3.50	1640	+000:02:43	700	1.38	1.44	381	792
4.00	1820	+000:03:01	700	1.38	1.51	314	621
4.50	2000	+000:03:19	700	1.38	1.54	267	498
5.00	2180	+000:03:37	700	1.38	1.61	238	427
Unconfined Trial # 20							
0.00	124	+000:00:12	100	1.38	0.86	1247	3049
0.25	274	+000:00:27	100	1.38	0.91	1225	2959
0.50	424	+000:00:42	100	1.38	0.94	1169	2816
0.75	574	+000:00:57	100	1.39	0.97	1104	2669
1.00	724	+000:01:12	100	1.38	0.97	1048	2558
1.50	904	+000:01:30	100	1.38	1.11	981	2359
2.00	1084	+000:01:48	100	1.38	1.17	845	1995
2.50	1264	+000:02:06	100	1.30	1.26	665	1496
3.00	1444	+000:02:24	100	1.56	1.35	525	1137
3.50	1624	+000:02:42	100	1.39	1.41	426	918
4.00	1804	+000:03:00	100	1.38	1.62	356	736
4.50	1984	+000:03:18	100	1.38	1.62	305	604
5.00	2164	+000:03:36	100	1.41	1.62	272	522

Table C.2: Unconfined Test Data (Continued)

Radial Position	Data Point #	Time	Time	CDPositi	MDPositi	Plate Temp	Heat Flux
(in)		(HR:MIN:SEC)	(ms)	(V)	(V)	(F)	(mV)
Unconfined Trial # 21							
0.00	130	+000:00:12	700	1.41	0.79	1063	2525
0.25	280	+000:00:27	700	1.42	0.83	1071	2517
0.50	430	+000:00:42	700	1.42	0.86	1039	2416
0.75	580	+000:00:57	700	1.31	0.89	953	2212
1.00	730	+000:01:12	700	1.45	0.95	854	1988
1.50	910	+000:01:30	700	1.44	1.01	719	1621
2.00	1090	+000:01:48	700	1.42	1.14	574	1249
2.50	1270	+000:02:06	700	1.42	1.30	446	939
3.00	1450	+000:02:24	700	1.38	1.20	356	718
3.50	1630	+000:02:42	700	1.42	1.37	298	549
4.00	1810	+000:03:00	700	1.42	1.44	259	455
4.50	1990	+000:03:18	700	1.42	1.53	229	379
5.00	2170	+000:03:36	700	1.41	1.56	210	351
Unconfined Trial # 22							
0.00	1810	+000:03:00	700	1.42	0.79	1139	2726
0.25	1960	+000:03:15	700	1.26	0.83	1153	2751
0.50	2110	+000:03:30	700	1.42	0.86	1134	2667
0.75	2260	+000:03:45	700	1.42	0.90	1057	2484
1.00	2410	+000:04:00	700	1.42	0.90	958	2264
1.50	2590	+000:04:18	700	1.44	1.02	847	1956
2.00	2770	+000:04:36	700	1.31	1.11	713	1604
2.50	2950	+000:04:54	700	1.42	1.20	565	1233
3.00	3130	+000:05:12	700	1.42	1.29	459	972
3.50	3310	+000:05:30	700	1.42	1.37	379	784
4.00	3490	+000:05:48	700	1.38	1.43	325	618
4.50	3670	+000:06:06	700	1.43	1.53	286	541
5.00	3850	+000:06:24	700	1.42	1.60	255	466
Unconfined Trial # 23							
0.00	140	+000:00:13	700	1.42	0.79	1180	2835
0.25	290	+000:00:28	700	1.31	0.82	1196	2877
0.50	440	+000:00:43	700	1.42	0.86	1179	2806
0.75	590	+000:00:58	700	1.42	0.90	1108	2645
1.00	740	+000:01:13	700	1.42	0.94	1027	2466
1.50	920	+000:01:31	700	1.42	1.03	937	2224
2.00	1100	+000:01:49	700	1.41	1.11	832	1925
2.50	1280	+000:02:07	700	1.41	1.32	682	1537
3.00	1460	+000:02:25	700	1.42	1.28	557	1227
3.50	1640	+000:02:43	700	1.74	1.36	461	959
4.00	1820	+000:03:01	700	1.42	1.45	393	798
4.50	2000	+000:03:19	700	1.42	1.53	341	663
5.00	2180	+000:03:37	700	1.42	1.61	303	563
Unconfined Trial # 24							
0.00	197	+000:00:19	400	1.38	0.80	1234	3002
0.25	347	+000:00:34	400	1.42	0.84	1252	3039
0.50	497	+000:00:49	400	1.33	0.86	1234	2969
0.75	647	+000:01:04	400	1.41	0.92	1165	2796
1.00	797	+000:01:19	400	1.41	0.94	1086	2629
1.50	977	+000:01:37	400	1.42	1.03	1015	2437
2.00	1157	+000:01:55	400	1.46	1.11	934	2202
2.50	1337	+000:02:13	400	1.41	1.21	784	1808
3.00	1517	+000:02:31	400	1.41	1.28	650	1462
3.50	1697	+000:02:49	400	1.42	1.36	541	1162
4.00	1877	+000:03:07	400	1.41	1.43	458	957
4.50	2057	+000:03:25	400	1.43	1.53	401	825
5.00	2237	+000:03:43	400	1.42	1.60	352	691

Table C.2: Unconfined Test Data (Continued)

Radial Position	Data Point #	Time	Time	CDPositi	MDPositi	Plate Temp	Heat Flux
(in)		(HR:MIN:SEC)	(ms)	(V)	(V)	(F)	(mV)
Unconfined Trial # 25							
0.00	150	+000:00:14	700	1.48	0.57	1012	2451
0.25	300	+000:00:29	700	1.39	0.61	999	2407
0.50	450	+000:00:44	700	1.49	0.64	960	2293
0.75	600	+000:00:59	700	1.49	0.69	892	2105
1.00	750	+000:01:14	700	1.48	0.65	812	1906
1.50	930	+000:01:32	700	1.49	0.68	693	1576
2.00	1110	+000:01:50	700	1.47	0.90	549	1201
2.50	1290	+000:02:08	700	1.48	0.98	411	859
3.00	1470	+000:02:26	700	1.48	1.21	324	643
3.50	1650	+000:02:45	700	1.46	0.97	268	506
4.00	1830	+000:03:02	700	1.49	1.24	231	405
4.50	2010	+000:03:20	700	1.55	1.33	209	328
5.00	2190	+000:03:38	700	1.49	1.41	191	281
Unconfined Trial # 26							
0.00	150	+000:00:14	700	1.48	0.61	1092	2635
0.25	300	+000:00:29	700	1.48	0.64	1072	2569
0.50	450	+000:00:44	700	1.49	0.68	1028	2445
0.75	600	+000:00:59	700	1.48	0.71	958	2280
1.00	750	+000:01:14	700	1.48	0.59	889	2130
1.50	930	+000:01:32	700	1.48	0.67	790	1844
2.00	1110	+000:01:50	700	1.48	0.92	651	1470
2.50	1290	+000:02:08	700	1.50	1.10	500	1088
3.00	1470	+000:02:26	700	1.45	1.08	391	811
3.50	1650	+000:02:44	700	1.48	1.04	319	627
4.00	1830	+000:03:02	700	1.50	1.26	269	498
4.50	2010	+000:03:20	700	1.49	1.35	241	429
5.00	2190	+000:03:38	700	1.49	1.48	218	373
Unconfined Trial # 27							
0.00	140	+000:00:13	700	1.48	0.60	1120	2713
0.25	290	+000:00:28	700	1.51	0.63	1097	2639
0.50	440	+000:00:43	700	1.49	0.67	1050	2516
0.75	590	+000:00:58	700	1.34	0.71	985	2371
1.00	740	+000:01:13	700	1.49	0.62	930	2236
1.50	920	+000:01:31	700	1.49	0.65	872	2066
2.00	1100	+000:01:49	700	1.48	0.91	767	1780
2.50	1280	+000:02:07	700	1.49	0.99	617	1382
3.00	1460	+000:02:25	700	1.54	1.08	491	1061
3.50	1640	+000:02:43	700	1.48	1.15	397	837
4.00	1820	+000:03:01	700	1.52	1.23	332	668
4.50	2000	+000:03:19	700	1.49	1.36	287	546
5.00	2180	+000:03:37	700	1.48	1.37	257	473
Unconfined Trial # 28							
0.00	140	+000:00:13	700	1.45	0.60	1176	2845
0.25	290	+000:00:28	700	1.49	0.62	1144	2744
0.50	440	+000:00:43	700	1.50	0.67	1084	2600
0.75	590	+000:00:58	700	1.42	0.69	1022	2472
1.00	740	+000:01:13	700	1.48	0.63	980	2378
1.50	920	+000:01:31	700	1.48	0.75	938	2245
2.00	1100	+000:01:49	700	1.49	0.90	825	1942
2.50	1280	+000:02:07	700	1.48	0.99	670	1520
3.00	1460	+000:02:25	700	1.52	1.06	542	1188
3.50	1640	+000:02:43	700	1.49	1.05	445	952
4.00	1820	+000:03:01	700	1.49	1.25	374	779
4.50	2000	+000:03:19	700	1.48	1.54	324	646
5.00	2180	+000:03:37	700	1.49	1.38	290	559

Table C.2: Unconfined Test Data (Continued)

Radial Position	Data Point #	Time	Time	CDPositi	MDPositi	Plate Temp	Heat Flux
(in)		(HR:MIN:SEC)	(ms)	(V)	(V)	(F)	(mV)
Unconfined Trial # 29							
0.00	160	+000:00:15	700	1.17	1.53	826	1925
0.25	310	+000:00:30	700	1.16	1.59	820	1913
0.50	460	+000:00:45	700	1.17	1.63	819	1918
0.75	610	+000:01:00	700	1.08	1.64	816	1917
1.00	760	+000:01:15	700	1.14	1.71	817	1919
1.50	940	+000:01:33	700	1.15	1.85	817	1921
2.00	1120	+000:01:51	700	1.15	1.88	793	1850
2.50	1300	+000:02:09	700	1.21	1.96	742	1719
3.00	1480	+000:02:27	700	1.14	2.02	700	1618
3.50	1660	+000:02:45	700	1.15	2.13	688	1577
4.00	1840	+000:03:03	700	1.15	2.21	667	1518
4.50	2020	+000:03:21	700	1.14	2.27	617	1404
5.00	2200	+000:03:39	700	1.16	2.37	550	1244
Unconfined Trial # 30							
0.00	170	+000:00:16	700	1.16	1.56	961	2314
0.25	320	+000:00:31	700	1.14	1.58	957	2312
0.50	470	+000:00:46	700	1.15	1.65	952	2331
0.75	620	+000:01:01	700	1.07	1.64	952	2313
1.00	770	+000:01:16	700	1.15	1.71	956	2323
1.50	950	+000:01:34	700	1.14	1.79	955	2345
2.00	1130	+000:01:52	700	1.14	1.88	934	2244
2.50	1310	+000:02:10	700	1.15	1.96	884	2151
3.00	1490	+000:02:28	700	1.14	2.04	834	2017
3.50	1670	+000:02:46	700	1.14	2.12	823	1992
4.00	1850	+000:03:04	700	1.21	2.21	809	1941
4.50	2030	+000:03:22	700	1.16	2.38	760	1808
5.00	2210	+000:03:40	700	1.14	2.37	691	1616
Unconfined Trial # 31							
0.00	150	+000:00:14	700	1.13	1.58	940	2255
0.25	300	+000:00:29	700	1.14	1.61	937	2252
0.50	450	+000:00:44	700	1.15	1.64	935	2253
0.75	600	+000:00:59	700	1.29	1.68	932	2247
1.00	750	+000:01:14	700	1.15	1.72	932	2249
1.50	930	+000:01:32	700	1.15	1.80	930	2249
2.00	1110	+000:01:50	700	1.15	1.88	909	2191
2.50	1290	+000:02:08	700	1.15	1.97	849	2055
3.00	1470	+000:02:26	700	1.14	2.05	809	1949
3.50	1650	+000:02:44	700	1.15	2.14	806	1944
4.00	1830	+000:03:02	700	1.08	2.23	797	1909
4.50	2010	+000:03:20	700	1.15	2.31	750	1773
5.00	2190	+000:03:38	700	1.15	2.36	681	1600
Unconfined Trial # 32							
0.00	130	+000:00:12	700	1.15	1.56	1018	2450
0.25	280	+000:00:27	700	1.08	1.59	1014	2455
0.50	430	+000:00:42	700	1.17	1.64	1013	2459
0.75	580	+000:00:57	700	1.15	1.68	1011	2464
1.00	730	+000:01:12	700	1.13	1.71	1011	2469
1.50	910	+000:01:30	700	1.15	1.78	1012	2469
2.00	1090	+000:01:48	700	1.14	1.92	990	2408
2.50	1270	+000:02:06	700	1.15	1.96	933	2257
3.00	1450	+000:02:24	700	1.15	1.96	888	2146
3.50	1630	+000:02:42	700	1.14	2.12	888	2141
4.00	1810	+000:03:00	700	1.06	2.20	883	2125
4.50	1990	+000:03:18	700	1.15	2.29	836	1994
5.00	2170	+000:03:36	700	1.15	2.37	762	1794

Table C.2: Unconfined Test Data (Continued)

Radial Position	Data Point #	Time	Time	CDPositi	MDPositi	Plate Temp	Heat Flux
(in)		(HR:MIN:SEC)	(ms)	(V)	(V)	(F)	(mV)
Unconfined Trial # 33							
0.00	150	+000:00:14	700	1.14	1.54	910	2146
0.25	300	+000:00:29	700	1.15	1.59	907	2140
0.50	450	+000:00:44	700	1.15	1.63	901	2132
0.75	600	+000:00:59	700	1.16	1.79	890	2110
1.00	750	+000:01:14	700	1.22	1.72	884	2091
1.50	930	+000:01:32	700	1.15	1.80	863	2027
2.00	1110	+000:01:50	700	1.14	1.88	834	1956
2.50	1290	+000:02:08	700	1.14	1.90	787	1829
3.00	1470	+000:02:26	700	1.15	2.04	733	1684
3.50	1650	+000:02:44	700	1.15	2.13	707	1630
4.00	1830	+000:03:02	700	1.15	2.31	702	1607
4.50	2010	+000:03:20	700	1.21	2.31	680	1545
5.00	2190	+000:03:38	700	1.15	2.38	636	1434
Unconfined Trial # 33 b							
0.00	120	+000:00:11	700	1.16	1.56	783	1810
0.25	270	+000:00:26	700	1.14	1.59	778	1803
0.50	420	+000:00:41	700	1.14	1.63	773	1794
0.75	570	+000:00:56	700	1.15	1.70	766	1785
1.00	720	+000:01:11	700	1.13	1.71	758	1763
1.50	900	+000:01:29	700	1.15	1.80	743	1718
2.00	1080	+000:01:47	700	1.15	1.87	722	1658
2.50	1260	+000:02:05	700	1.15	2.00	678	1538
3.00	1440	+000:02:23	700	1.14	2.05	624	1399
3.50	1620	+000:02:41	700	1.14	2.13	603	1352
4.00	1800	+000:03:07	700	1.14	2.29	572	1261
4.50	1980	+000:03:17	700	1.15	2.34	562	1246
5.00	2160	+000:03:35	700	1.14	2.37	512	1124
Unconfined Trial # 34							
0.00	150	+000:00:12	700	1.14	1.55	861	2027
0.25	300	+000:00:29	700	1.15	1.59	856	2012
0.50	450	+000:00:44	700	1.15	1.66	852	2009
0.75	600	+000:00:59	700	1.15	1.69	844	1984
1.00	750	+000:01:14	700	1.15	1.80	834	1967
1.50	930	+000:01:32	700	1.12	1.78	819	1917
2.00	1110	+000:01:50	700	1.15	1.88	798	1861
2.50	1290	+000:02:08	700	1.14	1.96	757	1750
3.00	1470	+000:02:26	700	1.15	2.09	709	1626
3.50	1650	+000:02:44	700	1.15	2.10	688	1574
4.00	1830	+000:03:02	700	1.15	2.21	684	1568
4.50	2010	+000:03:20	700	1.14	2.29	660	1499
5.00	2190	+000:03:38	700	1.14	2.42	616	1378
Unconfined Trial # 35							
0.00	405	+000:00:40	200	1.13	1.58	881	2069
0.25	555	+000:00:55	200	1.16	1.62	878	2064
0.50	705	+000:01:10	200	1.14	1.73	870	2046
0.75	855	+000:01:25	200	1.13	1.72	861	2025
1.00	1005	+000:01:40	200	1.16	1.74	853	2008
1.50	1185	+000:01:58	200	1.13	1.82	838	1967
2.00	1365	+000:02:16	200	1.17	1.91	812	1899
2.50	1545	+000:02:34	200	1.14	1.99	771	1788
3.00	1725	+000:02:52	200	1.15	2.08	725	1670
3.50	1905	+000:03:10	200	1.02	2.17	712	1640
4.00	2085	+000:03:28	200	1.20	2.24	711	1637
4.50	2265	+000:03:46	200	1.15	2.32	686	1568
5.00	2445	+000:04:04	200	1.15	2.32	645	1466

Table C.2: Unconfined Test Data (Continued)

Radial Position	Data Point #	Time	Time	CDPositi	MDPositi	Plate Temp	Heat Flux
(in)		(HR:MIN:SEC)	(ms)	(V)	(V)	(F)	(mV)
Unconfined Trial # 36							
0.00	110	+000:00:10	700	1.15	1.56	925	2190
0.25	260	+000:00:25	700	1.23	1.59	921	2182
0.50	410	+000:00:40	700	1.15	1.63	915	2167
0.75	560	+000:00:55	700	1.15	1.67	906	2147
1.00	710	+000:01:10	700	1.14	1.71	897	2127
1.50	890	+000:01:28	700	1.08	1.80	879	2079
2.00	1070	+000:01:46	700	1.15	1.88	856	2017
2.50	1250	+000:02:04	700	1.10	1.96	813	1899
3.00	1430	+000:02:22	700	1.14	2.04	765	1779
3.50	1610	+000:02:40	700	1.19	2.12	752	1745
4.00	1790	+000:02:58	700	1.15	2.21	756	1747
4.50	1970	+000:03:16	700	1.15	2.29	731	1686
5.00	2150	+000:03:34	700	1.15	2.37	679	1541

Table C.3: Confined Test Conditions

	Date	Pulsed or Steady	Tail Pipe Dia	Gap	Gas Flow	
Run			(mm)	(mm)	(L/m)	(scfm)
1	7-Jun	Pulsed	25	25	93	3.3
2	7-Jun	Pulsed	25	25	103	3.6
3	7-Jun	Pulsed	25	25	79	2.8
4	7-Jun	Pulsed	25	25	122	4.3
5	7-Jun	Pulsed	25	71	89	3.1
6	7-Jun	Pulsed	25	71	101	3.6
7	7-Jun	Pulsed	25	71	78.5	2.8
8	7-Jun	Pulsed	25	71	124	4.4
9	7-Jun	Steady	25	71	28	1.0
10	7-Jun	Steady	25	71	18	0.6
11	7-Jun	Steady	25	25	28	1.0
12	7-Jun	Steady	25	25	13	0.5
1	10-Jun	Pulsed	71	25	70	2.5
2	10-Jun	Pulsed	71	25	104	3.7
3	10-Jun	Pulsed	71	71	70	2.5
4	10-Jun	Pulsed	71	71	102	3.6
5	10-Jun	Pulsed	71	142	74	2.6
6	10-Jun	Pulsed	71	142	104	3.7
7	10-Jun	Steady	71	25	70	2.5
8	10-Jun	Steady	71	25	106	3.7
9	10-Jun	Steady	71	142	72	2.5
10	10-Jun	Steady	71	142	104	3.7
1	25-May	Steady	71	71	100	3.5
2	26-May	Steady	71	71	71	2.5

Table C.3: Confined Test Conditions (Continued)

	Air Settings		Air Flow	Exit Jet Temp	Pulse Pressure Data		
					Mean	Peak to Peak	Frequency
Run	(Hz)	(in H2O)	(scfm)	(deg F)	(psi)	(psi)	(Hz)
1	**25.7**	20.00	133.50	1800.00	13.25	59	135
2	**32.7**	40.00	176.25	1770.00	18.72	69	137
3	**14.3**	11.00	71.25	1960.00	3.80	23	114
4	**26.6**	32.00	138.75	2032.00	14.24	66	112
5	**25.6**	29.50	135.00	1800.00	12.47	60	133
6	**32.8**	40.50	180.00	1780.00	18.35	60	148
7	**14.3**	11.00	73.50	1933.00	4.17	28	112
8	**26.7**	33.00	135.00	2004.00	15.33	63	116
9	**11.3**	9.60	48.75	1920.00			
10	**7.2**	4.10	26.25	1770.00			
11	**11.3**	9.60	48.75	1830.00			
12	**7.3**	4.10	26.25	1770.00			
1	**14.5**	10.30	75.00	2017.00	1.20	50	153
2	**26.5**	29.00	135.00	2120.00	6.20	78	168
3	**14.5**	10.20	75.00	2035.00	-0.57	59	157
4	**26.6**	29.00	135.00	2110.00	2.30	98	173
5	**14.5**	16.20	75.00	2020.00	-0.18	58	155
6	**26.5**	29.30	135.00	2125.00	2.88	103	170
7	**12.6**	5.60	75.00	2011.00			
8	**24.5**	20.30	131.25	2117.00			
9	**12.6**	5.60	75.00	2000.00			
10	**24.4**	20.10	135.00	2125.00			
1	**21.3**	15.20	123.75	2080.00			
2	**12.6**	5.60	75.00	1970.00			

Table C.4: Confined Test Data

Radial Position	Data Point	Time	Time	CDPosition	MDPosition	Plate Temp	Heat Flux
(in)		(HR:MIN:SEC)	(ms)	(V)	(V)	(F)	(mV)
Confined Trial #1 7-Jun							
0.00	110	+000:00:10	700	1.24	0.66	1112	2595
0.25	260	+000:00:25	700	1.25	0.78	1118	2614
0.50	410	+000:00:40	700	1.24	0.79	1116	2603
0.75	560	+000:00:55	700	1.24	0.89	1110	2571
1.00	710	+000:01:10	700	1.22	0.94	1081	2483
1.50	890	+000:01:28	700	1.24	1.02	941	2154
2.00	1070	+000:01:46	700	1.24	1.11	856	1896
2.50	1250	+000:02:04	700	1.24	1.21	726	1621
3.00	1430	+000:02:22	700	1.22	1.31	597	1297
3.50	1610	+000:02:40	700	1.25	1.36	511	1047
4.00	1790	+000:02:58	700	1.23	1.44	455	903
4.50	1970	+000:03:16	700	1.24	1.52	403	814
5.00	2150	+000:03:34	700	1.24	1.57	354	670
Confined Trial #2 7-Jun							
0.00	140	+000:00:13	700	1.24	0.78	1249	2936
0.25	290	+000:00:28	700	1.24	0.51	1250	2933
0.50	440	+000:00:43	700	1.24	0.87	1250	2933
0.75	590	+000:00:58	700	1.24	0.89	1245	2906
1.00	740	+000:01:13	700	1.24	0.93	1212	2811
1.50	920	+000:01:31	700	1.24	1.00	1066	2479
2.00	1100	+000:01:49	700	1.24	1.10	986	2279
2.50	1280	+000:02:07	700	1.24	1.18	851	1958
3.00	1460	+000:02:25	700	1.25	1.31	704	1543
3.50	1640	+000:02:43	700	1.24	1.35	602	1304
4.00	1820	+000:03:01	700	1.25	1.58	534	1129
4.50	2000	+000:03:19	700	1.24	1.51	479	963
5.00	2180	+000:03:37	700	1.18	1.55	428	846
Confined Trial #3 7-Jun							
0.00	133	+000:00:13	0	1.25	0.79	1117	2564
0.25	283	+000:00:28	0	1.25	0.78	1119	2564
0.50	433	+000:00:43	0	1.24	0.89	1116	2525
0.75	583	+000:00:58	0	1.24	0.91	1105	2495
1.00	733	+000:01:13	0	1.24	0.95	1069	2398
1.50	913	+000:01:31	0	1.17	1.04	926	2079
2.00	1093	+000:01:49	0	1.24	1.12	816	1786
2.50	1273	+000:02:07	0	1.19	1.21	671	1426
3.00	1453	+000:02:25	0	1.25	1.14	550	1141
3.50	1633	+000:02:43	0	1.28	1.37	469	938
4.00	1813	+000:03:01	0	1.26	1.45	415	802
4.50	1993	+000:03:19	0	1.25	1.49	369	696
5.00	2173	+000:03:37	0	1.25	1.40	332	640
Confined Trial #4 7-Jun							
0.00	130	+000:00:12	700	1.24	0.76	1385	3436
0.25	280	+000:00:27	700	1.24	0.81	1391	3450
0.50	430	+000:00:42	700	1.24	0.87	1391	3445
0.75	580	+000:00:57	700	1.13	0.90	1382	3408
1.00	730	+000:01:12	700	1.24	0.95	1349	3314
1.50	910	+000:01:30	700	1.25	1.00	1189	2951
2.00	1090	+000:01:48	700	1.24	1.08	1099	2708
2.50	1270	+000:02:06	700	1.24	1.54	971	2390
3.00	1450	+000:02:24	700	1.26	1.22	822	1982
3.50	1630	+000:02:42	700	1.25	1.28	719	1683
4.00	1810	+000:03:00	700	1.23	1.47	652	1500
4.50	1990	+000:03:18	700	1.24	1.52	613	1383
5.00	2170	+000:03:36	700	1.24	1.57	558	1244

Table C.4: Confined Test Data (Continued)

Radial Position	Data Point	Time	Time	CDPositi	MDPositi	Plate Temp	Heat Flux
(in)		(HR:MIN:SEC)	(ms)	(V)	(V)	(F)	(mV)
Confined Trial #5 7-Jun							
0.00	140	+000:00:13	700	1.17	0.69	1050	2581
0.25	290	+000:00:28	700	1.18	0.72	1059	2601
0.50	440	+000:00:43	700	1.18	0.57	1045	2555
0.75	590	+000:00:58	700	1.17	0.79	1009	2461
1.00	740	+000:01:13	700	1.18	0.66	946	2301
1.50	920	+000:01:31	700	1.18	0.90	790	1881
2.00	1100	+000:01:49	700	1.18	0.99	685	1576
2.50	1280	+000:02:07	700	1.14	1.15	582	1310
3.00	1460	+000:02:25	700	1.18	1.12	469	998
3.50	1640	+000:02:43	700	1.19	1.24	376	749
4.00	1820	+000:03:01	700	1.18	1.30	312	592
4.50	2000	+000:03:19	700	1.18	1.37	272	495
5.00	2180	+000:03:37	700	1.17	1.43	242	417
Confined Trial #6 7-Jun							
0.00	130	+000:00:12	400	1.18	0.65	1119	2766
0.25	280	+000:00:27	700	1.18	0.64	1117	2761
0.50	430	+000:00:42	700	1.18	0.72	1101	2723
0.75	580	+000:00:57	700	1.30	0.76	1066	2623
1.00	730	+000:01:12	700	1.14	0.66	1007	2475
1.50	910	+000:01:30	700	1.18	0.84	853	2066
2.00	1090	+000:01:48	700	1.18	1.02	748	1759
2.50	1270	+000:02:06	700	1.18	1.09	639	1463
3.00	1450	+000:02:24	700	1.18	1.12	521	1135
3.50	1630	+000:02:42	700	1.18	1.23	424	888
4.00	1810	+000:03:00	700	1.18	1.33	348	679
4.50	1990	+000:03:18	700	1.18	1.41	300	557
5.00	2170	+000:03:36	700	1.19	1.45	264	468
Confined Trial #7 7-Jun							
0.00	130	+000:00:12	700	1.20	0.68	1043	2542
0.25	280	+000:00:27	700	1.29	0.71	1052	2564
0.50	430	+000:00:42	700	1.18	0.75	1042	2526
0.75	580	+000:00:57	700	1.24	0.78	999	2410
1.00	730	+000:01:12	700	1.18	0.67	927	2222
1.50	910	+000:01:30	700	1.18	0.94	747	1746
2.00	1090	+000:01:48	700	1.12	1.01	626	1405
2.50	1270	+000:02:06	700	1.17	1.06	522	1127
3.00	1450	+000:02:24	700	1.20	1.19	412	849
3.50	1630	+000:02:42	700	1.18	1.27	331	650
4.00	1810	+000:03:00	700	1.12	1.35	273	488
4.50	1990	+000:03:18	700	1.18	1.42	235	391
5.00	2170	+000:03:36	700	1.18	1.45	212	337
Confined Trial #8 7-Jun							
0.00	120	+000:00:11	700	1.18	0.71	1346	3339
0.25	270	+000:00:26	700	1.17	0.71	1340	3326
0.50	420	+000:00:41	700	1.18	0.77	1331	3272
0.75	570	+000:00:56	700	1.18	0.81	1297	3172
1.00	720	+000:01:11	700	1.19	0.67	1228	3010
1.50	900	+000:01:29	700	1.19	0.92	1043	2566
2.00	1080	+000:01:47	700	1.18	1.01	905	2179
2.50	1260	+000:02:05	700	1.18	1.09	767	1802
3.00	1440	+000:02:23	700	1.18	1.22	625	1415
3.50	1620	+000:02:41	700	1.18	1.25	511	1100
4.00	1800	+000:02:59	700	1.19	1.28	425	884
4.50	1980	+000:03:17	700	1.18	1.43	360	703
5.00	2160	+000:03:35	700	1.18	1.42	318	599

Table C.4: Confined Test Data (Continued)

Radial Position	Data Point	Time	Time	CDPosition	MDPosition	Plate Temp	Heat Flux
(in)		(HR:MIN:SEC)	(ms)	(V)	(V)	(F)	(mV)
Confined Trial #9 7-Jun							
0.00	135	+000:00:13	200	0.99	0.86	1047	2555
0.25	285	+000:00:28	200	1.05	0.62	1023	2499
0.50	435	+000:00:43	200	1.04	0.94	957	2338
0.75	585	+000:00:58	200	1.05	0.96	861	2083
1.00	735	+000:01:13	200	1.05	1.54	774	1854
1.50	915	+000:01:31	200	1.05	1.11	656	1522
2.00	1095	+000:01:49	200	1.04	1.21	541	1216
2.50	1275	+000:02:07	200	1.05	1.29	428	906
3.00	1455	+000:02:25	200	0.90	1.36	347	693
3.50	1635	+000:02:43	200	1.05	1.39	294	550
4.00	1815	+000:03:01	200	1.04	1.53	256	453
4.50	1995	+000:03:19	200	1.05	1.65	230	389
5.00	2175	+000:03:37	200	1.05	1.72	207	332
Confined Trial #10 7-Jun							
0.00	130	+000:00:12	700	1.05	1.01	803	1894
0.25	280	+000:00:27	700	1.05	0.97	784	1839
0.50	430	+000:00:42	700	1.06	0.97	738	1710
0.75	580	+000:00:57	700	1.08	1.04	674	1552
1.00	730	+000:01:12	700	1.05	1.06	608	1364
1.50	910	+000:01:30	700	0.99	0.95	510	1077
2.00	1090	+000:01:48	700	1.05	1.23	410	790
2.50	1270	+000:02:06	700	1.05	1.25	319	568
3.00	1450	+000:02:24	700	1.05	1.34	259	416
3.50	1630	+000:02:42	700	1.05	1.48	219	324
4.00	1810	+000:03:00	700	1.05	1.57	194	267
4.50	1990	+000:03:18	700	1.04	1.65	175	230
5.00	2170	+000:03:36	700	1.05	1.64	163	199
Confined Trial #11 7-Jun							
0.00	150	+000:00:14	700	1.35	1.24	1040	2570
0.25	300	+000:00:29	700	1.35	1.23	1020	2483
0.50	450	+000:00:44	700	1.35	1.22	966	2351
0.75	600	+000:00:59	700	1.37	0.94	900	2177
1.00	750	+000:01:14	700	1.34	1.31	849	2037
1.50	930	+000:01:32	700	1.40	1.39	730	1692
2.00	1110	+000:01:50	700	1.48	1.45	573	1284
2.50	1290	+000:02:08	700	1.35	1.56	455	972
3.00	1470	+000:02:26	700	1.35	1.64	380	785
3.50	1650	+000:02:44	700	1.34	1.73	328	645
4.00	1830	+000:03:02	700	1.38	1.82	291	558
4.50	2010	+000:03:20	700	1.47	1.89	266	480
5.00	2190	+000:03:38	700	1.35	1.80	253	454
Confined Trial #12 7-Jun							
0.00	120	+000:00:11	700	1.35	1.10	929	2271
0.25	270	+000:00:26	700	1.35	1.10	917	2223
0.50	420	+000:00:41	700	1.35	1.18	880	2129
0.75	570	+000:00:56	700	1.38	1.22	815	1971
1.00	720	+000:01:11	700	1.34	1.26	755	1790
1.50	900	+000:01:29	700	1.27	1.35	654	1500
2.00	1080	+000:01:47	700	1.31	1.42	512	1123
2.50	1260	+000:02:05	700	1.35	1.51	403	846
3.00	1440	+000:02:23	700	1.35	1.61	334	670
3.50	1620	+000:02:41	700	1.35	1.67	291	562
4.00	1800	+000:02:59	700	1.43	1.78	258	470
4.50	1980	+000:03:17	700	1.35	1.84	234	407
5.00	2160	+000:03:35	700	1.41	1.94	218	378

Table C.4: Confined Test Data (Continued)

Radial Position	Data Point	Time	Time	CDPosition	MDPosition	Plate Temp	Heat Flux
(in)		(HR:MIN:SEC)	(ms)	(V)	(V)	(F)	(mV)
Confined Trial #1 10-Jun							
0.00	140	+000:00:13	700	1.31	1.21	986	2443
0.25	290	+000:00:28	700	1.33	1.24	963	2380
0.50	440	+000:00:43	700	1.40	1.29	963	2367
0.75	590	+000:00:58	700	1.51	1.31	966	2378
1.00	740	+000:01:13	700	1.31	1.35	967	2372
1.50	920	+000:01:31	700	1.31	1.43	964	2379
2.00	1100	+000:01:49	700	1.32	1.50	928	2292
2.50	1280	+000:02:07	700	1.31	1.65	858	2098
3.00	1460	+000:02:25	700	1.25	1.66	814	1977
3.50	1640	+000:02:43	700	1.31	1.76	812	1975
4.00	1820	+000:03:01	700	1.31	1.95	817	1992
4.50	2000	+000:03:19	700	1.34	1.93	787	1917
5.00	2180	+000:03:37	700	1.31	1.97	725	1734
Confined Trial #2 10-Jun							
0.00	127	+000:00:12	400	1.32	1.19	1122	2804
0.25	277	+000:00:27	400	1.32	1.22	1123	2812
0.50	427	+000:00:42	400	1.24	1.27	1121	2801
0.75	577	+000:00:57	400	1.31	1.14	1121	2794
1.00	727	+000:01:12	400	1.32	1.33	1118	2787
1.50	907	+000:01:30	400	1.31	1.43	1103	2750
2.00	1087	+000:01:48	400	1.32	1.48	1065	2629
2.50	1267	+000:02:06	400	1.24	1.59	995	2446
3.00	1447	+000:02:24	400	1.34	1.68	958	2341
3.50	1627	+000:02:42	400	1.31	1.59	975	2391
4.00	1807	+000:03:00	400	1.31	1.82	999	2448
4.50	1987	+000:03:18	400	1.33	1.96	987	2423
5.00	2167	+000:03:36	400	1.40	1.92	954	2355
Confined Trial #3 10-Jun							
0.00	190	+000:00:18	700	2.21	1.24	842	2040
0.25	340	+000:00:33	700	1.21	1.30	845	2038
0.50	490	+000:00:48	700	1.21	1.34	843	2040
0.75	640	+000:01:03	700	1.20	1.38	841	2037
1.00	790	+000:01:18	700	1.21	1.53	839	2022
1.50	970	+000:01:36	700	1.19	1.49	814	1955
2.00	1150	+000:01:54	700	1.21	1.55	763	1808
2.50	1330	+000:02:12	700	1.17	1.65	693	1645
3.00	1510	+000:02:30	700	1.21	1.76	606	1375
3.50	1690	+000:02:48	700	1.22	1.84	554	1215
4.00	1870	+000:03:06	700	1.21	1.93	519	1129
4.50	2050	+000:03:24	700	1.02	2.02	492	1039
5.00	2230	+000:03:42	700	1.20	2.09	473	993
Confined Trial #4 10-Jun							
0.00	200	+000:00:19	700	1.20	1.26	982	2415
0.25	350	+000:00:34	700	1.21	1.30	980	2404
0.50	500	+000:00:49	700	1.21	1.34	975	2386
0.75	650	+000:01:04	700	1.23	1.37	967	2370
1.00	800	+000:01:19	700	1.20	1.41	958	2344
1.50	980	+000:01:37	700	0.84	1.48	931	2268
2.00	1160	+000:01:55	700	1.21	1.58	891	2154
2.50	1340	+000:02:13	700	1.17	1.65	832	1991
3.00	1520	+000:02:31	700	1.34	1.76	772	1829
3.50	1700	+000:02:49	700	1.09	1.83	739	1739
4.00	1880	+000:03:07	700	1.21	1.93	715	1682
4.50	2060	+000:03:25	700	1.16	2.02	681	1596
5.00	2240	+000:03:43	700	1.19	1.99	643	1485

Table C.4: Confined Test Data (Continued)

Radial Position	Data Point	Time	Time	CDPosition	MDPosition	Plate Temp	Heat Flux
(in)		(HR:MIN:SEC)	(ms)	(V)	(V)	(F)	(mV)
Confined Trial #5 10-Jun							
0.00	150	+000:00:14	700	1.06	1.19	505	1076
0.25	300	+000:00:29	700	1.13	1.23	503	1065
0.50	450	+000:00:44	700	1.13	1.27	504	1081
0.75	600	+000:00:59	700	1.13	1.31	510	1092
1.00	750	+000:01:14	700	0.97	1.35	505	1071
1.50	930	+000:01:32	700	1.13	1.42	489	1031
2.00	1110	+000:01:50	700	1.13	1.52	441	878
2.50	1290	+000:02:08	700	1.10	1.61	397	734
3.00	1470	+000:02:26	700	1.13	1.69	372	656
3.50	1650	+000:02:44	700	1.14	1.78	347	609
4.00	1830	+000:03:02	700	1.18	1.86	346	616
4.50	2010	+000:03:20	700	1.13	1.95	334	583
5.00	2190	+000:03:38	700	1.14	1.70	328	570
Confined Trial #6 10-Jun							
0.00	210	+000:00:20	700	1.14	1.18	816	1938
0.25	360	+000:00:35	700	1.14	1.18	813	1931
0.50	510	+000:00:50	700	1.19	1.26	811	1932
0.75	660	+000:01:05	700	1.16	1.30	792	1875
1.00	810	+000:01:20	700	1.13	1.33	780	1847
1.50	990	+000:01:38	700	1.12	1.42	748	1753
2.00	1170	+000:01:56	700	1.14	1.51	701	1622
2.50	1350	+000:02:14	700	1.11	1.58	635	1463
3.00	1530	+000:02:32	700	1.14	1.66	591	1316
3.50	1710	+000:02:50	700	1.14	1.75	550	1190
4.00	1890	+000:03:08	700	1.14	1.84	528	1143
4.50	2070	+000:03:26	700	1.09	1.93	474	986
5.00	2250	+000:03:44	700	1.18	1.88	436	832
Confined Trial #7 10-Jun							
0.00	210	+000:00:13	700	1.13	1.44	949	2331
0.25	360	+000:00:35	700	1.13	1.51	930	2284
0.50	510	+000:00:50	700	1.13	1.61	930	2284
0.75	660	+000:01:05	700	1.13	1.44	932	2290
1.00	810	+000:01:20	700	1.13	1.62	936	2300
1.50	990	+000:01:38	700	1.11	1.71	945	2320
2.00	1170	+000:01:56	700	1.13	1.78	935	2271
2.50	1350	+000:02:14	700	1.13	1.88	877	2114
3.00	1530	+000:02:32	700	1.13	1.96	808	1927
3.50	1710	+000:02:50	700	1.13	2.05	774	1828
4.00	1890	+000:03:08	700	1.07	2.14	762	1795
4.50	2070	+000:03:26	700	1.13	2.22	760	1788
5.00	2250	+000:03:44	700	1.16	2.21	738	1743
Confined Trial #8 10-Jun							
0.00	240	+000:00:23	700	1.13	1.47	1151	2882
0.25	390	+000:00:38	700	1.13	1.52	1148	2871
0.50	540	+000:00:53	700	1.17	1.54	1146	2865
0.75	690	+000:01:08	700	1.13	1.50	1144	2861
1.00	840	+000:01:23	700	1.13	1.61	1143	2853
1.50	1020	+000:01:41	700	1.06	1.71	1138	2835
2.00	1200	+000:01:59	700	1.14	1.79	1110	2758
2.50	1380	+000:02:17	700	1.13	1.88	1033	2554
3.00	1560	+000:02:35	700	1.13	1.96	956	2343
3.50	1740	+000:02:53	700	1.13	2.05	937	2288
4.00	1920	+000:03:11	700	1.13	2.13	933	2271
4.50	2100	+000:03:29	700	1.08	2.21	926	2256
5.00	2280	+000:03:47	700	1.06	2.23	914	2237

Table C.4: Confined Test Data (Continued)

Radial Position	Data Point	Time	Time	CDPosition	MDPosition	Plate Temp	Heat Flux
(in)		(HR:MIN:SEC)	(ms)	(V)	(V)	(F)	(mV)
Confined Trial #9 10-Jun							
0.00	170	+000:00:16	700	1.31	1.46	812	1940
0.25	320	+000:00:31	700	1.20	1.49	810	1935
0.50	470	+000:00:46	700	1.31	1.51	808	1925
0.75	620	+000:01:01	700	1.32	1.57	805	1916
1.00	770	+000:01:16	700	1.30	1.60	799	1893
1.50	950	+000:01:34	700	1.30	1.50	766	1801
2.00	1130	+000:01:52	700	1.15	1.84	704	1629
2.50	1310	+000:02:10	700	1.29	1.85	624	1405
3.00	1490	+000:02:28	700	1.30	1.95	565	1243
3.50	1670	+000:02:46	700	1.31	2.03	535	1168
4.00	1850	+000:03:04	700	1.35	2.12	518	1120
4.50	2030	+000:03:22	700	1.30	2.20	492	1056
5.00	2210	+000:03:40	700	1.29	2.19	462	993
Confined Trial #10 10-Jun							
0.00	170	+000:00:16	700	1.26	1.29	956	2346
0.25	320	+000:00:31	700	1.30	1.49	954	2338
0.50	470	+000:00:46	700	1.32	1.52	948	2320
0.75	620	+000:01:01	700	1.41	1.58	942	2301
1.00	770	+000:01:16	700	1.30	1.61	935	2282
1.50	950	+000:01:34	700	1.30	1.62	903	2188
2.00	1130	+000:01:52	700	1.29	1.80	840	2007
2.50	1310	+000:02:10	700	1.30	1.86	759	1778
3.00	1490	+000:02:28	700	1.29	1.96	698	1611
3.50	1670	+000:02:46	700	1.30	2.16	672	1542
4.00	1850	+000:03:04	700	1.31	2.12	664	1520
4.50	2030	+000:03:22	700	1.30	2.20	641	1456
5.00	2210	+000:03:40	700	1.19	2.09	615	1392
Confined Trial #1 25-May							
0.00	225	+000:00:22	200	1.27	1.63	959	2294
0.25	375	+000:00:37	200	1.27	1.67	958	2323
0.50	525	+000:00:52	200	1.27	1.69	954	2318
0.75	675	+000:01:07	200	1.28	1.74	947	2317
1.00	825	+000:01:22	200	1.23	1.76	938	2287
1.50	1005	+000:01:40	200	1.28	1.86	917	2242
2.00	1185	+000:01:58	200	1.24	1.95	899	2153
2.50	1365	+000:02:16	200	1.28	2.04	863	2108
3.00	1545	+000:02:34	200	1.28	2.10	810	1959
3.50	1725	+000:02:52	200	1.28	2.20	789	1901
4.00	1905	+000:03:10	200	1.28	2.29	794	1909
4.50	2085	+000:03:28	200	1.28	2.40	783	1850
5.00	2265	+000:03:46	200	1.28	2.35	757	1832
Confined Trial #2 25-May							
0.00	260	+000:00:25	700	1.26	1.62	804	1882
0.25	410	+000:00:40	700	1.30	1.66	799	1872
0.50	560	+000:00:55	700	1.28	1.70	793	1874
0.75	710	+000:01:10	700	1.27	1.71	788	1873
1.00	860	+000:01:25	700	1.28	1.81	782	1830
1.50	1040	+000:01:43	700	1.28	1.85	768	1831
2.00	1220	+000:02:01	700	1.30	1.94	747	1743
2.50	1400	+000:02:19	700	1.28	2.02	709	1660
3.00	1580	+000:02:37	700	1.28	2.11	652	1493
3.50	1760	+000:02:55	700	1.29	2.18	622	1433
4.00	1940	+000:03:13	700	1.28	2.28	619	1429
4.50	2120	+000:03:31	700	1.15	2.36	601	1379
5.00	2300	+000:03:49	700	1.28	2.39	569	1307

APPENDIX D

DATA SHEETS

THE HT-50 THERMAL FLUX METER

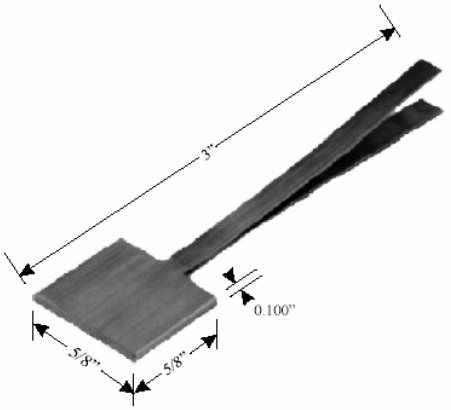

FOR PRECISE MEASUREMENT OF HEAT FLUXES

- Heat Fluxes To 10^6 Btu/hr ft²
- Temperature Range to 1800°F.
- Rapid Response (0.1 Secs.)
- Linear Output
- Accuracy 5%
- Negligible Thermal Resistance
- No Power Supply Required

APPLICATION

The Model HT-50 Thermal Flux Meter is a solid state, flat-plate, metallic transducer designed to measure heat flow directly. This transducer is placed upon any surface through which the heat flow is to be measured. The unit will measure heat flow to, or from any surface. In many cases, the transducers may also be installed internally within any barrier with no loss of accuracy.

Application areas include:

- Furnace/Boiler Heat Flow
- High Temperature Heat Transfer
- Engine Heat Loss Measurements
- Physical Property Determinations
- Aeronautical and Space Technology

OPERATION

The transducer may be attached to the heat transfer surface by either clamp, or ceramic cement. The D.C. signal generated by the transducer from the heat flow is conducted to the readout by means of a cable. When the transducer attains equilibrium (app. 0.1 sec.) with the surface, the generated voltage will be proportional to the heat flux. When this output voltage is multiplied by a specific calibration constant, which is supplied with each transducer, the resulting value will be heat loss/gain in terms of Btu/hr ft².

PRINCIPLE

The flow of heat to, or from a surface on which the transducer is placed creates a small temperature difference between the upper and lower surfaces of the transducer. These surfaces are in thermal contact with a miniature, high temperature thermopile which generates a direct current signal from this temperature difference. The thermoelectric element yields signals which may be measured by a microvolt meter. Because each unit is self-powered, no excitation voltage is necessary. The thermal resistance introduced by the transducer is negligible for all practical purposes.

CALIBRATION

ITI Thermal Flux Meters are individually calibrated at a base temperature of 70°F. An absolute calibration technique is used to determine the meter constant to the required accuracy, and verified by calculation. A temperature correction curve for elevated temperatures is also provided.

SPECIFICATIONS

Temperature Range	- 425°F. to 1800°F. (2000°F. in Vacuum)
Maximum Flux Density	10^6 Btu/hr ft²
Material	Stainless Steels
Time Constant	0.1 Secs.
Size	0.100"x 5/8"x 5/8"
Sensitivity	150 Btu/hr ft² μVolt
Accuracy	5%

ITI INTERNATIONAL THERMAL INSTRUMENT COMPANY
P.O. Box 309, Del Mar, California, 92014 (858) 755-4436 Fax (858) 755-6878

Figure D.1: Heat Flux Transducer Specifications

LX-PA SERIES
RATIOMETRIC VOLTAGE OUTPUT

The **UniMeasure LX-PA Series** linear position transducer with analog output is a low cost, compact alternative for use in light to moderate duty applications in dry environments. The plastic bodied device is ideal for high volume OEM situations where cost is a major consideration and in applications where small size or low weight are of paramount importance.

Model LX-PA is available in eleven different measurement ranges with a maximum range of 50" (1250 mm). The output is voltage from a potentiometric voltage divider circuit. In standard form, the electrical connections are made directly to the contacts on the potentiometer of the unit. Optional electrical cable attached to the potentiometer is available in various lengths. Standard potentiometer value is 1K ohm with optional values of 2K, 5K and 10K ohm available.

SPECIFICATIONS

General

Measurement Ranges	See Table 1
Sensing Device	Precision Potentiometer
Resolution	Essentially Infinite
Linearity	
2", 2.8", 3.8" 4.7" ranges	±1.0% Full Scale
10" to 25" ranges	±0.5% Full Scale
30" to 50" ranges	±0.25% Full Scale
Repeatability	±0.03% Full Scale
Construction	Thermoplastic Body
Cable	Ø.018 (0.46 mm) Jacketed Stainless Steel
Wire Rope Tension	See Table 1
Weight	3 oz. (85 gm)
Connections	Solder terminals
Dimensional Information	See Supplemental Data[1]
Life	
Ranges to 4.7"	1,000,000 full stroke cycles
Ranges 10" to 25"	250,000 full stroke cycles
Ranges 30" to 50"	125,000 full stroke cycles

Environmental

Operating Temperature	-25°C to 75°C
Storage Temperature	-50°C to 80°C
Operating Humidity	95 R.H. max. non-condensing
Vibration	15 G's 0.1 ms max.
Shock	50 G's 0.1 ms max.
Ingress Protection	NEMA 1, IP-40

Electrical

Input Impedance	1000 Ω ±15%
Output Impedance	0 to 1000 Ω
Excitation Voltage	25 Volts max. AC or DC

CIRCUIT DIAGRAM

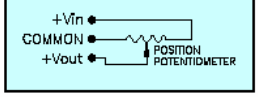

FOOTNOTES TO SPECIFICATIONS
1. Supplemental Data section located at end of LX Series pages.

TABLE 1

MODEL	RANGE (inch)	RANGE (mm)	NOMINAL OUTPUT (mV/V/in)	NOMINAL OUTPUT (mV/V/mm)	NOMINAL WIRE ROPE TENSION (oz)	NOMINAL WIRE ROPE TENSION (N)
LX-PA-2	2	50	469	18.5	16	4.4
LX-PA-2.8	2.8	70	341	13.4	14	3.9
LX-PA-3.8	3.8	96	258	10.1	11	3.1
LX-PA-4.7	4.7	120	207	8.1	8	2.2
LX-PA-10	10	250	88	3.5	16	4.4
LX-PA-15	15	380	64	2.5	14	3.9
LX-PA-20	20	500	49	1.9	11	3.1
LX-PA-25	25	625	39	1.5	8	2.2
LX-PA-30	30	750	32	1.3	14	3.9
LX-PA-40	40	1000	24	1.0	11	3.1
LX-PA-50	50	1250	20	0.8	8	2.2

Model Number Configuration

LX-PA-___-___-___

Range
- **2** ..... 2.0" (50 mm)
- **2.8** ..... 2.8" (70 mm)
- **3.8** ..... 3.8" (96 mm)
- **4.7** ..... 4.7" (120 mm)
- **10** ..... 10" (250 mm)
- **15** ..... 15" (390 mm)
- **20** ..... 20" (500 mm)
- **25** ..... 25" (640 mm)
- **30** ..... 30" (750 mm)
- **40** ..... 40" (1000 mm)
- **50** ..... 50" (1250 mm)

Potentiometer Value
- ✱ ..... 1K ohm
- **P2K** ..... 2K ohm
- **P5K** ..... 5K ohm
- **P10K** ..... 10K ohm

Electrical Cable Length
- ✱ ..... No Electrical Cable
- **LPM** ..... 150 mm (6") pigtail
- **L1M** ..... 1 m (3')
- **L2M** ..... 2 m (6.5')
- **L3M** ..... 3 m (10')
- **L4M** ..... 4 m (13.5')
- **L5M** ..... 5 m (16.5')

NOTE
1) —Asterisk items are standard configuration. No option designator is required.
2) Shaded options available at additional cost.

Example
LX-PA-20-L1M

UniMeasure | 4175 SW Research Way, Corvallis, OR 97333 | Tel: 541-757-3158 | Fax: 541-757-0858 | Email: sales@unimeasure.com

Figure D.2: Draw Wire Transducer Specifications
http://www.unimeasure.com/obj--pdf/pdf-lx-pa.pdf

Specifications

GENERAL
System Requirements: 80386 CPU or better; bidirectional parallel port; Microsoft Windows with 8 MB RAM for DaqView software
Power Consumption:
DAQBOOK-200: 620 mA @ 12 Vdc;
Operating Ambient: 0 to 50°C; 0 to 95% RH, non-condensing
Storage Temperature: 0 to 70°C
Dimensions: 3.5 x 21.6 x 27.9 cm (1⅜ x 8.5 x 11")
Weight: 2.5 kg (5 lb)

A/D SPECIFICATIONS
Type: successive approximation
Resolution: DAQBOOK-200: 16-bit
Conversion Time: 8 µs; on non-EPP systems, 30k-50k samples/s, system dependent
Monotonicity: no missing codes
Linearity: ±1 bit
Zero Drift: ±10 ppm/°C max
Gain Drift: ±30 ppm/°C max

SAMPLE AND HOLD AMPLIFIER
Acquisition Time: 2 µs
Aperture Uncertainty: 100 ps

ANALOG OUTPUTS/DAQBOOK-200
Channels: 16 single-ended, 8 differential, expandable up to 256 differential; single-ended/differential operation is software programmable
Connector: DB37 male, P1
Resolution: 16-bits
Ranges: unipolar/bipolar operation is software programmable on a per-channel basis
Unipolar: 0 to 10 V, 0 to 5 V, 0 to 2.5 V, 0 to 1.25 V
Bipolar: 0 to ±5 V, 0 to ±2.5 V, 0 to ±0.125 V, 0 to ±0.625 V
Maximum Overvoltage: 30 Vdc input current
Differential: 150 pA typ, 0.2 µA max
Single-ended: 250 pA typ, 0.4 µA max
Input Impedance: 100 MΩ
Gain Temp. Coefficient: 3 ppm/°C typ
Offset Temp. Coefficient: 12 µV/°C max

TRIGGERING/DAQBOOK-200
Analog Trigger
Programmable Level Range: 0 to ±5 V
Trigger to A/D Latency: 10 µs max
Digital Trigger
Logic Level Range: 0.8 V low, 2.2 V high
Trigger to A/D Latency: 10 µs max
Software Trigger
Trigger to A/D Latency: dependent on PC speed
Pre-Trigger: up to 65,536 scans

SEQUENCER/DAQBOOK-200
Randomly programmable for channel & gain; DAQBOOK-200 is also randomly programmable for unipolar/bipolar ranges
Depth: 512 location
Channel to Channel Rate: 10 µs/channel, fixed
Maximum Repeat Rate: 100 kHz
Minimum Repeat Rate: 10 hours
Expansion Channel Sample Rate: same as on-board channels, 10 µs/channel

ANALOG OUTPUTS/DAQBOOK-200
Channels: 2
Connector: DB37 male, P1
Resolution: 12-bits
Voltage Ranges: 0 to 5 Vdc with built-in reference; 0 up to ±10 Vdc with external reference
Maximum Output Current: 10 mA

GENERAL PURPOSE DIGITAL I/O
DAQBOOK-200
Channels: 24 expandable up to 192
Connector: DB37 male, P2
Device: 82C55
Output Voltage Levels
Minimum "1" Voltage: 3.0 @ 2.5 mA sourcing
Maximum "0" Voltage: 0.4 @ 2.5 mA sinking
Output Current
Maximum Source Current: 2.5 mA
Maximum Sink Current: -2.5 mA
Input Voltage Levels
Minimum Required "1" Voltage Level: 2 V
Maximum Allowed "0" Voltage Level: 0.8 V
Output Float Leakage Current: 10 µA

OMB-DAQBOOK Series
System Examples

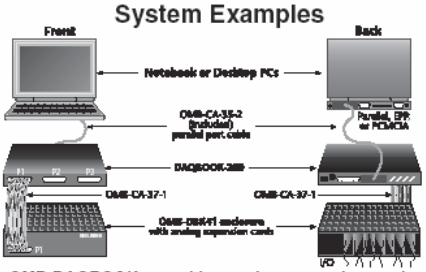

The OMB-DAQBOOK-200 with 8 analog expansion cards housed in one OMB-DBK41 ten-slot expansion card enclosure.

The OMB-DAQBOOK-200 with 18 analog expansion cards and two OMB-DBK32A power supply cards housed in two OMB-DBK41 ten-slot expansion card enclosures.

C-47

Figure D.3: Daqbook/216 Specifications
http://www.omega.com/DAS/pdf/OMB-DAQBOOK.pdf

Step Motor Systems

S6961/2
Smart Drive

Overview

IDC's S6961 (1–axis) and S6962 (2–axes) Microstepping Smart Drives are user friendly systems that offer you many compelling features and benefits. Consider these systems when your motion control application requires:

- A well integrated motion controller, microstepping drive, operator interface, power supply, 30 I/O, and built-in OPTO 22 I/O rack
- A simple Machine Controller
- Configurable I/O
- Go Immediate Mode. This mode of operation allows the controller to multitask between motion control and I/O operations. Immediate Mode also allows each axis to move completely independently of the other axis
- Interrupts
- Linear interpolation and registration
- Accepts encoder feedback for stall detect, closed loop operation and position maintenance
- Coordinated motion between two axes
- 1–99 axes of immediate control via host RS-232C communication
- Optional analog I/O for:
  - Reading an analog input proportional to temperature, distance, or pressure
  - Setting an analog output to control position of another axis of motion (for use with a D2500, H3501/4501, or B8501 analog position controls)

Motion Control

- 6K memory for up to 199 user programs (30K, 400 programs optional)
- User scaling of position, velocity, and acceleration
- Descriptive variables, math and conditional branching
- High-speed interrupt driven inputs–registration
- S6962–linear interpolated vector moves
- Windows Application Developer software included. See page G-35

Optional Keypad

- Both a programming tool and an operator interface
- Menu-driven setup, on-line Help Function, Diagnostic Screens, Trace Mode provides straight forward set up, troubleshooting and program debugging
- Easy to read backlit 40 character display
- Attaches to control or mounts remotely
- Scratch-proof, large keys
- Displays current position and I/O status
- Keypad is protected to Nema 4 (IP65) when panel mounted

OPTO Compatible I/O

- Accepts OPTO–22 (G4) digital modules and Grayhill (G5) analog and temperature modules
- 100% solid state, opto–isolation to 4000 volts
- 8 positions, all bidirectional
- Specify (intermix) OPTO I/O modules: for AC, DC, analog, and temperature signals

Drive Performance

- The S6961 and S6962 feature the same outstanding dynamic performance and reliability as our S6002 micristepping drive, described on page G-21

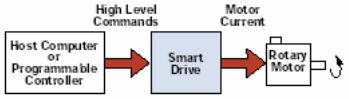

Compatible Mechanics:
EC2-S, EC3-S, EC4-S, EC5-S
NV-S, N2-S, R2A-S, R3-S, R4-S
Positioning Tables

Industrial Devices Corporation
707-789-1000 • 800-747-0064 • E-mail: info@idcmotion.com

Figure D.4: Position Controller Specifications
http://www.idcmotion.com/pdf/7040.pdf

R2A-S/P Rodless Actuator
50 lbs Payload
Step Motor

Performance

Belt-Drive Models

R2A-S32T-20T
R2A-S32V-20T

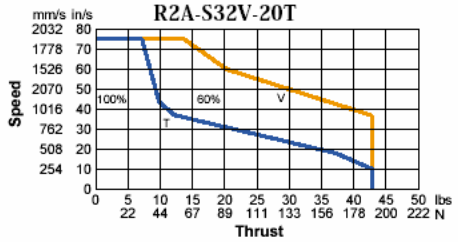

R2A-S32(T/V)-20T: 2:1 Timing Belt, 3 inch/rev Belt		
Travel per Motor Rev	1.50 in	38.10 mm
Repeatability	±0.004 in	±0.10 mm
Belt Accuracy	±0.010 in/ft	±0.25 mm

R2A-P22T-35T
R2A-P22V-35T

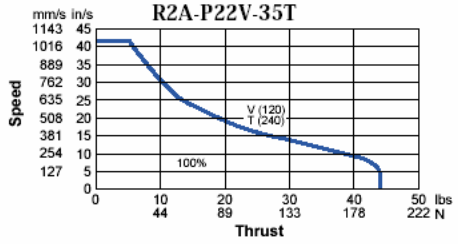

R2A-P22(T/V)-35T: 3.5:1 Helical Gears, 3 inch/rev Drive Belt		
Travel per Motor Rev	0.84 in	21.34 mm
Repeatability	±0.004 in	±0.10 mm
Belt Accuracy	±0.010 in/ft	±0.25 mm

R2A-P22T-120T
R2A-P22V-120T

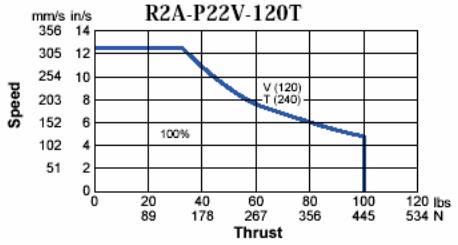

R2A-P22(T/V)-120T: 12:1 Helical Gears, 3 inch/rev Drive Belt		
Travel per Motor Rev	0.25 in	6.35 mm
Repeatability	±0.004 in	±0.10 mm
Belt Accuracy	±0.010 in/ft	±0.25 mm

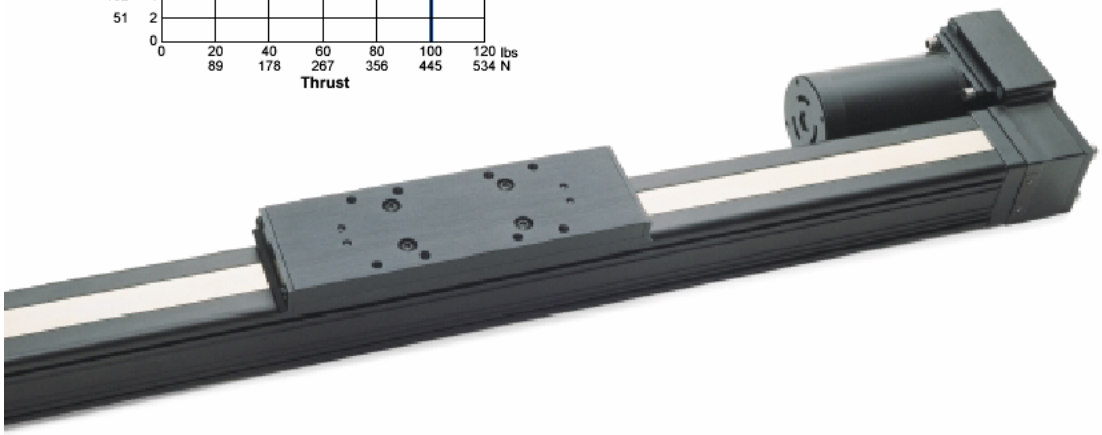

- Performance using S6000 Series, [illegible], and [illegible] Controls.
- Repeatability and Accuracy will be affected by belt stretch under heavier loads.

Industrial Devices Corporation
707-789-1000 • 800-747-0064 • E-mail: info@idcmotion.com

Figure D.5: Linear Actuator Specifications
http://www.idcmotion.com/pdf/2024.pdf

APPENDIX E

SAMPLE CALCULATIONS

- Calculating h, the heat transfer coefficient using Newton' Law of Cooling

  Newton's Law of Cooling:

$$q'' = h\left(T_{jet} - T_{surface}\right) \qquad \text{Eq (E.1)}$$

  Re arranged:

$$h = \frac{q''}{\left(T_{jet} - T_{surface}\right)} \qquad \text{Eq (E.2)}$$

  Data from the centerline for unconfined Trial #1:

  q"=87011 w/m^2

  T_{jet}=1383 k

  $T_{surface}$=495 k

$$h = \frac{87011}{1383 - 495} = 98.1 W / m^2 k \qquad \text{Eq (E.3)}$$

- Calculating $\bar{h}$, average heat transfer coefficient

  In this case the weighted average of h for each data point is used. The weight is the donut shaped area over which each value of h corresponds divided by the total area, denoted A.

  For example the weight of the first h, corresponding to the area with an inner radius of 0 m and an outer radius of 0.00635 m, the tail pipe centerline is calculated as follows:

$$A_1 = \frac{\pi * \left({r_{position2}}^2 - r_{position1} \right)}{\pi * r_{total}} = \frac{\pi * \left(0.00635^2 - 0^2 \right)}{\pi * 0.127^2} = 0.0025 \qquad \text{Eq (E.4)}$$

Now the weighted h is calculated. This example shows how this is done for the first data point in the unconfined test #1:

$$h_{A1} = h_1 * A_1 = 0.0025 * 98.1 = 0.24 \qquad \text{Eq (E.5)}$$

Finally $\overline{h}$ is the sum of all the weighted h values, final results is shown for unconfined trial #1.

$$\overline{h} = h_{A1} + ... + h_{An} = 61.2 \qquad \text{Eq (E.6)}$$

- Calculating $\overline{Nu}$, the average Nusselt number from experimental results.

  The following example calculates the average Nusselt number for unconfined trial #1:

$$\overline{Nu} = \frac{\overline{h}D}{k} = \frac{61.2 * 0.071}{89.4} = 49 \qquad \text{Eq (E.7)}$$

- Calculating the Reynolds number

  The Reynolds number equation is:

$$\text{Re} = \frac{\rho V D}{\mu} \qquad \text{Eq (E.8)}$$

  For the unconfined trial #1:

$$\text{Re} = \frac{0.252 * 36 * 0.071}{0.000208} = 3100 \qquad \text{Eq (E.9)}$$

- Calculating $\overline{Nu}$, from Martin's (1977) equation using unconfined trial #1.

  Note that this is a pulse combustion trial and Martin's (1977) equation is for steady impingement. The numbers are used for consistency with the rest of the calculations

The equations are as follows:

$$\frac{\overline{Nu}}{\mathrm{Pr}^{0.42}} = G\left(\frac{r}{D}, \frac{H}{D}\right) F_1(\mathrm{Re}) \qquad \text{Eq (3.10)}$$

$$F_1 = 2\,\mathrm{Re}^{0.5}\left(1 + 0.005\,\mathrm{Re}^{0.55}\right)^{0.5} \qquad \text{Eq (3.11)}$$

$$G = \frac{D}{r}\frac{1 - 1.1D/r}{1 + 0.1(H/D - 6)D/r} \qquad \text{Eq (3.12)}$$

Using sample data with Pr = 0.705:

$$F_1 = 2 * 3100^{0.5}\left(1 + 0.0005 * 3100^{0.55}\right)^{0.5} = 132 \qquad \text{Eq (3.13)}$$

$$G = \frac{0.071}{0.20}\frac{1 - 1.1 * 0.071/0.20}{1 + 0.1(0.071/0.071 - 6)0.071/0.20} = 0.26 \qquad \text{Eq (3.14)}$$

$$\overline{Nu} = 132 * 0.26 * 0.705^{0.42} = 30 \qquad \text{Eq (3.15)}$$

REFERENCES

Azevedo, L. F. A., Webb, B. W., Queiroz, M., (1994). "Pulsed Air Jet Impingement Heat Transfer" *Experimental Thermal and Fluid Science*, pp. 206-213

Barattini and D. J. Sailor, (1997) "Pulsed Impingement Heat Transfer Enhancement Between an Air Jet and a Heated Surface," Presented at the 1997 ASEE/GSW Annual Conference

Eibeck, P.A., J. O. Keller, T.T. Bramlette, and D. J. Sailor, (1991). " Pulse Combustion: Tailpipe Exit Jet Characteristics" Combust. *Sci. and Tech, Vol*. 94, pp. 167-192

Eibeck, P.A., J. O. Keller, T.T. Bramlette, and D. J. Sailor, (1991). " Pulse Combustion: Impinging Jet Heat Transfer Enhancement" *Combust. Sci. and Tech*, Vol. 94, pp. 147-165

Gemmen, R. S., J. O. Keller and V. S. Arpaci (1993). "Heat/Mass Transfer from a Cylinder in the Strongly Oscillating Flow of a Pulse combustor Tailpipe*" Combust. Sci. Tech*. Vol. 94, pp 103-130

Hanby, V. I. (1969) "Convective Heat Transfer in a Gas-Fired Pulsating Combustor," *Journal of Engineering for Power*, Vol. 91, Series A, N0. 1 pp. 48-52

Hwang, S.D. and H.H. Cho (2001). "Effects of Acoustic Excitation Positions on Heat Transfer and Flow in Axisymmetric Impinging Jet: Main Jet Excitation and Shear Layer Excitation*," International Journal of Heat and Fluid Flow*, Vol. 24 pp 199-209

Jambunathan, K., E. Lai, M. A. Moss and B. L. Button, (1992). "A Review of Heat Transfer Data for Scircular Jet Impingement", *Int. J. Heat and Fluid Flow*, Vol 13, No. 2 pp. 106-115

Kudra, T., M. Benali, and I. Zbicinski, (2003). "Pulse Combustion Drying: Aerodynamics, Heat Transfer, and Drying Kinetics" *Drying Technology* Vol. 21, No. 4, pp. 629-655

Martin, H., (1977). "Heat and Mass Transfer Between Impinging Gas Jets and Solid Surfaces", *Advances in Heat Transfer*, (edited by T. Irvine and J. P. Hartnett), Vol. 13, pp. 1-60.

Mladin, E. C. and D. A. Zumbrunnen, (1996). "Local Convective Heat Transfer to Submerged Pulsating Jets" *Int. J. Heat and Fluid Flow.* Vol 40, No. 14, pp. 3305-3321

Nevins, R. G., and H. D. Ball, (1962). "Heat Transfer Between a Flat Plate and a Pulsating Impinging Jet," *Proceedings of the 1961-62 Int'l Developments in Heat Transfer* pp. 510-516

Shaddix, Christopher R., (1998) "*Practical Aspects of Correcting Thermocouple Measurements for Radiation Loss,*" Proceedings of 1998 Fall Meeting of Western States Section/The Combustion Institute

States, R., (2003) "Tutorial: Air Hood Optimization After Pad Retrofit", Presented at ISA Expo 2003

Tavener, J. P., D. Southworth, D. Ayres, N. Davies. (2002) "*Industrial Measurement with Very Short Immersion*" http://www.isotechna.com/

Zbicinski, I., M. Benali, T. Kudra, (2002). "Pulse Combustion: An Advancement Technology for Efficient Drying", *Chem. Eng. Technol*. Vol. 25, pp. 687-691

Zumbrunnen, D. A., and M. Aziz, (1993). "Convective Heat Transfer Enhancement Due to Intermittency in an Impinging Jet," *Journal of Heat Transfer*, Vol. 115, February, pp. 91-98